polymers

MDPI

Article

Multiscale Experimental Evaluation of Agarose-Based Semi-Interpenetrating Polymer Network Hydrogels as Materials with Tunable Rheological and Transport Performance

Monika Trudicova [1], Jiri Smilek [1], Michal Kalina [1], Marcela Smilkova [1], Katerina Adamkova [2], Kamila Hrubanova [2], Vladislav Krzyzanek [2] and Petr Sedlacek [1,*]

[1] Faculty of Chemistry, Brno University of Technology, Purkynova 118, 61200 Brno, Czech Republic; xctrudicova@fch.vut.cz (M.T.); smilek@fch.vut.cz (J.S.); kalina-m@fch.vut.cz (M.K.); smilkova@fch.vut.cz (M.S.)

[2] Institute of Scientific Instruments of the Czech Academy of Sciences, Kralovopolska 147, 61264 Brno, Czech Republic; katka@isibrno.cz (K.A.); hrubanova@isibrno.cz (K.H.); krzyzanek@isibrno.cz (V.K.)

* Correspondence: sedlacek-p@fch.vut.cz; Tel.: +420-541-149-486

Received: 25 September 2020; Accepted: 29 October 2020; Published: 31 October 2020

Abstract: This study introduces an original concept in the development of hydrogel materials for controlled release of charged organic compounds based on semi-interpenetrating polymer networks composed by an inert gel-forming polymer component and interpenetrating linear polyelectrolyte with specific binding affinity towards the carried active compound. As it is experimentally illustrated on the prototype hydrogels prepared from agarose interpenetrated by poly(styrene sulfonate) (PSS) and alginate (ALG), respectively, the main benefit brought by this concept is represented by the ability to tune the mechanical and transport performance of the material independently via manipulating the relative content of the two structural components. A unique analytical methodology is proposed to provide complex insight into composition–structure–performance relationships in the hydrogel material combining methods of analysis on the macroscopic scale, but also in the specific microcosms of the gel network. Rheological analysis has confirmed that the complex modulus of the gels can be adjusted in a wide range by the gelling component (agarose) with negligible effect of the interpenetrating component (PSS or ALG). On the other hand, the content of PSS as low as 0.01 wt.% of the gel resulted in a more than 10-fold decrease of diffusivity of model-charged organic solute (Rhodamine 6G).

Keywords: hydrogels; semi-interpenetrating polymer networks; controlled release systems; rheology; diffusion; cryo-scanning electron microscopy

1. Introduction

Hydrogel represents a three-dimensional, water-swollen network assembled from cross-linked chains of either polymer molecules or partially coagulated colloidal particles. Because a macromolecular gel network can be formed from virtually any water-soluble polymer, hydrogel materials generally encompass a wide range of chemical compositions possessing a great variety of miscellaneous physicochemical functionalities that can be exploited in numerous applications [1]. Among them, the biomedical use of hydrogels has attracted particular interest since their first appearance. In a fact, hydrogels were the first biomaterials designed intentionally for the use in the human body [2,3]. The main benefits regarding their biomedical application include a combination of high water content and physicochemical similarity to the native extracellular matrix [4] which together results in their high

biocompatibility. Furthermore, their internal structure, as well as the rate of degradation or dissolution in vivo, can be tuned by controlling their chemical composition, type and density of the cross-links, etc. Since the first pioneer works on covalently cross-linked poly(2-hydroxyethyl methacrylate) gels published by Wichterle and Lim in 1960 [3], significant progress has been made in the field of hydrogel design for biomaterial use, in particular in improving the physical form of the hydrogel delivery (including micro- or nanoparticulate gels [5,6], gel films [7,8], etc.), in providing a specific response to a change in the external conditions (such as temperature [9,10], pH [11,12] or concentration of a particular biomolecule [13,14]), or in obtaining materials with precisely designed internal architecture such as the superporous gels [15,16], hydrogels self-assembled from biopolymers produced by genetically engineered microorganisms [17,18], dual network gels [19,20] and many others. Hence, until now, hydrogel materials have not only gained a prominent position in the field of medical research but have also been put into common practice in tissue engineering [21,22], regenerative medicine [23,24], diagnostic [25,26] or separation techniques [27,28], cell immobilization and cultivation and, perhaps most exclusively, in drug-delivery applications [29].

Despite many beneficial properties, hydrogels have also some specific limitations and risks regarding their uses in the development of drug-delivery systems [29]. For example, poor mechanical properties (i.e., low tensile strength) of the gels compared to 'hard' drug-delivery systems such as nanoparticles may lead to a premature disintegration of the gel carrier and instantaneous release of the active substance under a mechanical strain [30]. Perhaps even more important are the specific limitations connected to the transport properties of the gels. Drug loading capacity, as a complex product of multiple influences (drug solubility in water, its partition between gel and solution, or its effect on the stability of the gel network junctions) is usually limited even in the case of hydrophilic active substances [31,32]. Moreover, high water content and large pore size indispensably result in rapid drug release on a time scale of hours to days which again barely competes with the long-term release profiles of other delivery systems such as microspheres [33]. Until now, a range of strategies has been proposed to improve the partition of the active substance in the gel and to retard its release from the hydrogel carrier. These strategies usually aim at supporting the binding (either chemical or physical) between the drug and the polymer network. Hence, numerous procedures have been explored to incorporate monomers with a specific ionic or non-ionic affinity to the drug into the preparation of synthetic polymer networks [34], to exploit the presence of native functional groups of biopolymers (e.g., carbohydrates) in their physically cross-linked gels [35,36] or to conjugate the drug to the gel network via covalent bonds prone to enzymatic or chemical cleavage in situ [37].

In the present work, we put forward an alternative strategy, which aims to address both the aforementioned issues of the hydrogel drug carriers independently to each other. Our hydrogel system is based on semi-interpenetrating polymer networks (semiIPNs) which, together with interpenetrating polymer networks (IPNs), belong to the class of polymer blends. IPNs are defined by International Union of Pure and Applied Chemistry (IUPAC) as "A polymer comprising two or more networks which are at least partially interlaced on a molecular scale but not covalently bonded to each other and cannot be separated unless chemical bonds are broken." [38] SemiIPNs differ from the IPNs in the fact that the chains of the second polymer are dispersed in the network formed by the first polymer without forming a separate network and, consequently, the linear polymer component can in principle be separated from the constituent polymer network without breaking chemical bonds [38]. In recent years, both IPNs and semiIPNs have attracted special attention in novel material applications mainly due to the possibility of combining favorable properties of each polymer component to the final properties superior to those provided by the two polymer constituents alone. Hence, several IPN- and semiIPN-based hydrogel compositions have recently been proposed for application in tissue engineering [39] and in controlled-release (CR) systems [40], where the synergistic effect brought by the combination of the two polymer component is primarily focused on the specific improvement of mechanical properties, biocompatibility, thermal stability or chemical resistance of the gel.

In our study, we introduce a different approach to the utilization of semiIPN hydrogels in drug-delivery systems. Rather than focusing on a specific polymer composition developing carriers of hydrophilic (in particular ionic) active compounds based on semiIPN hydrogels which comprise a 'structure–ruling' gel-forming component, with a low affinity to the drug substance, interpenetrated by a 'binding' component that does not interfere with the internal morphology and the mechanical properties of the gel but significantly improves hydrogel reactivity. We hypothesize that such a system would allow an independent dual-tuning of mechanical and transport performance via manipulating the relative content of the two structural components. As a prototype material, we here introduce hydrogels based on an agarose network interpenetrated by a linear polyelectrolyte component. Agarose is involved in the study as a model representative of thermomelting polysaccharides which form physical hydrogels via thermally induced phase separation. Among versatile applications of agarose [41], its use in tissue engineering [42] and drug delivery [43] has recently attracted special attention mainly for its great biocompatibility, temperature-dependent behavior [43,44], and multiple options of manipulating its internal architecture [45,46]. As an interpenetrating component, two structurally distinct linear polyanions, alginate and poly(styrenesulfonate), are used in this study to provide an attractive binding affinity towards model low-molecular solute—Rhodamine 6G. This compound was used mainly for its complex molecular structure combining highly hydrophilic positively charged nitrogen atom with neighboring aromatic structural moieties, which represents a common structural motif widespread in different groups in pharmaceuticals [47,48].

The main aim of the study is to test the ability of the system to tailor the chemical structure and internal morphology of the proposed semiIPN hydrogels separately and, consequently, to manipulate its mechanical (rheological) and transport properties independently. To evaluate the relation between internal structure (both physical and chemical), mechanical properties, and transport performance of the resulting gels, we present a unique analytical approach, where the three fundamental material qualities (structure, rheological properties, and transport performance) are studied both on the macroscopic (i.e., the sample-averaged) and the microscopic scale.

2. Materials and Methods

2.1. Preparation of the Gels

All hydrogels, utilized in this study were prepared via the thermoreversible gelation of the aqueous solution of agarose (Type I, low electroendoosmosis; Sigma-Aldrich, Prague, Czech Republic). Agarose hydrogels (without any addition of a polyelectrolyte component) were prepared from the aqueous solution of agarose (concentration of agarose in solution/gel: 0.5%, 1%, 2%, and 4% by weight), while agarose-based semiIPN gels from the aqueous solution of agarose (1 wt.%) with a corresponding addition of a dissolved polyelectrolyte (0.002, 0.005 and 0.010% by weight). As a polyelectrolyte component, alginic acid sodium salt (ALG; Sigma-Aldrich, Prague, Czech Republic, 180947, average MW 120–160 kDa, M/G ratio 1.33 [49]) and poly(sodium 4-styrenesulfonate) (PSS; Sigma-Aldrich, Prague, Czech Republic, average MW 70 kDa), respectively, were used.

The gelation proceeded as follows: the accurately weighed amount of agarose powder was dispersed in deionized water (preparation of agarose gels) or in the aqueous solution of the respective polyelectrolyte of the required concentration (semiIPN gels), respectively. The mixture was at first slowly heated with continuous stirring to 85 °C and then maintained at the constant temperature until the solution turned transparent. Subsequently, the solution was degassed in an ultrasonic bath (1 min. at 85 °C) and slowly poured into the corresponding container (according to the needs of subsequent analysis) which was then stored in a closed bottle above the water-level (i.e., at 100% relative humidity to prevent unwanted surface evaporation of water). Upon the gradual cooling to room temperature (approximately 45 min), the mixture gradually gelled.

2.2. Turbidimetry

For the turbidimetric experiment, the respective heated and degassed agarose solution (with or without the respective polyelectrolyte component) was poured and let to cross-link in the poly(methyl methacrylate) cuvettes for spectrophotometry ($10 \times 10 \times 45$ mm^3). Subsequently, the ultraviolet–visible (UV-VIS) transmittance spectrum of the gel was collected in the wavelength range 300–800 nm on Hitachi U3900 spectrophotometer (Tokyo, Japan), whereby deionized water was used as a reference sample. From the transmittance spectrum, optical densities (OD) in the spectral range of 700 to 800 nm (where no specific light absorption by the gel components is expected) were calculated according to OD (λ) = $-\log T(\lambda)$. From the optical density, turbidity was calculated (considering optical path length = 10 mm) from $\tau(\lambda) = 2.3$ OD (λ). Calculated turbidities in the spectral range 700–800 nm were plotted as $\log\tau(\lambda) = f(\log\lambda)$ and the linear fit of the plot was performed using MS Excel. The wavelength exponent then was determined as the slope of the linear fit and further transformed into the correlation length (in μm) using data published by Aymard [50]. Finally, the correlation length value is presented as an effective value of mesh size determined from turbidimetry.

2.3. Oscillatory Rheometry

For the analysis of macroscopic viscoelastic behavior of a hydrogel sample, the circular cut of the gel (40 mm in diameter, 1.1 mm in height), gelled in a Petri dish before the analysis, was placed on the bottom Peltier plate of the Rheometer AR-G2 (TA Instruments, New Castle, DE, USA) pre-tempered to 25 °C. The oscillatory analysis was performed using plate-plate geometry (titanium plate sensor, 40 mm in diameter) at a constant temperature of 25 °C. The upper rheometer shaft with geometry was moved into the trim gap (1020 μm) and excess of hydrogel outside of both plates was cut away by a spatula. The geometry gap (1000 μm) was reached (normal force during compressing did not exceed 5 N). Due to the high content of water in hydrogels, the solvent trap was used to prevent the potential change in viscoelastic properties due to the evaporation of the dispersion medium. Frequency sweep measurements were performed on the whole set of hydrogel samples in duplicate. The conditioning step (25 °C, 5 min) preceded before each measurement. Thanks to the conditioning step, each hydrogel was relaxed and tempered to the required temperature before measurement. Firstly, the linear viscoelastic region (LVR) was determined by strain sweep test at a constant frequency of oscillation (1 Hz) in the range 0.01–1000%, 6 points per decade (Figure S2 in Supplementary Materials). The constant amplitude of deformation chosen from the LVR (0.5%) was used for all frequency sweep measurements. Frequency sweep measurements were performed on the whole set of hydrogel samples in duplicate (at least) with parameters as follows: 0.01–20 Hz, 6 points per decade, decimal logarithmic mode. The relative deviation of the duplicate measurements never exceeded 10% (in terms of elastic (storage) modulus G' and viscous (loss) modulus G'', respectively). From the recorded values of G' and G'', the corresponding values of complex modulus $|G^*|$ and phase angle δ were calculated according to:

$$|G^*| = \sqrt{(G')^2 + (G'')^2} \tag{1}$$

$$\delta = \operatorname{arctg}\frac{G''}{G'} \tag{2}$$

To calculate the effective mesh size from frequency sweep data, frequency dependencies of elastic and viscous moduli were fitted (using least square regression algorithm) with a generalized Maxwell model [51] using the procedure described by Pescolido et al. [52]. Fitting functions were as follows:

$$G' = \sum_{i=1}^{n} G_i \frac{(2\pi f\lambda_i)^2}{1 + (2\pi f\lambda_i)^2} \tag{3}$$

$$G'' = \sum_{i=1}^{n} G_i \frac{2\pi f\lambda_i}{1 + (2\pi f\lambda_i)^2} \tag{4}$$

where f is the frequency of oscillations (in Hz), $n = 4$ is the number of considered Maxwell elements (determined via the statistical procedure described in [53]), G_i and λ_i represents the corresponding spring constant and relaxation time, respectively, of the i-th Maxwell element. Data fitting was performed using the Solver tool in MS Excel. Based on the results of the data fitting, hydrogel shear modulus was calculated as the sum of the spring constants of Maxwell elements $G = \sum_{i=1}^{n} G_i$ and transformed into the density of crosslinking ρ_x and into the average network mesh size ξ, according to:

$$\rho_x = \frac{G}{RT} \tag{5}$$

and,

$$\xi = \sqrt[3]{\frac{6}{\pi \rho_x N_A}} \tag{6}$$

where T is the thermodynamic temperature, while R and N_A the universal gas constant and Avogadro constant, respectively.

2.4. Microrheometry

A colloidal analyzer Zetasizer Nano ZS (Malvern Panalytical Ltd., Great Malvern, UK) was used to collect dynamic light scattering (DLS) microrheological data. This method is based on observing the movement of tracer particles with defined particle size (polystyrene monodisperse with nominal particle size 100 nm, Sigma-Aldrich, Prague, Czech Republic) in the sample via monitoring the time development of intensity of the light scattered by these particles. The tracer particles were homogeneously incorporated inside the analyzed hydrogels during the initial preparation step (they were added to the mixture before heating up to dissolve agarose powder). The experimental parameters of DLS microrheological measurements were set as follows: temperature: 25 °C, equilibration time: 60 s, duration of one run: 10 s, number of runs: 12, number of measurements of each sample: 5. Each sample was prepared and analyzed in three replicates. The main experimental outcomes from DLS microrheology was the dependence of mean square displacement (MSD) of tracer particles in the studied hydrogels on the observation time. From the respective MSD, viscoelastic parameters (primarily the storage and loss moduli) were calculated in the Microrheology software tool in Zetasizer Software (Malvern Panalytical Ltd., Great Malvern, UK). Other viscoelastic parameters (complex modulus, phase angle) were calculated using equations shown above for the oscillatory rheology.

2.5. Macroscopic Diffusion Experiments

The whole set of prepared hydrogels was subjected to diffusion experiments proposed and optimized in our previous study [54,55]. For this purpose, hydrogel samples were prepared directly in PMMA cuvettes for spectrophotometry similarly to turbidimetry analysis. In this case, the cuvettes were overfilled with the solution to achieve the concave meniscus of the agarose solution at the cuvette edge. After the solidification (approximately 30 min, room temperature), the excess hydrogel was cut away to obtain a flat hydrogel surface at the open orifice of the cuvette.

The hydrogel-filled cuvettes were then immersed in a solution of model solute to study its diffusion in the gels qualitatively and quantitatively. As the model solute, positively charged organic dye Rhodamine 6G (R6G, dye content > 95 wt.%, Sigma-Aldrich, Prague, Czech Republic) was used. The concentration of the source solution of R6G in the diffusion experiment was 0.01 g.dm^{-3}, the solution was continuously stirred via a magnetic stirrer (250 RPM) during the whole diffusion experiment. At selected times (24, 48, and 72 h), the cuvettes were taken out of the solution and the UV-VIS absorption spectra were measured in the 300 to 800 nm spectral range at various distances from the orifice on Varian Cary 50 UV–VIS spectrophotometer (Varian, Inc., Paolo Alto, California, USA) equipped with the custom-made accessory providing controlled fine vertical movement of the cuvette in the spectrophotometer (for details on the accessory, see [56]). For a determination of R6G

concentration in the gel from the recorded spectra, a set of reference hydrogel samples was prepared for every tested agarose-polyelectrolyte composition. In the reference hydrogel samples, a known concentration of homogeneously dispersed R6G was provided by the addition of the corresponding amount of R6G to the agarose solution before its gelation. Further data processing of the spectra (suppression of the light scattering background signal) was described in detail previously [54,56]. Diffusion experiments were performed in duplicates for each of the analyzed hydrogel compositions.

Each concentration profile (dependence of R6G concentration on the position in the gel, i.e., on distance from the solution/gel interface) determined for a particular hydrogel at the time of diffusion t were fitted by following diffusion equation (for the derivation, see [57]) using the Solver tool in MS Excel:

$$c(x) = c_0 \cdot erfc \frac{x}{\sqrt{4D_{eff}t}} \quad (7)$$

where $c(x)$ and c_0 are concentrations of R6G in the gel (in g·m^{-3}) at distance x from the interface or at the interface, respectively, and D_{eff} is the effective diffusion coefficient of R6G in the gel. From the fitting parameters (D_{eff}, c_0) the rate of R6G diffusion and its partition in the gel is described quantitatively. The partition coefficient is then calculated as the ratio of the interface concentrations of R6G in the gel and the solution (c_{sol}), respectively:

$$\varepsilon = c_0 / c_{sol} \quad (8)$$

Mean values and standard deviations of these parameters were calculated by averaging the results for three diffusion times and duplicated measurements.

2.6. Fluorescence Correlation Spectroscopy

Self-diffusion of the molecules of the model solute (R6G) was studied by fluorescence correlation spectroscopy (FCS). For this purpose, the homogeneous distribution of the R6G molecules (concentration in the order of nM) was achieved similarly to the preparation of reference hydrogel samples for the evaluation of macro-diffusion experiments.

The FCS measurements were performed on MicroTime 200 instrument (PicoQuant, Berlin, Germany) equipped with a fluorescence microscope Olympus IX71 (Olympus, Tokio, Japan) (setup of the system: laser wavelength 510 nm, dichroic mirror 514/640 nm, emission filter 550/49, laser intensity 6.6 μW). Moreover, during FCS measurements, two single photon avalanche diode detectors were used, which allowed us to use cross-correlation for data evaluation. To maintain uniform measurement conditions, at the beginning of the experiment the vertical (xz) scan was performed and the position of the glass-gel interface was identified. Afterward, a horizontal (xy) scan was performed 5 μm above the glass surface and three different positions were chosen for measurements for each sample. Subsequently, for FCS analysis each hydrogel sample was prepared in five replicates. The main outcome from FCS analysis is the coefficient of self-diffusion of R6G in each hydrogel sample.

2.7. Scanning Electron Microscopy Imaging

For the scanning electron microscopy (SEM) imaging of the internal structures of the gels, samples were first cryogenically fixed. Small copper-based thin-wall tubes with a diameter of approximately 1 mm were at first filled with the particular hydrogel sample—each tube was filled by performing a horizontal motion through the already gelled agarose or agarose/polyelectrolyte solution using tweezers so that the hydrogel protruded from the tube at both ends. The plunge-freezing technique of fixation was used, where a small amount of hydrogel is rapidly cooled by immersion in cryogen (liquid nitrogen in this case). After having been plunge-frozen, the tubes containing hydrogel samples were kept at cryogenic temperatures throughout the whole experiment including the imaging. Before the imaging, freeze-fracture was also applied by cutting off the protruding part and scratching the surface superficially with a sharp blade at high vacuum and low temperature in the EM ACE600 preparation chamber (Leica microsystems, Vienna, Austria). Three successive steps of freeze etching to reveal

the internal microstructure were applied. During each of the etching steps, the temperature was increased to −100 °C, and after it stabilized, decreased back to −120 °C. All the frozen samples were imaged in the SEM Magellan 400L (FEI-Thermo Fisher Scientific, Hillsboro, OR, USA) equipped by a temperature-controlled cryo-stage at the temperature of −120 °C; the imaging was performed before any freeze etching and after each freeze etching step.

Image processing and analysis of the cryo-SEM images was performed in ImageJ open-source image processing toolbox (National Institute of Health, Bethesda, Maryland, USA and Laboratory for Optical and Computational Instrumentation, University of Wisconsin, Madison, USA; version 1.51, [58,59]). For this purpose, square sections of the raw cryo-SEM images (512 × 512 pixels) were processed by the following procedures: contrast and brightness of the section were first adjusted according to the image histogram and the bandpass filter was used to suppress lightening inhomogeneities and horizontal stripes. Then the processed images need to be converted from grayscale to black and white projections in an effort to display only the uppermost layer of the 3D network structure. For this conversion, the image sections were thresholded using the MaxEntropy algorithm. Subsequently, the actual analysis of the internal structure proceeded using 'Analyze particles' and 'Analyze skeleton' commands (details are provided in the Results section).

3. Results

3.1. Mechanical Properties of the Gels

Overall viscoelastic properties of the semiIPN gel samples were examined by standard techniques of oscillatory rheometry. Results of the frequency sweeps are shown for agarose gels and selected semiIPN gels in Figure 1a,b (corresponding frequency dependencies of storage and loss moduli as the raw experimental data are provided in Figure S1 in Supplementary Materials). As can be seen, the value of complex modulus (calculated using Equation (1)) is almost frequency-independent for all analyzed hydrogels (see Figure 1a). This represents a characteristic rheological feature of densely cross-linked gel networks where the deformation response in the linear viscoelastic region is not significantly affected by the timescale of the deformation [60–62]. Perhaps more important, it can be seen in the same figure that the overall stiffness of semiIPN gels can be adjusted over a wide range of values by alternating the concentration of the network-making component. In the case of agarose gels, changing the concentration of agarose from 0.5% to 4% by weight shifts the complex modulus of the gels to the values higher by more than two orders of magnitude. On the other hand, the presence of the interpenetrating polyelectrolyte components (PSS and ALG) in the range of concentrations used in this work (max. 0.01% by weight of the gels) does not affect the stiffness of the gel severely (see Figure 1, for other concentrations of polyelectrolytes, see Figures S2 and S3 in Supplementary Materials). The frequency dependence of the phase-shift angle (calculated using Equation (2)) illustrates the relative contribution of the elastic and viscous type of deformation on different time scales (see Figure 1b). It can be seen that even at the lowest frequencies of the oscillatory shear deformation, the phase-shift angle is still lower than 45° for all prepared gels (including as well the semiIPN gels with lower content of polyelectrolyte component, data shown in Figure S3 Supplementary Materials). In other words, even for the slowest deformations that take place on the longest timescales, the gel is deformed predominantly elastically. At the deformation timescale of seconds, the value of phase angle is so low for all gels (<10°), that their deformation behavior resembles ideal solids. Finally, it should be also mentioned that all prepared hydrogels were subjected also to complementary oscillatory tests such as amplitude sweep (alternatively called strain sweep) and relaxation tests. Although all the particular results are not shown here (see results of the strain sweep test in Figure S4 in Supplementary Materials), they can be concluded similarly—differences in the deformation response of the gels caused by the presence of interpenetrating polyelectrolyte component was insignificant compared to the impact of the different content of the gel-forming component (agarose).

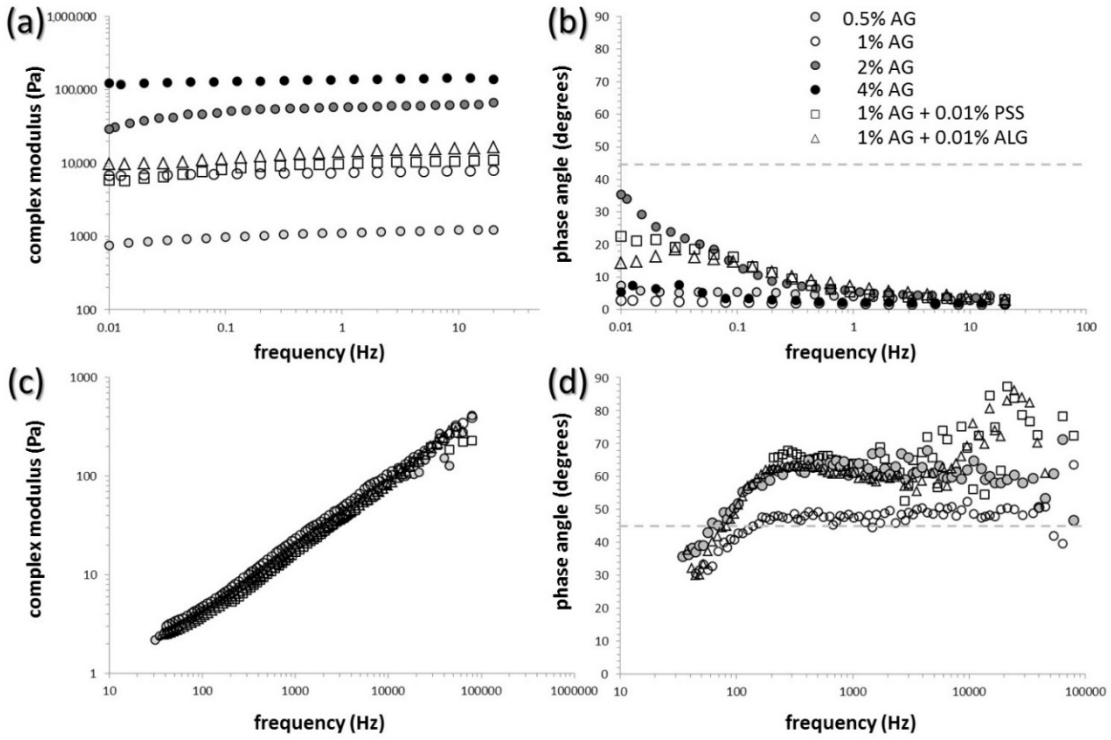

Figure 1. Parameters of viscoelasticity of the gels determined on macroscopic (**a**,**b**) and microscopic scale (**c**,**d**). Frequency dependence of the complex modulus (**a**,**c**) and the phase angle (**b**,**d**), respectively.

The microrheological assay describes the deformation behavior of the gels from a different perspective. The method based on DLS observation was used for monitoring the thermal motion of standard tracer microparticles incorporated into the internal structure of the gels. In this approach, from the scattering correlogram (a function which correlates the scattering intensity over time), the mean square displacement function of the tracer particles is derived and the basic viscoelastic parameters (storage and loss moduli and the others related with these two) are calculated for individual characteristic times or frequencies. This approach therefore provides a microrheometric analog to standard oscillatory frequency sweep tests—viscoelastic parameters which are obtained are the same in their essence for both methods; nevertheless, in the case of microrheology, they characterize viscoelasticity of that part of the internal space of the hydrogel where the thermal motion of the tracer particles takes place.

Basic results of the DLS microrheology are presented in Figure 1c,d and Figure S5 in Supplementary Materials. Figure 1c,d show frequency dependencies of complex moduli and phase angles, respectively, derived from the thermal motion of tracer microparticles in the internal pores of the particular hydrogel structure. As can be seen, the results of this experiment show fundamental differences as compared to the results of common oscillatory (macro)rheometry assay. Complex moduli of the gels determined by DLS microrheometry are significantly lower and considerably more dependent on the frequency of the deformation. Furthermore, as far as the frequency-dependent complex moduli (as well as complex viscosity, an alternative quantitative parameter describing stiffness of the material) of all tested gels (again, including the other PSS and ALG containing semiIPN gels presented graphically in Figure S5 in Supplementary Materials) show virtually the same values, and it can be deduced that the local environments of the microparticle motion in particular gels provide similar deformation response. Contrarily to the classical oscillatory rheometry, the viscous character of the deformation behavior predominates (note the values of phase angle > 45° in Figure 1d). This is reasonable from the point of view that the thermal motion of the particles takes place in the liquid pores of the hydrogel matrix and that the microrheological approach, therefore, provides insight into the deformation behavior of

this local microenvironment. Furthermore, it can be seen from the frequency dependencies of phase angles that while the lowest applied frequencies induce the most viscous deformation response in the case of oscillatory macrorheometric analysis, the opposite is observed for the microrheology assay (most elastic response is measured for the lowest characteristic frequencies). Again, this apparent discrepancy of the viscoelastic properties arises from the essential difference between the two rheometric approaches. While for the oscillatory rheometry the lowest frequencies characterize the slowest applied oscillatory deformation where the liquid-like character of the material is most manifested, in the case of microrheology the lowest frequencies correspond to the longest correlation time where the trace particle motion reaches also more distant surroundings of the particle. Therefore, the presence of a polymer network that surrounds liquid pores filled with tracer particles affects the particle motion most strongly just for the lowest frequencies. It can be seen in Figure 1d that concerning both discussed aspects of the viscoelastic response of tested gels on the microscopic scale, no fundamental differences were found for the gels no matter what the content of gel-forming or interpenetrating component was.

3.2. Transport Properties of the Gels

Similarly to the investigation of mechanical properties of the gels, also the analysis of transport performance towards the model hydrophilic solute (Rhodamine 6G, R6G) was performed using both a macro- and a micro-scale approach. The results of the diffusion experiments are shown in Figure 2 and Tables 1 and 2. Firstly, macroscopic investigation of the diffusion of R6G from source solution into the gels was involved using the methodology developed in our previous work [37–39]. It can be seen in Figure 2a,c that, using this simple method, the effects of the interpenetrated components on the rate of transport in the gels can be evaluated even visually. In particular, the picture in Figure 2a shows that the presence of interpenetrating PSS chains severely affects (decelerates) the rate of R6G diffusion in the gel and that the effect correlates with the content of PSS in the gels. Furthermore, different color saturation in the gel near the interface with the source solution indicates that also the partition of the R6G between the solution and the gel is affected by the presence of PSS. On the other hand, no such effects can be observed in the case of ALG's presence in the gels (see Figure 2c). These visual observations can easily be transformed into quantitative information by measuring UV-VIS spectra at different positions in the gels. Using the calibration method based on gels prepared with a known content of R6G, concentration profiles of R6G can be determined for different gel compositions and for various times of the diffusion experiment. A comparison of such concentration profiles corresponding to gels with different contents of PSS and ALG is shown in Figure 2b,d, respectively.

By the regression of the concentration profiles (using fitting Equation (7)), effective diffusion coefficients (D_{eff}) and boundary concentrations of R6G in the gel (c_0) can be calculated (see Tables 1 and 2). It can be seen that the comparison of absolute values of the calculated diffusivities agrees well with the qualitative features discussed based on the visual investigation of the gels. The presence of PSS in the gel reduces the effective diffusivity of R6G significantly; the highest content of PSS reduced the diffusivity by more than 90% of the value corresponding to the agarose gel with no interpenetrating component. The effect of ALG was much less pronounced and rather inverse at first sight—the presence of ALG in the gels slightly increases the average diffusivity. Nevertheless, taking into account the confidence interval of the diffusivity values, no definite conclusions can be derived for an effect of ALG on the rate of R6G diffusion in the gels.

A similar difference in effects of the two interpenetrating polyelectrolytes was observed also for partition coefficients calculated using Equation (8). While the concentration of R6G in the gel at the boundary with the source solution was not significantly affected even by the highest concentration (0.01 wt.%) of ALG as compared to the reference agarose gel (see Table 2), the same content of PSS increased the partition drastically (to more than 10-fold higher average concentration compared to reference agarose gel). In a fact, partition coefficients determined in this study illustrate the dynamic partitioning of the solute during its diffusion into the gel. Equilibrium distribution of the solute between the solution and the gel could be described more accurately by the results of equilibrium

absorption experiments such as those described in our previous study [55]. On the other hand, the diffusion experiments proposed here benefits mainly from providing the simultaneous monitoring of partitioning and diffusion parameters in the single experiment.

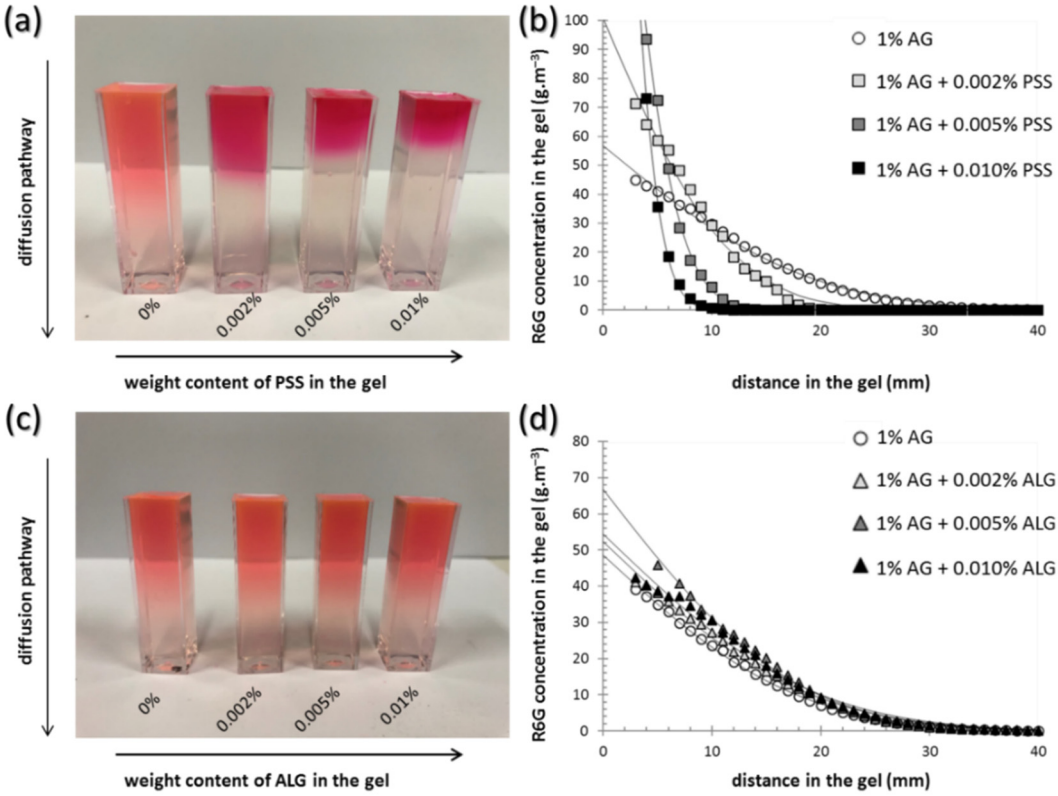

Figure 2. Diffusion of Rhodamine 6G (R6G) in the gels investigated on the macroscopic scale. (**a**,**c**) Visual comparison of agarose gels (1 wt.% of agarose) with different content of the interpenetrating component after 72 h of diffusion of R6G from solution. (**b**,**d**) Experimentally determined concentration profiles of the same gels.

Table 1. Summarized results of investigation of R6G diffusion on the macroscopic and molecular scale in hydrogels with/without poly(styrene sulfonate) (PSS).

Weight Content of PSS in the Gel	Macroscopic Diffusivity D_{eff} ($\mu m^2 \cdot s^{-1}$)	FCS Diffusivity * D_s ($\mu m^2 \cdot s^{-1}$)	Partition Coefficient ε (-)	Fluorescence Lifetime τ (ns)
0%	389 ± 7	343 ± 7	5.3 ± 2.0	4.21 ± 0.06
0.002%	158 ± 27	196 ± 27	10.2 ± 2.6	4.21 ± 0.09
0.005%	52 ± 25	148 ± 25	31.0 ± 10.1	4.27 ± 0.07
0.010%	27 ± 22	106 ± 22	64.8 ± 36.7	4.30 ± 0.06

* self-diffusion coefficients determined via fluorescence correlation spectroscopy.

Table 2. Summarized results of investigation of R6G diffusion on the macroscopic and molecular scale in hydrogels with/without alginate (ALG).

Weight Content of ALG in the Gel	Macroscopic Diffusivity D_{eff} ($\mu m^2 \cdot s^{-1}$)	FCS Diffusivity D_s ($\mu m^2 \cdot s^{-1}$)	Partition Coefficient ε (-)	Fluorescence Lifetime τ (ns)
0%	333 ± 33	385 ± 15	7.0 ± 1.6	3.70 ± 0.02
0.002%	379 ± 27	309 ± 21	6.4 ± 1.2	3.73 ± 0.03
0.005%	379 ± 46	304 ± 48	6.4 ± 1.0	3.69 ± 0.01
0.010%	394 ± 42	298 ± 21	6.1 ± 1.0	3.64 ± 0.01

FCS analysis provides a complementary view on the transport properties of the gels as far as self-diffusion of individual, homogeneously distributed R6G molecules is monitored. Self-diffusion

coefficient (D_s) of the R6G molecules in a respective gel is determined here from the time evolution of correlation function that characterizes the time scales of fluctuations in the intensity of the R6G fluorescence. Different diffusion models can be used in the mathematical evaluation of the correlation function. In our work, we have applied the simplest model involving a single characteristic decay-time to the autocorrelation function providing one global diffusion coefficient of the present chromophores. The diffusion coefficient values determined for the semiIPN hydrogels are summarized in Tables 1 and 2. It can be seen that for both polyelectrolyte components interpenetrating the agarose matrix, the self-diffusivity of R6G decreases with the concentration of the binding component in the gel, only the exact extent of the suppression of P6G diffusivity is different for PSS and ALG, respectively. In the case of PSS, the effect is slightly less pronounced than in the case of effective diffusivities determined by the macroscopic diffusion assay. On the other hand, a modest reduction of the rate of thermal motion of R6G is here found out also for ALG, unlike the macroscopic assay. The apparent discrepancy between the results of macroscopic and FCS diffusivity assays may be attributed to the different experimental conditions as well as to the distinct physical phenomena behind the two methods. First, the macroscopic diffusion assay uses the concentration of tracked diffusion probe (R6G) orders of magnitude higher than FCS. The relative content of freely moving RG6 molecules, not affected by the interpenetrated polyelectrolyte, must be significantly different in the two methods. Therefore, macroscopic diffusion assay may not be sufficiently sensitive to detect an effect of weakly binding components (such as ALG). On the other side, when the binding is strong enough to entirely immobilize the fluorescent molecule, this molecule becomes "invisible" for the FCS methods and the average self-diffusivity determined by FCS may be overvalued. Actually, in contrast to the macro-scale experiments with the UV-VIS absorption detection of diffusing R6G, the FCS technique can analyze only the motion of fluorescence-emitting molecules. Therefore, the strongly physically bound R6G molecules that lose the light-emitting ability via static fluorescence quenching are not monitored and do not contribute to the calculated diffusion coefficient any more. In general, results of the FCS diffusivity assay confirm that R6G molecules are subjected to an attractive interaction with both the polyelectrolyte components, whereby the interaction is significantly stronger in the case of PSS.

Aside from the determination of the self-diffusion coefficient of a solute, the FCS method can also provide some additional parameters which might be interpreted concerning the mode of binding of the solute by the polymer network. For instance, in the case of time-resolved FCS technique, the average diffusion coefficients of R6G in the analyzed volume are complemented with corresponding average fluorescence lifetimes. Tables 1 and 2 show the values of the average fluorescence lifetime of R6G determined by TCSPC (time-correlated single photon counting) analysis of the time-resolved FCS experiment. Once again, a dissimilar effect has risen from the presence of ALG and PSS, respectively. The presence of PSS in the gel matrix leads to a slightly increased value of fluorescence lifetime, while higher content of ALG rather decreases the value. As far as the fluorescence lifetime is inversely proportional to rates of non-radiative de-excitation processes, its value is sensitive to a local environment in which a motion of the molecule occurs. In particular, the increase in fluorescence lifetime can be explained in terms of loss of the rotational freedom of the fluorophore caused by the R6G binding by PSS.

On the other hand, the R6G fluorescence lifetime, the value of which usually varies around 4 ns [63], is known to be highly concentration-dependent, as Förster energy transfer between monomers and weakly fluorescent stable dimers at higher R6G concentrations decreases the quantum yield and causes the fluorescence lifetime shortening [64]. Therefore, a decrease of fluorescence lifetimes in the gel with the highest ALG content may be assigned to a change in the spatial distribution of R6G molecules in the gel, which does not alter the rotational freedom significantly but causes colocalization of R6G molecules and the formation of R6G dimers. Similarly, concentration effects may explain also a difference in the average fluorescence lifetimes determined for agarose gels without polyelectrolyte components in the two independent experimental batches (compare the values for 0% ALG and PSS, in Tables 1 and 2, respectively). As far as all the analyzed gels in the respective experimental batch

were prepared simultaneously using the same R6G source solution and gelation conditions, it can be expected that the total R6G concentration in the gels is well comparable. On the other hand, in the case of a very low concentration of the R6G in the gel (order of nM), this is difficult to reproduce among the different experimental batches.

The qualitative difference in the effects of PSS and ALG on the fluorescence lifetime can be attributed to the dissimilar types of solute binding by the two polyelectrolytes. Electrostatic binding between opposite charges on the functional moieties of ALG and R6G molecules is less orientation-specific and, therefore, does not limit the rotation of the electrostatically bound R6G molecules significantly. On the other hand, this binding concentrates the fluorophore in the vicinity of oppositely charged polyelectrolyte which may enhance its aggregation. Unlike that, the presence of benzene moieties in the molecular structure of PSS complements the electrostatic attraction of R6G molecules with the planar stacking of the π electron-rich aromatic systems which results in significant loss of the rotational freedom of R6G and the corresponding increase in fluorescence lifetime.

3.3. Characterization of the Internal Structure of the Gels

Because both mechanical and transport properties of hydrogels are inevitably coupled with their internal structure, for a reasonable interpretation of results provided by the diffusion and rheological analyses of the studied hydrogels it is essential to provide their qualitative and, at best, quantitative structural characterization. For this purpose, we have included in our study also a complex structural assay comprising methods of either direct visualization or an indirect physicochemical mapping of the hydrogel network morphology.

For an indirect structural investigation of the agarose-based semiIPN hydrogels, we have at first utilized a simple turbidimetric assay, where turbidity is calculated from the optical density of the gels (determined by a standard transmission UV-VIS spectrometer) and plotted in log-log coordinates versus wavelength of the incident light. The exact mathematical apparatus for extracting internal structure parameters from such turbidity spectra was first proposed by Doty and Steiner [65] and further utilized by numerous authors [50,66–69]. We have followed the data-processing procedure that has been successfully applied by Aymard on various aqueous dispersions including swelled agarose hydrogels [50]. In this approach, linear regression of the log-log turbidity spectrum is performed in the range of wavelengths from 700 to 800 nm, and from the slope of the fitting line, the mesh size of an average scattering unit is determined (the log-log plots used for the calculation of the effective mesh size are shown in Figure S6 in Supplementary Materials). Aymard interprets the mesh size as the average distance between entanglements in the hydrogel network and, therefore, a value of this parameter can be taken as a rough estimate of the dimensions of pores in the gels. Mesh size values, determined from the turbidity data, are summarized in Figure 3a. As expected, the effective mesh size decreases significantly with the concentration of agarose in the gel as an indicator of the increasing density of crosslinking in the gel network. The order of magnitude of the calculated mesh sizes is in good agreement with the published range of pore sizes in agarose gels between 80 and 500 nm [70,71]. It was expected that the minor addition of polyelectrolyte interpenetrating components (PSS or ALG) will not remarkably alter the internal structure of the gels. It can be seen in Figure 3a that the addition of 0.01 wt.% of PSS or ALG increased in mesh size. The result can seem surprising as far as any addition of other polymer components should result in presence of more scattering centers which would hereby rather decrease the calculated mesh size value. Nevertheless, it must be emphasized that the method only characterizes a mean isometric dimension of the average scattering unit in the gel, and provides limited information about the other qualitative and quantitative structural parameters such as the actual shape of the network pores, width of the pore size distribution, etc. Therefore, conclusions about the results shown in Figure 3a should, rather, be about how the presence of minor contents of interpenetrating components does not significantly (in terms of the orders of magnitude) affect the size of the representative scatterer in the gel.

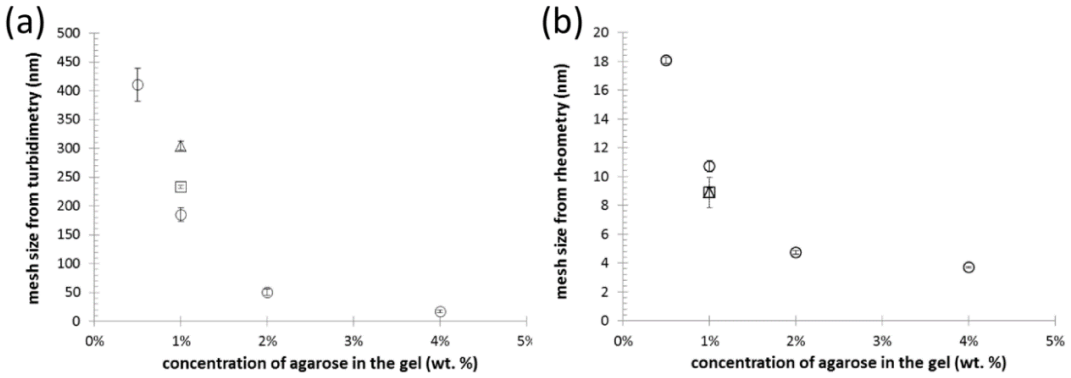

Figure 3. Results of indirect structural mapping of the hydrogels with different concentrations of agarose (○) and of the gels containing 1 wt.% of agarose-based interpenetrated by 0.01 wt.% of PSS (□) and ALG (△), respectively. The analysis-specific effective mesh sizes were calculated from the results of turbidimetry (**a**) and (macro)rheometry (**b**), respectively.

Not only the light scattering, but also the mechanical properties (mainly the elastic component of the deformation response) of the polymer networks are fundamentally connected with their crosslinking densities. Therefore, the results of rheometric assays may be used for the determination of effective mesh size, which in this case represents the mean size of the elastically active sections of polymer chains. Calculation of the mesh sizes from frequency sweep tests (using Equations (3) to (6)) is based on the rubber elasticity theory [72]. Although the validity of this theory for gels has continuously been questioned [73,74], it has been repeatedly utilized to calculate the mesh size of hydrogels based on rheometric parameters [52,75]. Previously, we have applied this approach in the determination of mesh size of polysaccharide-based phase-separated hydrogels [76]. The results of the calculations for the gels studied in the current study are shown in Figure 3b. As with the turbidimetry-derived values, also in this case the mesh sizes should be used for qualitative monitoring of changes in the internal structure rather than to provide absolute dimensions of the hydrogel pores. Again, it is evident that the increasing agarose content results in decreasing mesh size as a result of a more densely physically crosslinked agarose network. Compared to the turbidity-based mesh sizes, it can be seen that much lower values of the mesh size are calculated from the results of oscillatory rheometry. The elastically active chain sections differ naturally from those that participate in light scattering. Further comparing the results with published values of agarose gels pore sizes, it is also evident that the mesh size is significantly lower than the mean pore size. This is not a surprising fact when considering that also other than physical and chemical junction in the gel network (e.g., mechanical entanglements of the free polymer chains) can contribute to the elastic response to deformation. In this perspective, the most important outcome of this indirect structural mapping is that, in accordance with results from turbidimetry, no fundamental effect of the presence of interpenetrating polyelectrolyte component was observed (compare the effective mesh sizes for 1wt.% agarose gels with similar agarose gels containing also 0.01 wt.% ALG or PSS in Figure 3) as compared with the principal influence of the network-forming agarose component.

The gross picture of the morphology of the gels, provided by indirect structural mapping with rheometry and turbidimetry, was further refined by direct visualization of their internal porous structure by scanning electron microscopy (SEM). Cryogenic SEM (cryo-SEM) imaging was applied because aqueous samples cannot be directly observed in a high vacuum that needs to be maintained in the SEM chamber without any preceding stabilization. Therefore, the cryogenic fixation of the sample was performed via rapid cooling provided by the plunging of the sample in liquid nitrogen. To visualize the internal structure of a hydrogel sample, plunge freezing is followed by freeze-fracture (scratching the sample at high vacuum and cryogenic temperature) and freeze etching (letting the frozen water sublime to reveal the sample surface). Although plunging is not an optimal cryogenic

fixation method for preparation of such hydrated samples in electron microscopy because of the Leidenfrost effect during which a thermally insulating film of vaporized nitrogen forms around the sample, preventing fast cooling and allowing water ice crystals to form inside the specimen [77,78], it could be also beneficial in the case of hydrogel structural studies. We assume that the size and distribution of the ice crystals correspond to the chemical composition of the hydrogels and the amount of free water.

Results of the cryo-SEM imaging of the gels with different content of agarose (with the absence of an interpenetrating component) are shown in Figure 4, while the results for semiIPN hydrogels with the highest content of the respective interpenetrating component are provided in Figure 5. As expected, the principal role of agarose concentration in controlling the density of the crosslinking of the hydrogel network is obvious. On the other hand, as can be seen in Figure 5, even the highest applied concentration of an interpenetrating component (ALG or PSS) does not induce noticeable changes in the internal structure of the gels. Taking a closer look at the cryo-SEM images, it can be concluded that the plunge freezing of the gels in liquid nitrogen satisfactorily preserved the internal structure of the gels that is in correlation with the other applied methods. The network structure is largely isomorphic, with no apparent signs of anisotropic deformation during cooling. Nevertheless, some structural artifacts can be found in the images (such as those marked with arrows in Figure 4) indicating that the formation of ice crystals was not completely prevented.

The cryo-SEM images such as those shown in Figures 4 and 5 serve primarily as a visual illustration of the qualitative characteristics of the internal structure of the studied gel networks. From this point of view, the visual evaluation of the cryo-SEM images confirms the qualitative findings provided by indirect structure-mapping methods (turbidimetry, rheometry), i.e., the principle that the network-forming role of agarose is not particularly disturbed by a presence of the polyelectrolyte component. Nevertheless, cryo-SEM imaging can also be further processed to support these qualitative conclusions from some quantitative outcomes. For this purpose, we have applied two techniques of the image processing that are implemented in the open-source scientific image-processing toolbox ImageJ and that are suggested for the analysis of porous structures.

Firstly, the 'Analyze particles' tool (an automatic particle segmentation algorithm implemented in ImageJ) was used to identify individual pores in the image of the gel network. The outlines of the pores detected in the binary projection (Figure 6b) of an original image (Figure 6a) are shown in Figure 6c. As a numerical result of the Analyze particles tool, every outlined pore is described by its area and perimeter. Wherever it is necessary to take care of the pores which are displayed in the binary picture touching one another, the Watershed algorithm can be used before particle analysis. This algorithm uses a density profile to determine if one object with a peninsula should be two objects. If it determines that they should, it will draw a line to separate them. From the particle analysis, the distribution of pore areas and perimeters is obtained and processed into statistical parameters, e.g., average or mean values. The box plot projection of the pore areas and perimeters is shown in Figure 7a,b. These results again confirm that the size of pores, detected in the cryo-SEM images, decreases significantly with the increasing concentration of agarose in the gel. Once again, no such considerable pore size reduction is found for the semiIPN gels as a result of the presence of polyelectrolyte component.

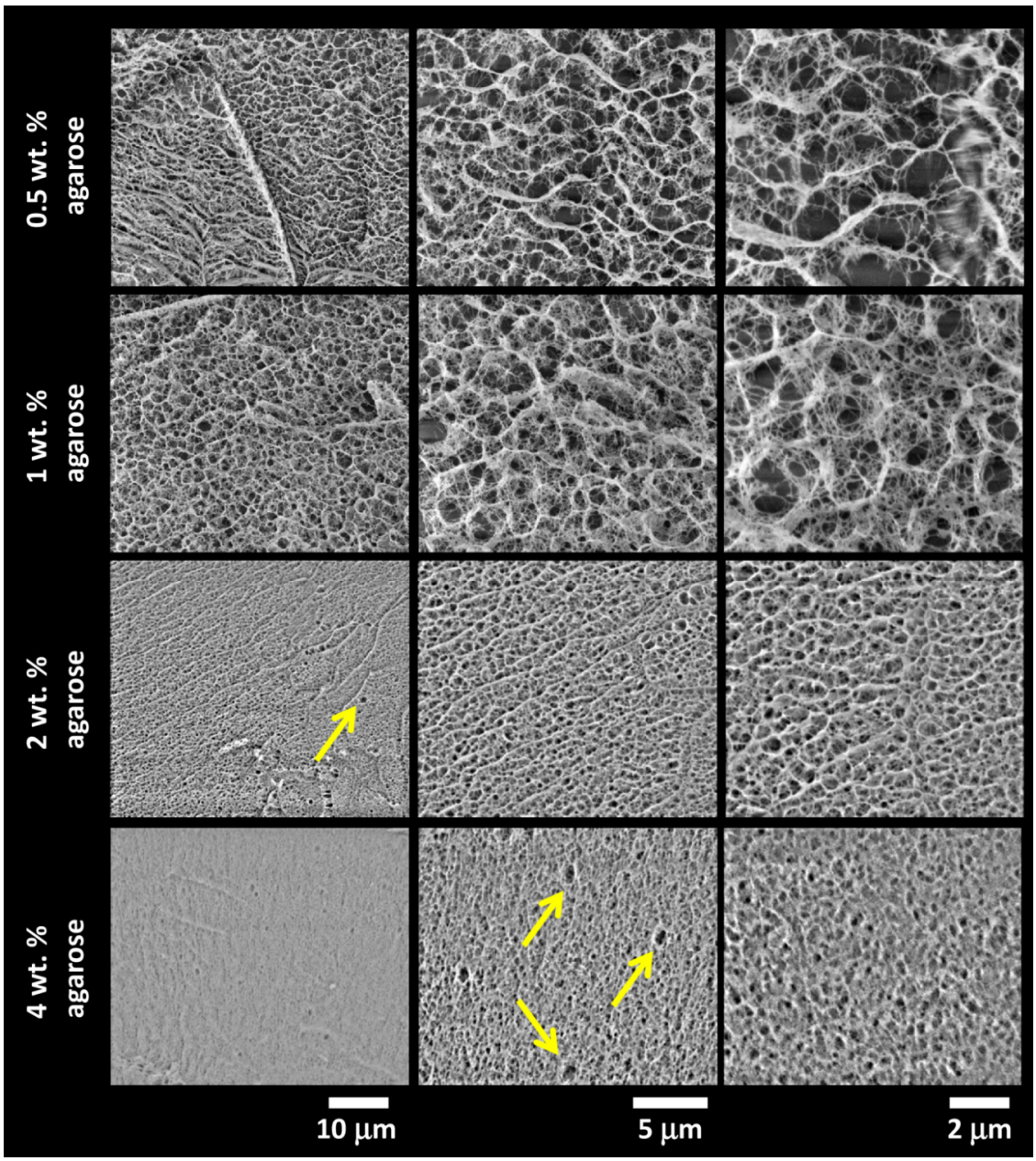

Figure 4. Results of cryogenic scanning electron microscopy (cryo-SEM) imaging of the internal structure of the plunge-frozen hydrogels with various content of agarose (with the absence of an interpenetrating polyelectrolyte component). Structure alterations caused by the formation of ice crystals are marked with arrows.

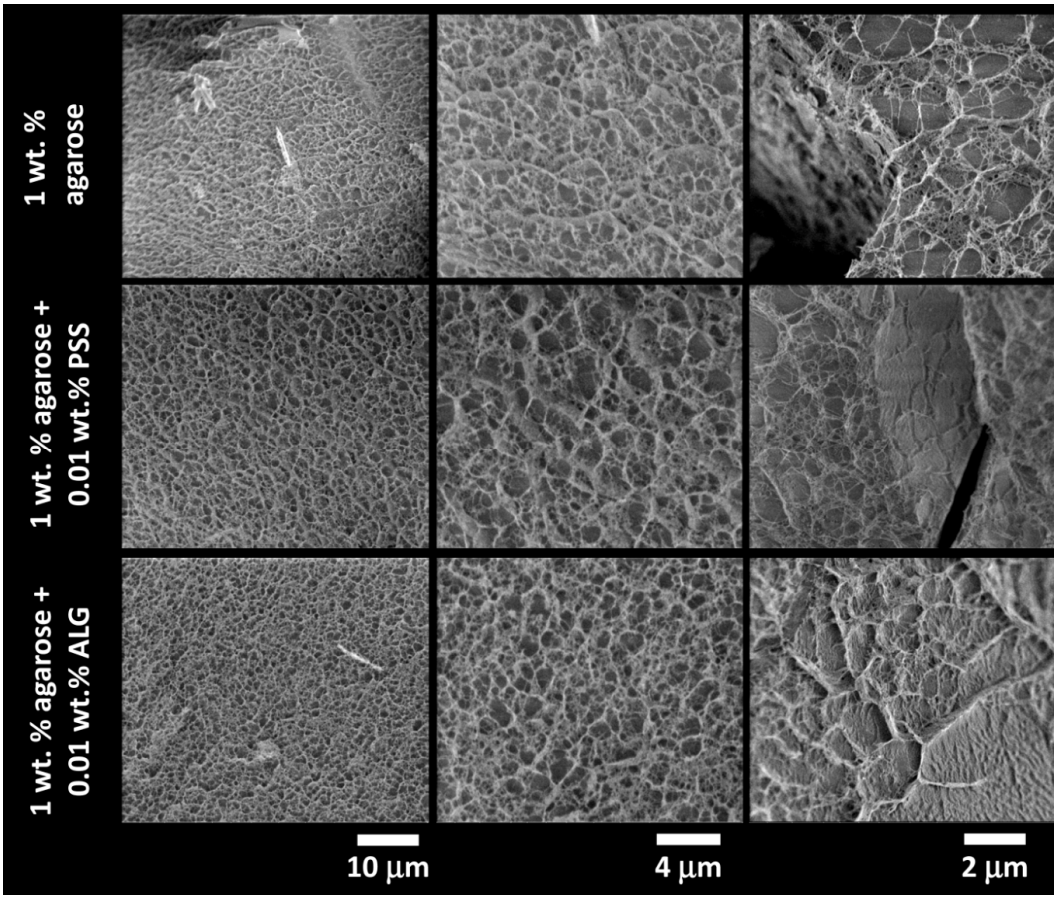

Figure 5. Results of cryo-SEM imaging of the internal structure of the plunge-frozen 1wt.% agarose hydrogels with and without the presence of an interpenetrating polyelectrolyte component (0.01 wt.% of PSS and ALG, respectively).

Pore areas/perimeters are not in their absolute values reasonably comparable with the results of indirect structural analyses summarized in Figure 3. Furthermore, as can be seen in Figure 6c, the pores detected in the cryo-SEM images have complex, rarely isometric shapes and, therefore, neither pore areas nor pore perimeters can be simply transformed to an isometric representation of the pore size, such as the diameters in the case of circular pore projections. Therefore, aside from the 'Analyse particles' approach, we used also another image analysis option implemented in the ImageJ toolbox—the 'Analyze skeleton' tool. In this procedure, the network structure displayed in the analyzed image is first skeletonized, i.e., replaced by the line skeleton using a topology-maintaining medial axis thinning algorithm (example of the skeletonized representation of the processed image is shown in Figure 6d). Using the subsequent analysis tool, branches and junctions of such a skeleton are classified, counted, and measured. The Box plot which represents the statistical treatment of branch sizes, detected in the skeleton of cryo-SEM images of analyzed hydrogels, is shown in Figure 7c. Unlike the areas or perimeters of the pores, the mesh size represents a linear size parameter and as such can be directly compared with the effective mesh sizes determined by turbidimetry or rheometry. As can be seen in Figure 7c, the effect of agarose content in the gel surpasses the influence of the interpenetrating component also in the distribution of branch sizes. Increasing concentration of agarose induces denser crosslinking which results in shorter branches in the skeletonized image. The mean values of the branch sizes are in the order of hundreds of nm, which represents larger pore dimensions compared to the values determined by indirect structural techniques (Figure 3) as well as to the published pore sizes detected in agarose gels by other techniques [70,71]. This is probably caused by the partial expansion

of dispersed water resulting from its imperfect vitrification and partial crystallization (see the signs of ice formation mentioned above).

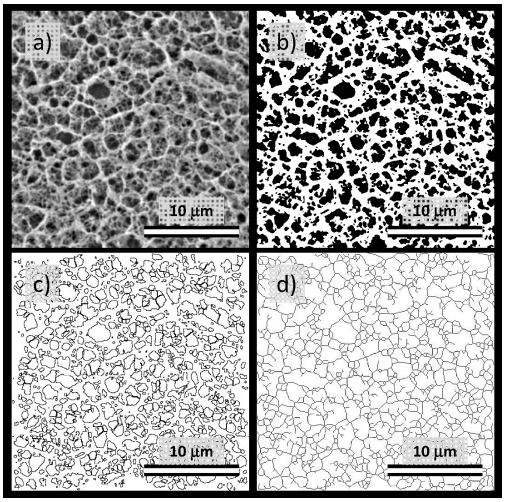

Figure 6. Processing of cryo-SEM images using the tools implemented in ImageJ software ((National Institute of Health, Bethesda, MD, USA and Laboratory for Optical and Computational Instrumentation, University of Wisconsin, Madison, WI, USA). Scalebar = 10 µm. (**a**) Original image (1 wt.% agarose gel without any interpenetrating component). (**b**) Binary projection (grayscale thresholding using MaxEntropy algorithm) of the original image. (**c**) An image mask is provided by the application of the 'Analyze particles' tool. (**d**) Image mask is provided by the application of the 'Analyze skeleton' tool.

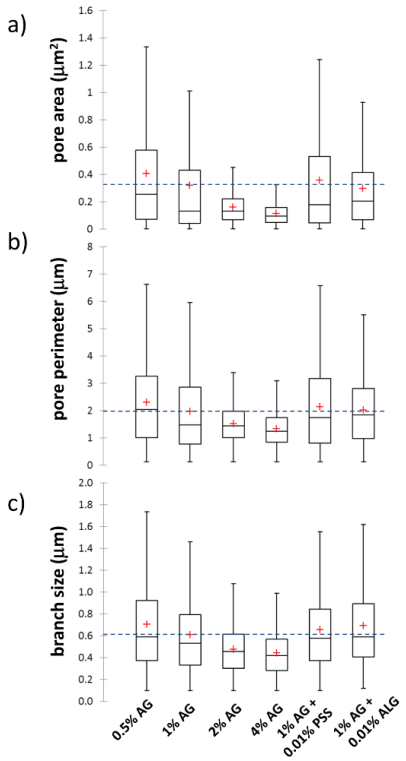

Figure 7. Box plots of pore size parameters determined from analysis of cryo-SEM images using ImageJ software. (**a**,**b**) Pore areas and perimeters determined using the 'Analyze Particles' tool. (**c**) Branch sizes using the 'Analyze skeleton' tool. Blue dashed lines in the box plots represent the mean values of the displayed parameters for 1 wt.% agarose gels without the presence of an interpenetrating polyelectrolyte component.

4. Discussion

The work presented here was set two major objectives. The first was to evaluate a simple material strategy proposed for the development of hydrogel-based controlled release systems that would allow independent tuning of their mechanical and transport features. The strategy is based on hybrid (dual component) hydrogels that consist of a network formed by a hydrophilic gelling component with reduced affinity to bind the carried active substance, interpenetrated by chains of a linear polymer that possess functional groups prone to a strong attractive interaction with the active substance. The second objective was to propose and test an appropriate analytical methodology that could provide a complex insight into composition–structure–performance relationships in the resulting hydrogel materials with the main concern on mechanical and transport properties investigated not only on the macroscopic scale but also in the specific microcosms of the aqueous gel pores. Combining these two central viewpoints, the presented study represents a fundamental contribution to the state of the art in controlled release systems with the potential to open up a new area of research and development of hydrogel-based CR materials.

The idea of semiIPN hydrogels with rheological and transport properties tunable independently via manipulating the relative composition of a network-making and a binding component is amazingly simple and it is surprising that, to our best knowledge, no systematic effort has been made to evaluate the potential of the use of such materials in the development of novel CR systems. The approach has a great advantage in its modularity—a broad portfolio of gel-making hydrophilic polymers with a limited capacity of physical binding by strong interactions such as coulomb forces or hydrogen bonds can be found, including the materials most routinely used in research and development of the first generation hydrogels for drug-delivery systems (e.g., poly(vinyl alcohol) [79], poly(2-hydroxyethyl methacrylate) [3,80], poly(ethylene glycols) [81] or thermomelting polysaccharides like gellan, dextran or agar [82,83]). During their gelation process, all these matrices allow easy incorporation of the interpenetrating component—a linear hydrophilic polymer with the chemical structure selected concerning specific binding preferences of intended carried substance. In our study, charged polymers were suggested as the interpenetrating component as they are generally applicable as a binding component in CR systems carrying ionic active compounds. A wide range of polyelectrolytes bearing various densities of positive or negative charges in combination with diverse accompanying chemical functionalities may be found among natural polymers (anionic and cationic polysaccharides such as alginate, hyaluronan, chitosan, polypeptides poly-γ-glutamate, poly-lysine), their chemically modified analogs (trimethyl chitosan, quaternized dextran, etc.) or among fully synthetic polymers (e.g., polymerized substituted acrylic monomers like polyacrylates, polyacrylamides, substituted polystyrenes, etc.). As a prototype material, agarose-based hydrogels interpenetrated by a minor content (less than or equal to 1:100 ratio by weight) of anionic polyelectrolytes (PSS and ALG) were prepared and analyzed in this work. The structure, mechanical properties, and transport of positively charged organic solute (Rhodamine 6G) in these gels were described thoroughly.

As expected, it was confirmed experimentally that the internal structure of the prepared gels in terms of their crosslinking density and corresponding internal porosity is principally governed by the concentration of agarose as the network-forming component (see the schematic representation of the effect in Figure 8a,b). As far as the morphology of the gel network predetermines its overall deformation response, also the mechanical performance of the gels is ruled by the content of agarose. By manipulating the concentration of the network-making component (agarose), the stiffness of the prepared gels may be altered over several orders of magnitude while the predominantly elastic (solid-like) rheological behavior typical for densely cross-linked hydrogels always prevails. Controlled stiffness of the hydrogel drug-delivery system is, on the one hand, a special concern mainly in load-bearing applications where the risk of premature mechanical destruction of a carrier is followed by a flow-away of the active compound which must be taken into account. On the other hand, a direct in vivo application of the highly elastic hydrogel materials may be problematic and limited to special physical forms such as gel micro- or nano-spheres [29]. Nevertheless, several strategies have

been proposed to overcome this hydrogel-delivery issue. One of the most common approaches is based on the injection of a viscous polymer solution followed by in situ crosslinking induced by an appropriate environmental trigger. One example which may be fully compatible with the proposed strategy of a semiIPN-based hydrogel-controlled release system is represented by block copolymers with hydrophobic domains which can crosslink at increased (physiological) temperatures via reverse thermal gelation caused by an entropically driven aggregation of the hydrophobic blocks (e.g., triblock ABA copolymers of A = poly(ethylene oxide) (PEO) and B = poly(propylene oxide) (PPO) [84]). The controlled interpenetration of the networks prepared from these temperature-sensitive sol-gel systems with a linear binding polymer component should be free of experimental difficulties as far as several PEO-based semiIPN systems have already been studied [85,86]. From this perspective, the proposed hybrid-network concept was proved to provide the expected ability to manipulate easily the material viscoelasticity with existing options on how to meet the specific requirements on flow properties of materials used in contemporary CR applications.

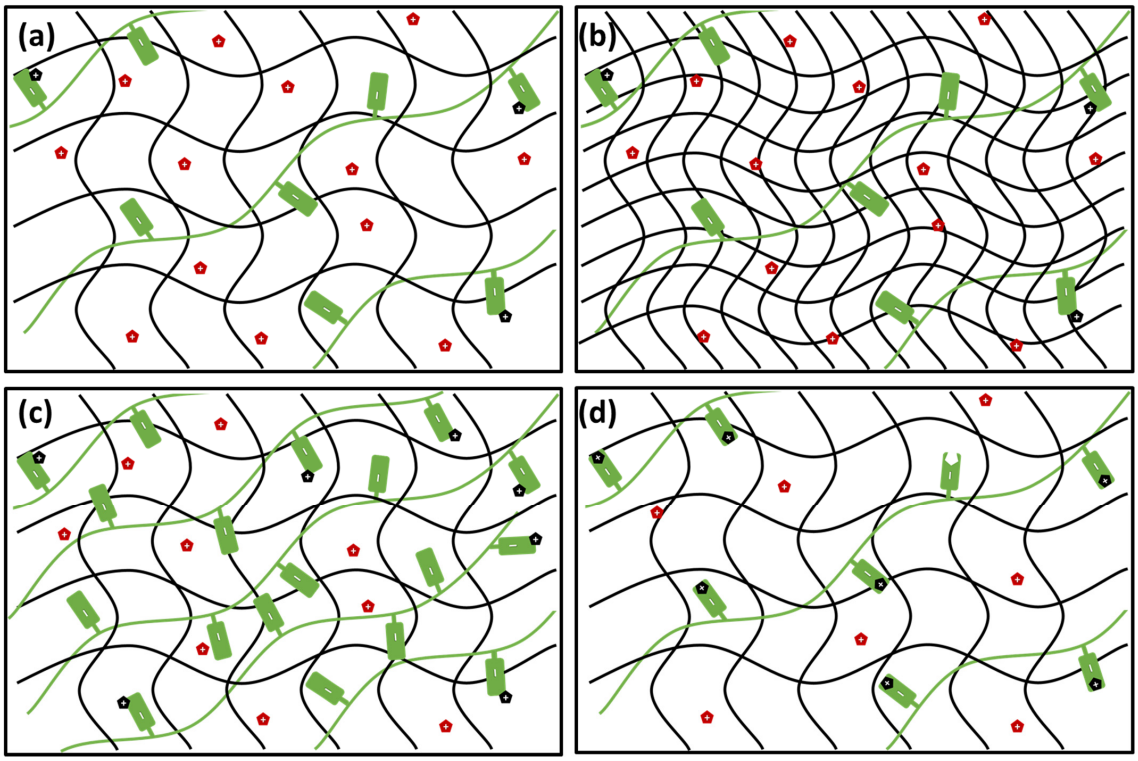

Figure 8. Schematic representation of the proposed concept of use of semiIPN hydrogels as controlled release (CR) systems with tunable rheological and transport properties. (**a**) Gelling component (black) with interpenetrating polyanion (green) possess universal binding affinity towards cations (red = free cations, black = bound cations). (**b**) With increasing content of the gelling component, gel stiffness and rigidity is increased with a negligible effect on the binding and diffusion of the cations. (**c**) With increasing content of the interpenetrating component, number of binding sites is increased affecting the transport properties of the gel with no effect on the mechanical properties. (**d**) Higher affinity of the binding sites (such as those provided for organic ions by PSS as compared with ALG) enhance the binding effectivity and shows more pronounced influence on the transport properties of the gel.

Furthermore, it was confirmed by the systematic diffusion-mapping assay that transport of the carried compounds in the dual-component gels may be significantly influenced even by a trace content of a suitable interpenetrating component (again, the schematic representation of the effect is provided in Figure 8a,c). In the present work, we focused our attention on the molecular transport of Rhodamine 6G. This model solute was used on the one side for its specific molecular structure combining the positive charge on nitrogen atom with aromatic structural residues. This specific structural motif is common

for numerous pharmaceutically active substances, e.g., for local anesthetics [47] or antibiotics [48]. Furthermore, well-described light absorption and emission behavior of R6G allows for the combination of various spectrometric techniques in the investigation of its transport in the hydrogel matrix on a different scale (macroscopic vs. microscopic scale). Results of experiments monitoring the diffusion of R6G from a source solution into the gels containing PSS confirmed that increasing the content of the interpenetrating component gradually suppresses the rate of R6G transport. In terms of the relative decrease in diffusion coefficient compared to a respective agarose gel, for the gels with ratio 1:100 (PSS to agarose) by weight, more than 90% decrease in diffusion coefficient was found for interpenetrated poly(styrene sulfonate). No such great alteration of R6G mobility may be achieved by manipulating the content of agarose itself, as was experimentally proved in our previous study [87]. Furthermore, not only the diffusion rate but also the partitioning of the solute in the gel is influenced significantly (more than a 10-fold increase in the partition coefficient was found in the case of PSS). Enhanced partitioning of the active compound may significantly increase the loading capacity of the drug carrier and consequently improve its pharmacokinetic profile [29]. On the other hand, a comparison of diffusion-related behavior of the gels interpenetrated by ALG and PSS, respectively, confirms that the degree to which the transport performance of the gel can be influenced is significantly dependent on the type of interaction between the active substance and the binding component (schematically represented in Figure 8a,d). In the case of ALG the binding of R6G is provided by the Coulomb electrostatic attraction alone while in the presence of PSS, we assume the stacking of aromatic moieties contributes to the binding significantly. This results in the fact that the extent to which the diffusion of R6G is affected (or, more precisely, the levels of R6G concentration at which these effects are manifested) differs significantly for the two interpenetrated polyelectrolytes.

Overall, on the example of prototype semiIPN hydrogels (in particular those containing PSS), it is illustrated that the transport properties of this type of hybrid network system may be altered greatly without any significant influence on their internal morphology and, hence, independently on their mechanical behavior. Furthermore, this strategy is not necessarily limited to the transport of hydrophilic active substances. Recently, several approaches have been proposed for the modification of hydrogels to provide controlled transport of water-insoluble solutes [88]. In our previous work, we have developed and characterized hydrogel systems with hydrophobic domains formed by surfactant micelles [89,90]. Controlled incorporation of such mechanically trapped hydrophobic domains in a supporting structure-defining hydrogel network could open new horizons in an independent tuning of mechanical and release behavior also for non-polar drug-releasing systems.

As was already noted, an additional merit of the present study is represented by the unique methodology that was utilized in providing the morphological, rheological, and also transport characterization of the studied hydrogels not only on the macroscopic but also on a microscopic scale. It was confirmed that this original analytical approach is highly beneficial in explaining the causal link between chemical composition, internal morphology, and mechanical and transport properties of the gels. For instance, our results clearly illustrate how the oscillatory (macro-)rheometry is complemented with the information provided by microrheometry in the completion of the overview of specific contributions of the polymer network and the surrounding aqueous solution, respectively, to the elastic and viscous components of the deformation response. Similarly, the involvement of a self-diffusion assay on the scale of individual molecules in parallel to common macroscopic monitoring of the diffusion of the same substance in the concentration gradient helps to explain how the binding of individual molecules in their local environment affects the rate of their molecular transport. Of course, the particular techniques described here do not represent the only and irreplaceable analytical option. For example, alternative techniques suggested for microrheological characterization of hydrogels include video microscopy [91] or fluorescence correlation spectroscopy [92]. Similarly, macroscopic diffusion experiments with hydrogels are often performed in a diffusion cell apparatus [87] while the self-diffusion of the solutes in the gels is commonly monitored via nuclear magnetic resonance

(NMR) [93]. Nevertheless, a combination of the macroscopic and microscopic scale of the analysis in a single study is still rather scarce.

Finally, for a reasonable discussion of deformation or transport performance of hydrogel materials, it is always necessary to have at one's disposal an analytical tool for mapping changes in the internal structure of the gel. Here, we have shown that cryo-SEM imaging of the gels provides detailed qualitative (and in combination with appropriate image processing techniques also quantitative) structural information. As noted, some indicators of alteration of the internal structure by the freezing artifacts can be found in our results. Nevertheless, this could be overcome e.g., by the utilization of a more appropriate cryofixation technique such as high-pressure freezing [94]. Aside from the direct visualization of the internal structure, our study also shows that valuable approximate structural information can be achieved also from much more accessible techniques of indirect structural mapping such as turbidimetry, rheometry, and additionally, for example, also differential scanning calorimetry [95].

5. Conclusions

It this study, we have experimentally verified through the results of a complex multiscale analysis of structure, viscoelastic, and transport properties of model agarose-based hydrogels with interpenetrating polyelectrolyte components that the concept of semiIPN gels containing an inert polymer network interpenetrated by a linear polymer component with the properly selected binding functionality can be successfully applied in the development of hydrogel materials with the ability of independent manipulation of mechanical and transport properties. Such materials possess a great application potential in controlled release systems, where one of the fundamental selection criteria for a suitable material candidate is represented by agreeing the required viscoelasticity and release-kinetic properties. In so far as this concept in general necessitates minimal requirements in the gelation procedure, it may be easily implemented in diverse state-of-the-art approaches in hydrogel preparation. Therefore, we believe that the presented work may become a stepping stone for a brand-new direction in the research and development of hydrogel-based controlled release systems. Furthermore, the original analytical approach designed and applied in this study is proposed as the methodological framework for these follow-up studies providing complex insights into composition–structure–performance relationships in developed hydrogel material.

Supplementary Materials: The following are available online at http://www.mdpi.com/2073-4360/12/11/2561/s1, Figure S1: Results of frequency sweep rheometry tests for various compositions of agarose-based hydrogels presented as frequency dependencies of storage (a) and loss (b) moduli, respectively. Figure S2: Results of frequency sweep rheometry tests for hydrogels with different contents of interpenetrating components—PSS (a,b) and ALG (c,d)—represented by frequency dependencies of storage (a,c) and loss (c,d) moduli. Figure S3: Results of frequency sweep rheometry tests for hydrogels with different contents of interpenetrating components—PSS (a,b) and ALG (c,d)—represented by frequency dependencies of complex moduli (a,c) and phase angle (b,d). Figure S4: Results of strain sweep rheometry tests for various compositions of agarose-based hydrogels presented as frequency dependencies of storage (a), loss (b) and complex (c) moduli, and phase angle (d), respectively. Figure S5: Results of DLS microrheometry tests for hydrogels with different contents of interpenetrating components—PSS (a, b) and ALG (c,d)—represented by frequency dependencies of complex moduli (a,c) and phase angle (b,d). Figure S6: Results of turbidimetry presented as log-log plot of turbidity vs. wavelength (between 700 and 800 nm). Slope of the linear regression was used to calculate the effective mesh size according to Aymard [50].

Author Contributions: Conceptualization, P.S., J.S. and M.K.; methodology, P.S., J.S., M.K. and V.K.; investigation, M.T., M.S., K.A. and K.H.; writing—original draft preparation, P.S., J.S. and M.K.; supervision, P.S.; project administration, P.S.; funding acquisition, P.S. All authors have read and agreed to the published version of the manuscript.

Funding: This research was funded by the Ministry of Education, Youth and Sports of the Czech Republic grant numbers REG LO1211 and COST LD15047 and by Czech Science Foundation grant number GA17-15451S. The APC was funded by Materials Research Centre at Faculty of Chemistry, Brno University of Technology.

Conflicts of Interest: The authors declare no conflict of interest.

References

1. Ahmed, E.M. Hydrogel: Preparation, characterization, and applications: A review. *J. Adv. Res.* **2015**, *6*, 105–121. [CrossRef] [PubMed]
2. Kopeček, J. Hydrogel biomaterials: A smart future? *Biomaterials* **2007**, *28*, 5185–5192. [CrossRef] [PubMed]
3. Wichterle, O.; Lím, D. Hydrophilic Gels for Biological Use. *Nature* **1960**, *185*, 117–118. [CrossRef]
4. Geckil, H.; Xu, F.; Zhang, X.; Moon, S.; Demirci, U. Engineering hydrogels as extracellular matrix mimics. *Nanomedicine* **2010**, *5*, 469–484. [CrossRef] [PubMed]
5. Oh, J.K.; Drumright, R.; Siegwart, D.J.; Matyjaszewski, K. The development of microgels/nanogels for drug delivery applications. *Prog. Polym. Sci.* **2008**, *33*, 448–477. [CrossRef]
6. Vinogradov, S.V.; Bronich, T.K.; Kabanov, A.V. Nanosized cationic hydrogels for drug delivery: Preparation, properties and interactions with cells. *Adv. Drug Deliver. Rev.* **2002**, *54*, 135–147. [CrossRef]
7. Tokarev, I.; Minko, S. Stimuli-responsive hydrogel thin films. *Soft Matter* **2009**, *5*, 511–524. [CrossRef]
8. Ishihara, K.; Ueda, T.; Nakabayashi, N. Preparation of Phospholipid Polylners and Their Properties as Polymer Hydrogel Membranes. *Polym. J.* **1990**, *22*, 355–360. [CrossRef]
9. Klouda, L.; Mikos, A.G. Thermoresponsive hydrogels in biomedical applications. *Eur. J. Pharm. Biopharm.* **2008**, *68*, 34–45. [CrossRef]
10. Klouda, L. Thermoresponsive hydrogels in biomedical applications. *Eur. J. Pharm. Biopharm.* **2015**, *97*, 338–349. [CrossRef]
11. Qiu, Y.; Park, K. Environment-sensitive hydrogels for drug delivery. *Adv. Drug Deliver. Rev.* **2001**, *53*, 321–339. [CrossRef]
12. Gupta, P.; Vermani, K.; Garg, S. Hydrogels: From controlled release to pH-responsive drug delivery. *Drug Discov. Today* **2002**, *7*, 569–579. [CrossRef]
13. Miyata, T.; Asami, N.; Uragami, T. A reversibly antigen-responsive hydrogel. *Nature* **1999**, *399*, 766–769. [CrossRef] [PubMed]
14. Miyata, T.; Uragami, T.; Nakamae, K. Biomolecule-sensitive hydrogels. *Adv. Drug Deliver. Rev.* **2002**, *54*, 79–98. [CrossRef]
15. Spiller, K.L.; Laurencin, S.J.; Charlton, D.; Maher, S.A.; Lowman, A.M. Superporous hydrogels for cartilage repair: Evaluation of the morphological and mechanical properties. *Acta Biomater.* **2008**, *4*, 17–25. [CrossRef] [PubMed]
16. Chen, J.; Park, H.; Park, K. Synthesis of superporous hydrogels: Hydrogels with fast swelling and superabsorbent properties. *J. Biomed. Mater. Res.* **1999**, *44*, 53–62. [CrossRef]
17. Petka, W.A.; Harden, J.L.; McGrath, K.P.; Wirtz, D.; Tirrell, D.A. Reversible Hydrogels from Self-Assembling Artificial Proteins. *Science* **1998**, *281*, 389–392. [CrossRef]
18. Ehrick, J.D.; Deo, S.K.; Browning, T.W.; Bachas, L.G.; Madou, M.J.; Daunert, S. Genetically engineered protein in hydrogels tailors stimuli-responsive characteristics. *Nat. Mater.* **2005**, *4*, 298–302. [CrossRef]
19. Gong, J.P.; Katsuyama, Y.; Kurokawa, T.; Osada, Y. Double-Network Hydrogels with Extremely High Mechanical Strength. *Adv. Mater.* **2003**, *15*, 1155–1158. [CrossRef]
20. Yasuda, K.; Ping Gong, J.; Katsuyama, Y.; Nakayama, A.; Tanabe, Y.; Kondo, E.; Ueno, M.; Osada, Y. Biomechanical properties of high-toughness double network hydrogels. *Biomaterials* **2005**, *26*, 4468–4475. [CrossRef]
21. Lee, K.Y.; Mooney, D.J. Hydrogels for Tissue Engineering. *Chem. Rev.* **2001**, *101*, 1869–1880. [CrossRef] [PubMed]
22. Drury, J.L.; Mooney, D.J. Hydrogels for tissue engineering: Scaffold design variables and applications. *Biomaterials* **2003**, *24*, 4337–4351. [CrossRef]
23. Slaughter, B.V.; Khurshid, S.S.; Fisher, O.Z.; Khademhosseini, A.; Peppas, N.A. Hydrogels in Regenerative Medicine. *Adv. Mater.* **2009**, *21*, 3307–3329. [CrossRef]
24. Annabi, N.; Tamayol, A.; Uquillas, J.A.; Akbari, M.; Bertassoni, L.E.; Cha, C.; Camci-Unal, G.; Dokmeci, M.R.; Peppas, N.A.; Khademhosseini, A. 25th Anniversary Article: Rational Design and Applications of Hydrogels in Regenerative Medicine. *Adv. Mater.* **2014**, *26*, 85–124. [CrossRef] [PubMed]
25. van der Linden, H.J.; Herber, S.; Olthuis, W.; Bergveld, P. Stimulus-sensitive hydrogels and their applications in chemical (micro)analysis. *Analyst* **2003**, *128*, 325–331. [CrossRef]

26. Rubina, A.Y.; Pan'kov, S.V.; Dementieva, E.I.; Pen'kov, D.N.; Butygin, A.V.; Vasiliskov, V.A.; Chudinov, A.V.; Mikheikin, A.L.; Mikhailovich, V.M.; Mirzabekov, A.D. Hydrogel drop microchips with immobilized DNA: Properties and methods for large-scale production. *Anal. Biochem.* **2004**, *325*, 92–106. [CrossRef]
27. Wang, K.L.; Burban, J.H.; Cussler, E.L. Hydrogels as separation agents. In *Responsive Gels: Volume Transitions II.*; Springer: Berlin/Heidelberg, Germany, 1993; pp. 67–79.
28. Ozay, O.; Ekici, S.; Baran, Y.; Kubilay, S.; Aktas, N.; Sahiner, N. Utilization of magnetic hydrogels in the separation of toxic metal ions from aqueous environments. *Desalination* **2010**, *260*, 57–64. [CrossRef]
29. Hoare, T.R.; Kohane, D.S. Hydrogels in drug delivery: Progress and challenges. *Polymer* **2008**, *49*, 1993–2007. [CrossRef]
30. Narayanaswamy, R.; Torchilin, V.P. Hydrogels and Their Applications in Targeted Drug Delivery. *Molecules* **2019**, *24*, 603. [CrossRef] [PubMed]
31. Li, J.; Mooney, D.J. Designing hydrogels for controlled drug delivery. *Nat. Rev. Mater.* **2016**, *1*, 1–17. [CrossRef]
32. Trongsatitkul, T.; Budhlall, B.M. Microgels or microcapsules? Role of morphology on the release kinetics of thermoresponsive PNIPAm-co-PEGMa hydrogels. *Polym. Chem.* **2013**, *4*, 1502–1516. [CrossRef]
33. Perugini, P.; Genta, I.; Conti, B.; Modena, T.; Pavanetto, F. Long-term release of clodronate from biodegradable microspheres. *AAPS PharmSciTech* **2001**, *2*, 6–14. [CrossRef]
34. Lee, B.H.; Lee, Y.M.; Sohn, Y.S.; Song, S.-C. A Thermosensitive Poly(organophosphazene) Gel. *Macromolecules* **2002**, *35*, 3876–3879. [CrossRef]
35. Andrade-Vivero, P.; Fernandez-Gabriel, E.; Alvarez-Lorenzo, C.; Concheiro, A. Improving the Loading and Release of NSAIDs from pHEMA Hydrogels by Copolymerization with Functionalized Monomers. *J. Pharm. Sci.* **2007**, *96*, 802–813. [CrossRef] [PubMed]
36. Sato, T.; Uchida, R.; Tanigawa, H.; Uno, K.; Murakami, A. Application of polymer gels containing side-chain phosphate groups to drug-delivery contact lenses. *J. Appl. Polym. Sci.* **2005**, *98*, 731–735. [CrossRef]
37. Young, S.; Wong, M.; Tabata, Y.; Mikos, A.G. Gelatin as a delivery vehicle for the controlled release of bioactive molecules. *J. Control. Release* **2005**, *109*, 256–274. [CrossRef]
38. Jenkins, A.D.; Kratochvíl, P.; Stepto, R.F.T.; Suter, U.W. Glossary of basic terms in polymer science (IUPAC Recommendations 1996). *Pure Appl. Chem.* **1996**, *68*, 2287–2311. [CrossRef]
39. Zoratto, N.; Matricardi, P. Semi-IPNs and IPN-based hydrogels. In *Polymeric Gels*; Woodhead Publishing: Cambridge, UK, 2018; pp. 91–124.
40. Aminabhavi, T.M.; Nadagouda, M.N.; More, U.A.; Joshi, S.D.; Kulkarni, V.H.; Noolvi, M.N.; Kulkarni, P.V. Controlled release of therapeutics using interpenetrating polymeric networks. *Expert Opin. Drug Deliv.* **2015**, *12*, 669–688. [CrossRef] [PubMed]
41. Rinaudo, M. Main properties and current applications of some polysaccharides as biomaterials. *Polym. Int.* **2008**, *57*, 397–430. [CrossRef]
42. Zarrintaj, P.; Manouchehri, S.; Ahmadi, Z.; Saeb, M.R.; Urbanska, A.M.; Kaplan, D.L.; Mozafari, M. Agarose-based biomaterials for tissue engineering. *Carbohydr. Polym.* **2018**, *187*, 66–84. [CrossRef]
43. Wang, N.; Wu, X.S. Preparation and Characterization of Agarose Hydrogel Nanoparticles for Protein and Peptide Drug Delivery. *Pharm. Dev. Technol.* **1997**, *2*, 135–142. [CrossRef] [PubMed]
44. Liang, S.; Xu, J.; Weng, L.; Dai, H.; Zhang, X.; Zhang, L. Protein diffusion in agarose hydrogel in situ measured by improved refractive index method. *J. Control. Release* **2006**, *115*, 189–196. [CrossRef] [PubMed]
45. Marras-Marquez, T.; Peña, J.; Veiga-Ochoa, M.D. Agarose drug delivery systems upgraded by surfactants inclusion: Critical role of the pore architecture. *Carbohydr. Polym.* **2014**, *103*, 359–368. [CrossRef]
46. Meilander, N.J.; Yu, X.; Ziats, N.P.; Bellamkonda, R.V. Lipid-based microtubular drug delivery vehicles. *J. Control. Release* **2001**, *71*, 141–152. [CrossRef]
47. Narahashi, T.; Yamada, M.; Frazier, D.T. Cationic Forms of Local Anaesthetics block Action Potentials from Inside the Nerve Membrane. *Nature* **1969**, *223*, 748–749. [CrossRef]
48. Gunasekaran, P.; Rajasekaran, G.; Han, E.H.; Chung, Y.-H.; Choi, Y.-J.; Yang, Y.J.; Lee, J.E.; Kim, H.N.; Lee, K.; Kim, J.-S.; et al. Cationic Amphipathic Triazines with Potent Anti-bacterial, Anti-inflammatory and Anti-atopic Dermatitis Properties. *Sci. Rep.* **2019**, *9*, 1292. [CrossRef]
49. Broderick, E.; Lyons, H.; Pembroke, T.; Byrne, H.; Murray, B.; Hall, M. The characterisation of a novel, covalently modified, amphiphilic alginate derivative, which retains gelling and non-toxic properties. *J. Colloid Interface Sci.* **2006**, *298*, 154–161. [CrossRef] [PubMed]

50. Aymard, P.; Martin, D.R.; Plucknett, K.; Foster, T.J.; Clark, A.H.; Norton, I.T. Influence of thermal history on the structural and mechanical properties of agarose gels. *Biopolymers* **2001**, *59*, 131–144. [CrossRef]
51. Lapasin, R.; Pricl, S. *Rheology of Industrial Polysaccharides: Theory and Applications*; Springer: Boston, MA, USA, 1995; ISBN 978-1-4613-5915-9.
52. Pescosolido, L.; Feruglio, L.; Farra, R.; Fiorentino, S.; Colombo, I.; Coviello, T.; Matricardi, P.; Hennink, W.E.; Vermonden, T.; Grassi, M. Mesh size distribution determination of interpenetrating polymer network hydrogels. *Soft Matter* **2012**, *8*, 7708–7715. [CrossRef]
53. Draper, N.R.; Smith, H. *Applied Regression Analysis*; John Wiley & Sons, Inc: New York, NY, USA, 1996.
54. Sedláček, P.; Smilek, J.; Klučáková, M. How the interactions with humic acids affect the mobility of ionic dyes in hydrogels—2. Non-stationary diffusion experiments. *React. Funct. Polym.* **2014**, *75*, 41–50. [CrossRef]
55. Smilek, J.; Sedláček, P.; Kalina, M.; Klučáková, M. On the role of humic acids' carboxyl groups in the binding of charged organic compounds. *Chemosphere* **2015**, *138*, 503–510. [CrossRef] [PubMed]
56. Sedláček, P.; Smilek, J.; Laštůvková, M.; Kalina, M.; Klučáková, M. Hydrogels: Invaluable experimental tool for demonstrating diffusion phenomena in physical chemistry laboratory courses. *J. Mater. Educ.* **2017**, *39*, 59–90.
57. Crank, J. *The Mathematics of Diffusion*; Oxford University Press Inc: New York, NY, USA, 1979.
58. ImageJ Website. Available online: https://imagej.nih.gov/ij/ (accessed on 20 August 2020).
59. Schneider, C.A.; Rasband, W.S.; Eliceiri, K.W. NIH Image to ImageJ: 25 years of image analysis. *Nat. Methods* **2012**, *9*, 671–675. [CrossRef] [PubMed]
60. Normand, V.; Lootens, D.L.; Amici, E.; Plucknett, K.P.; Aymard, P. New Insight into Agarose Gel Mechanical Properties. *Biomacromolecules* **2000**, *1*, 730–738. [CrossRef]
61. Grillet, A.M.; Wyatt, N.B.; Gloe, L.M. Polymer Gel Rheology and Adhesion. In *Rheology*; InTech: Rijeka, Croatia, 2012; pp. 59–80.
62. Weng, L.; Chen, X.; Chen, W. Rheological Characterization of in Situ Crosslinkable Hydrogels Formulated from Oxidized Dextran and *N* -Carboxyethyl Chitosan. *Biomacromolecules* **2007**, *8*, 1109–1115. [CrossRef] [PubMed]
63. Trenkmann, I.; Bok, S.; Korampally, V.R.; Gangopadhyay, S.; Graaf, H.; von Borczyskowski, C. Counting single Rhodamine 6G dye molecules in organosilicate nanoparticles. *Chem. Phys.* **2012**, *406*, 41–46. [CrossRef]
64. Penzkofer, A.; Leupacher, W. Fluorescence behaviour of highly concentrated rhodamine 6G solutions. *J. Lumin.* **1987**, *37*, 61–72. [CrossRef]
65. Doty, P.; Steiner, R.F. Light Scattering and Spectrophotometry of Colloidal Solutions. *J. Chem. Phys.* **1950**, *18*, 1211–1220. [CrossRef]
66. Horne, D.S. Determination of the fractal dimension using turbidimetric techniques. Application to aggregating protein systems. *Faraday Discuss. Chem. Soc.* **1987**, *83*, 259–280. [CrossRef]
67. Camerini-Otero, R.D.; Day, L.A. The wavelength dependence of the turbidity of solutions of macromolecules. *Biopolymers* **1978**, *17*, 2241–2249. [CrossRef]
68. Leone, M.; Sciortino, F.; Migliore, M.; Fornili, S.L.; Vittorelli, M.B.P. Order parameters of gels and gelation kinetics of aqueous agarose systems: Relation to the spinodal decomposition of the sol. *Biopolymers* **1987**, *26*, 743–761. [CrossRef]
69. Aymard, P.; Williams, M.A.K.; Clark, A.H.; Norton, I.T. A Turbidimetric Study of Phase Separating Biopolymer Mixtures during Thermal Ramping. *Langmuir* **2000**, *16*, 7383–7391. [CrossRef]
70. Singh, T.R.R. *Hydrogels*; CRC Press: Boca Raton, FL, USA, 2018; ISBN 9781315152226.
71. Stellwagen, N.C. Effect of the electric field on the apparent mobility of large DNA fragments in agarose gels. *Biopolymers* **1985**, *24*, 2243–2255. [CrossRef]
72. Flory, P.J. *Principles of Polymer Chemistry*; Cornell University Press: Ithaca, New York, NY, USA, 1953.
73. Larson, R.G. *The Structure and Rheology of Complex Fluids*; Oxford University Press Inc.: New York, NY, USA, 1999.
74. Chai, Q.; Jiao, Y.; Yu, X. Hydrogels for Biomedical Applications: Their Characteristics and the Mechanisms behind Them. *Gels* **2017**, *3*, 6. [CrossRef]
75. Calhoun, M.A.; Bentil, S.A.; Elliott, E.; Otero, J.J.; Winter, J.O.; Dupaix, R.B. Beyond linear elastic modulus: Viscoelastic models for brain and brain mimetic hydrogels. *ACS Biomater. Sci. Eng.* **2019**, *5*, 3964–3973. [CrossRef]

76. Smilek, J.; Jarábková, S.; Velcer, T.; Pekař, M. Compositional and Temperature Effects on the Rheological Properties of Polyelectrolyte–Surfactant Hydrogels. *Polymers* **2019**, *11*, 927. [CrossRef]
77. Galway, M.E.; Heckman, J.W., Jr.; Hyde, G.J.; Fowke, L.C. Advances in high-pressure and plunge-freeze fixation. In *Methods in Cell Biology*; Academic Press: Cambridge, MA, USA, 1995; Volume 49, pp. 3–19. [CrossRef]
78. Hrubanova, K.; Nebesarova, J.; Ruzicka, F.; Krzyzanek, V. The innovation of cryo-SEM freeze-fracturing methodology demonstrated on high pressure frozen biofilm. *Micron* **2018**, *110*, 28–35. [CrossRef]
79. Paradossi, G.; Cavalieri, F.; Chiessi, E.; Spagnoli, C.; Cowman, M.K. Poly (vinyl alcohol) as versatile biomaterial for potential biomedical applications. *J. Mater. Sci. Mater.* **2003**, *14*, 687–691. [CrossRef]
80. Holly, F.J.; Refojo, M.F. Wettability of hydrogels I. Poly(2-hydroxyethyl methacrylate). *J. Biomed. Mater. Res.* **1975**, *9*, 315–326. [CrossRef]
81. Zhu, J. Bioactive modification of poly(ethylene glycol) hydrogels for tissue engineering. *Biomaterials* **2010**, *31*, 4639–4656. [CrossRef]
82. Osmałek, T.; Froelich, A.; Tasarek, S. Application of gellan gum in pharmacy and medicine. *Int. J. Pharm.* **2014**, *466*, 328–340. [CrossRef] [PubMed]
83. Park, H.; Park, K.; Shalaby, W.S.W. *Biodegradable Hydrogels for Drug Delivery*; CRC Press: Boca Raton, FL, USA, 2011.
84. Xiong, X.Y.; Tam, K.C.; Gan, L.H. Polymeric Nanostructures for Drug Delivery Applications Based on Pluronic Copolymer Systems. *J. Nanosci. Nanotechno.* **2006**, *6*, 2638–2650. [CrossRef] [PubMed]
85. Amiji, M.; Tailor, R.; Ly, M.-K.; Goreham, J. Gelatin-Poly(Ethylene Oxide) Semi-interpenetrating Polymer Network with pH-Sensitive Swelling and Enzyme-Degradable Properties for Oral Drug Delivery. *Drug Dev. Ind. Pharm.* **1997**, *23*, 575–582. [CrossRef]
86. Elisseeff, J.; McIntosh, W.; Anseth, K.; Riley, S.; Ragan, P.; Langer, R. Photoencapsulation of chondrocytes in poly(ethylene oxide)-based semi-interpenetrating networks. *J. Biomed. Mater. Res.* **2000**, *51*, 164–171. [CrossRef]
87. Sedláček, P.; Smilek, J.; Klučáková, M. How the interactions with humic acids affect the mobility of ionic dyes in hydrogels—Results from diffusion cells. *React. Funct. Polym.* **2013**, *73*, 1500–1509. [CrossRef]
88. Larrañeta, E.; Stewart, S.; Ervine, M.; Al-Kasasbeh, R.; Donnelly, R. Hydrogels for Hydrophobic Drug Delivery. Classification, Synthesis and Applications. *J. Funct. Biomater.* **2018**, *9*, 13. [CrossRef]
89. Venerová, T.; Pekař, M. Rheological properties of gels formed by physical interactions between hyaluronan and cationic surfactants. *Carbohydr. Polym.* **2017**, *170*, 176–181. [CrossRef]
90. Enev, V.; Sedláček, P.; Jarábková, S.; Velcer, T.; Pekař, M. ATR-FTIR spectroscopy and thermogravimetry characterization of water in polyelectrolyte-surfactant hydrogels. *Colloids Surf. A* **2019**, *575*, 1–9. [CrossRef]
91. Moschakis, T. Microrheology and particle tracking in food gels and emulsions. *Curr. Opin. Colloid Interface Sci.* **2013**, *18*, 311–323. [CrossRef]
92. Rathgeber, S.; Beauvisage, H.-J.; Chevreau, H.; Willenbacher, N.; Oelschlaeger, C. Microrheology with Fluorescence Correlation Spectroscopy. *Langmuir* **2009**, *25*, 6368–6376. [CrossRef]
93. García-Aparicio, C.; Quijada-Garrido, I.; Garrido, L. Diffusion of small molecules in a chitosan/water gel determined by proton localized NMR spectroscopy. *J. Colloid Interface Sci.* **2012**, *368*, 14–20. [CrossRef] [PubMed]
94. Severs, N.; Shotton, D. Rapid Freezing of Biological Specimens for Freeze Fracture and Deep Etching. *Cell Biol.* **2006**, *3*, 249–255.
95. Landry, M.R. Thermoporometry by differential scanning calorimetry: Experimental considerations and applications. *Thermochim. Acta* **2005**, *433*, 27–50. [CrossRef]

Plant Methods

METHODOLOGY

Open Access

A simple technique for assessing the cuticular diffusion of humic acid biostimulants

Marcela Smilkova[1], Jiri Smilek[2], Michal Kalina[2], Martina Klucakova[1], Miloslav Pekar[1] and Petr Sedlacek[1*]

Abstract

Background: Experimental determination of the extent and rate of transport of liquid humates supplied to plants is critical in testing physiological effects of such biostimulants which are often supplied as foliar sprays. Therefore, an original experimental method for the qualitative investigation and quantitative description of the penetration of humates through plant cuticles is proposed, tested, and evaluated.

Results: The proposed method involves the isolation of model plant leaf cuticles and the subsequent in vitro evaluation of cuticular humate transport. The employed novel methodology is based on a simple diffusion couple arrangement involving continuous spectrophotometric determination of the amount of penetrated humate in a hydrogel diffusion medium. *Prunus laurocerasus* leaf cuticles were isolated by chemical and enzymatic treatment and the rate of cuticular penetration of a commercial humate (lignohumate) was estimated over time in quantitative and qualitative terms. Different rates of lignohumate transport were determined for abaxial and adaxial leaf cuticles also in relation to the different cuticular extraction methods tested.

Conclusions: The proposed methodology represents a simple and cheap experimental tool for the study on the trans-cuticular penetration of humic-based biostimulants.

Keywords: Diffusion, Hydrogel, *Prunus laurocerasus*, Liquid fertilization, Humic substances, Plant cuticle

Background

Foliar application of fertilizers and biostimulants has become a popular method in the field of agronomy and the plant nutrition since its first use in the early twentieth century. Nowadays, foliar uptake of nutrients widely complements standard root fertilizer treatments [1, 2]. Most aerial plant organs (leaves, stem, etc.) are long-known to be able to take up nutrients from sprays [3, 4]. Transcuticular penetration into leaf tissues and sorption on the leaf surface plays a key role in the foliar application of nutrients [5–7], surfactants [8, 9] and different types of pesticides [10–15].

Bidirectional transport of diverse substances in and out of plants is controlled primarily by the plant cuticle [16], a membrane which covers the aerial plant parts and forms the natural interface between plant organs and a surrounding environment [17]. From a chemical point of view, it can be considered as a heterogeneous composite material which is formed by lipophilic components such as waxes, water insoluble polymers cutin and/or cutan and phenolic compounds like flavonoids, mixed together with hydrophilic polar compounds such as polysaccharides [18].

The cuticle plays its biological role principally as a barrier to control the movement of gases, water and solutes and to impart pathogen resistance [17, 19–21]. Furthermore, it protects a plant against abiotic factors such as rain, frost and ultraviolet light [21, 22], and also against adverse biotic impacts of insects, pests, mycosis, etc. [20, 23]. Naturally, as the correct functioning

*Correspondence: sedlacek-p@fch.vut.cz
[1] Institute of Physical and Applied Chemistry, Brno University of Technology, Faculty of Chemistry, Purkynova 464/118, 612 00 Brno, Czech Republic
Full list of author information is available at the end of the article

of plant cuticles is crucial for the well-balanced uptake of nutrients, minerals, adjuvants, or for plant growth preparation, cuticle-penetration experiments as well as laboratory studies of the structural physico-chemical properties of cuticles are an essential part of plant-nutrition research.

For more than 50 years, scientists have continuously been focusing their experiments on the penetration of active compounds through plant cuticles, or on their adsorption on the cuticle surface [3, 24]. For the purpose of the experimental determination of the extent and rate of foliar absorption of a nutrient, several techniques directly involving intact leaves were tested, e.g. dipping, brushing, sticking, spraying, or the droplet method [3]. However, attention has gradually been paid also to experiments performed with cuticles in an isolated form. The first successful attempts at cuticle isolation were made by Orgell, who developed a method based on the treatment of leaves by pectinase [25]. A chemical alternative to this enzymatic method is isolating cuticles with zinc chloride as introduced by Holloway and Baker [26] and further utilized by Solel and Edgington [10, 27, 28]. Various experimental settings have been used for cuticular permeability trials, such as a sole transpiration chamber [29], a side-by-side transport chamber, in which the cuticle is located between two compartments filled with donor and receptor solution [24], or a tube-in-tube setup, where the cuticle is affixed on the opening of small tube filled with deionized water and submerged in the larger tube with a donor solution [30].

Either in experiments performed with intact plant organs or with those utilizing isolated plant cuticles, another crucial step in the development of a particular methodology for studying foliar absorption is the use of an analytical method for the quantification of the cuticle-permeating compound. Foliar uptake of inorganic compounds has been often studied by means of radioactive isotope methods, where different radioactive isotopes of elements are used e.g. ^{14}C [30, 31], ^{32}P [32–35], ^{42}K or ^{45}Ca [36], or ^{86}Rb, ^{45}Ca, ^{36}Cl and ^{35}S [37]. Radionuclide assays have also been utilized successfully in foliar absorption studies of organic compounds such as urea [30] and atrazine [11]. Among other methods for studying the foliar uptake of organic molecules, HPLC was used to determine the quantity of the organic dye Congo Red and fungicides on the leaf surface [38]. Another experimental approach is based on tracking the penetrating compounds indirectly by observing their effects. This approach was used, for example, by Solel and Edgington [10] or, more recently, by Zelena and Veverka [13], who studied the rate of the transcuticular movement of fungicides by measuring the propagation of inhibitory zones in agar gel fed with a fungus sensitive to the tested fungicide. The fungicide was always applied on top of the cuticle, placed in the center of the agar-filled Petri dish.

Humic substances are complex organic mixtures that fulfil a range of important functions in ecosystems and that are essential for their proper functioning. They represent an essential fraction of the natural organic matter of soils, peats, and young coals. In a dissolved form, they can also be found in aquatic systems such as rivers and lakes. A growing understanding of the positive effects of the presence of humic substances in their natural habitats has motivated the preparation of commercial products based on isolated natural or artificially synthesized humic substances. Positive impacts of the utilization of humic-based soil amendments on the chemical [39, 40], physical [41, 42], and microbial [43] fitness of soils have been thoroughly documented. Apart from the application of humic-based materials into soil, the foliar application of soluble humates has gradually become a popular way of application as well. This was initiated by numerous reports on the biostimulant effects of humates, namely on the effect on plant growth [44, 45] and nutrient uptake [46], hormone-like [47, 48] and enzyme-promoting effects [49, 50], as well as some effects enhancing photosynthesis and seed-germination [51, 52]. In particular, in greenhouse experiments using cuttings and young olive plants, Fernandez-Escobar found foliar-applied humic substances extracted from leonardite to have an effect on olive growth [53]; the tested leonardite extracts stimulated shoot growth and promoted the accumulation of elements in leaves. Maibodi et al. suggested that foliar application of humic substances might be of benefit with respect to enhancing nutrient uptake, root development, and drought resistance in ryegrass [54]. In addition, Bettoni [55] showed that a combination of foliar and immersion methods represented the most effective way of applying humic substances originating from leonardite, as far as the tested onion bulb yield and quality was concerned.

However, there is raising debate concerning the generally accepted beneficial effects of commercial humates in agriculture. Olk et al. [56] and Rose et al. [57] reviewed information on the benefits of using humic preparations in agriculture and stressed still ambiguous results. Similarly, Lyons and Genc [58] has pointed out that there is a surprising lack of evidence regarding the effectiveness of the on-farm application of humates, the findings concerning their beneficial effects being inconsistent. Among other recommendations, these authors call for a comprehensive physico-chemical characterization of humates and for a careful assessment of the mechanism of their foliar action. Thereby, the experimental determination of the rate of absorption and transport of humate solutions applied to plants also as foliar sprays

is critical as preliminary step for assessing their biological effects. Recently, some attempts have been made in describing the root pathway of the humate absorption. For instance, Kulikova studied the uptake of leonardite humic substances by plant root and its transport and spatial distribution among the plant tissues using microautoradiography [59]. Nevertheless, as yet, no experimental procedure has been proposed for a systematic assay of the transcuticular uptake of humates. The aim of this paper is hence to introduce an original in vitro technique as a simple experimental option for this task. The proposed method enables the investigation and quantitative description of the penetration of humates through the plant cuticle via spectrophotometric monitoring of the diffusion of humates through an isolated plant cuticle fixed between a donor and an acceptor agarose hydrogels forming the common diffusion couple arrangement. The basic design of the method follows on from our previous work [60, 61]. The usability of the technique was tested on artificial lignohumate as a model commercial product and on cuticles obtained by enzymatic and chemical means of isolation.

Materials and methods

Isolation and characterization of cuticles

Leaf cuticles were isolated by two different methods (chemical and enzymatic) as described previously [10, 25]. In both cases, plant cuticles were isolated from *Prunus laurocerasus* (see "Results" and "Discussion"). Firstly, undamaged, young, fully-expanded leaves were immersed in distilled water. For the every plant leaf, the leaf blade (the lamina) was carefully cut off by scalpel from the other leaf parts (veins, petiole). In the case of enzymatic isolation, the lamina was then immersed into the isolation solution consisting of citric buffer (0.1 M and pH 3.5), supplemented with 2.5 wt% of pectinase from *Aspergillus niger* (> 1 units/mg, Sigma-Aldrich), 2.5 wt% of cellulase from *Trichoderma logibrachiatum* (> 1 units/mg, Sigma-Aldrich) and 0.25 wt% of sodium azide (p.a., Sigma-Aldrich). After 6 weeks, the leaf tissue, including isolated cuticles, was placed in distilled water and degraded mesophyll was gently removed by brushing. The chemical isolation procedure differed only in the composition of the isolation solution, i.e. 60 wt% zinc chloride (≥ 97%, Sigma-Aldrich) dissolved in concentrated hydrochloric acid (35%, Penta), and the shorter time duration of the chemical treatment (3 days).

Plant cuticles isolated by both the above mentioned methods were characterized by optical microscopy (Olympus IX71, objective Olympus PLN, magnification 20×, numerical aperture 0.40), by which differences in abaxial (stomatous) and adaxial (astomatous) cuticles were compared and the average radius of stomata was determined (for the optical microscope images of the cuticles, see Fig. 1). Optical microscopy was also used in order to eliminate physically damaged cuticles. The morphology of isolated plant cuticles, especially average cuticle thickness and roughness, was determined by mechanical profilometer (DEKTA kXT, Bruker). VISION 64 was used as the control software and the pressure value of the stylus was set at 3 mg.

Preparation of hydrogels

All hydrogels used in this work were prepared via the thermoreversible gelation of agarose (< 10% moisture content, Sigma-Aldrich). These hydrogels acted as supporting matrix in which diffusion experiments on the active compound were performed. Lignohumate A was kindly provided by the Amagro (Prague, Czech Republic) and used as model active compound. It represents a commercial mixture of potassium humates and fulvates prepared by hydrolytic-oxidative conversion of technical lignosulfonates under strictly controlled conditions [62, 63]. The method of preparation of hydrogels is described in detail in our previous studies [60, 64]. Donor hydrogels containing 1 wt% agarose with the addition of 1 wt% potassium lignohumate (Lignohumate A) dissolved in distillated water and acceptor hydrogels consisting of only 1 wt% agarose were prepared in PMMA cuvettes (dimensions $10 \times 10 \times 45$ mm). The thermoreversible gelation of agarose took place at ambient temperature and 100% relative humidity for at least 45 min. After the gelation process was completed, excess gel mass above the cuvette edge was cut off by scalpel for all prepared hydrogels. This provided a flat gel surface that allows even contact with the cuticle and with the second hydrogel in the diffusion couple arrangement (see below). This arrangement was obtained in the way that every single isolated plant cuticle was carefully placed between the donor and acceptor hydrogels and the contact area of both cuvettes was isolated from surroundings by parafilm to prevent unfavorable drying.

Diffusion experiments

Both abaxial and adaxial cuticles isolated by the two different isolation methods (chemical and enzymatic) were subjected to diffusion experiments. As can be seen in Fig. 2, the diffusion couple was formed by two agarose hydrogels—a hydrogel with an homogenously dispersed humate inside (i.e. the donor hydrogel) and a hydrogel with no initial content of the humate (i.e. the acceptor hydrogel)—and the isolated cuticle separating the two gels. As the humate can move freely inside the agarose matrix, it penetrates the cuticle and flows across the concentration gradient from the donor to the acceptor gel. These diffusion experiments were performed with 10 repetitions for abaxial and adaxial cuticles, respectively.

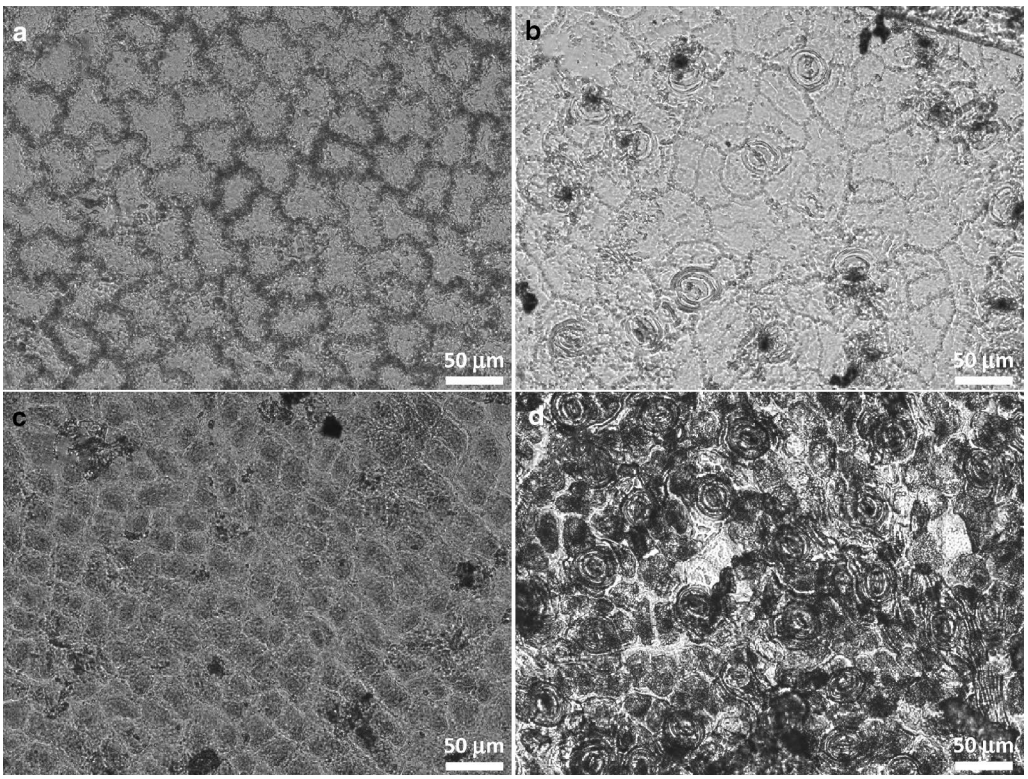

Fig. 1 Optical micrographs of the isolated cuticles. Adaxial (**a**, **c**) and abaxial (**b**, **d**) cuticles isolated by chemical (**a**, **b**) and enzymatical (**c**, **d**) methods, respectively

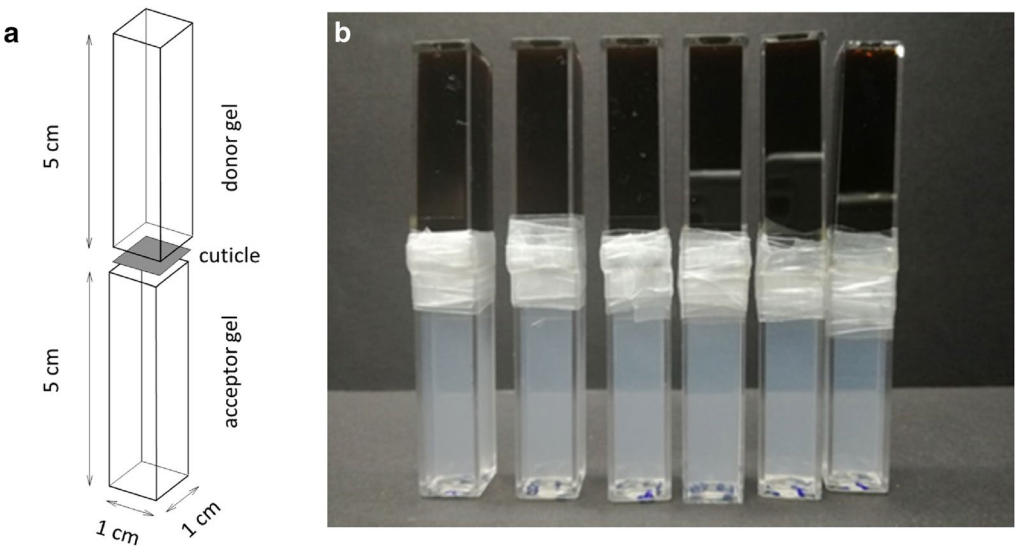

Fig. 2 Schematic drawing of the diffusion couple arrangement (individual parts are shifted for clarity) (**a**). Picture of the diffusion couple at the beginning of the experiment (**b**)

During the diffusion experiments, all the diffusion couples were placed in a closed container above water level (to maintain constant humidity of the surroundings). Experimental conditions—in particular, relative humidity (100%) and temperature (25 °C)—were held constant during the whole experimental period.

The transport of lignohumate through the plant cuticle into the acceptor hydrogel was measured by a UV–VIS spectrophotometry (Varian Cary 50). At selected time intervals, the cuvettes were taken out and UV–VIS spectra of lignohumate in acceptor hydrogels were collected at distances from the hydrogel-cuticle interface ranging from 3 to 40 mm (with 1 or 2 mm increment in distance depending on the actual rate of the color change). The measurement of UV–VIS absorbance at different distances from the interface was performed by means of a special in-house made accessory providing controlled fine vertical movement of the cuvette in the spectrophotometer (see [65] for more detail and picture of the used cuvette holder).

Results

Isolation and characterization of cuticles

Two methods of cuticle isolation were tested. The main advantage of the enzymatic method is the use of less harmful isolation agents. The procedure is, therefore, more user-friendly and suitable for routine laboratory use. Furthermore, the presence of any structural artifacts arising from chemical damage to the cuticle is less likely than in the case of more drastic chemical treatment in hydrochloric acid. On the other hand, the enzymatic method is significantly more time-consuming in comparison with chemical isolation. In our study, however, both techniques resulted in the isolation of cuticles which were strong and easy to manipulate. Optical microscopy was used in order to exclude mechanically damaged cuticles, to distinguish between abaxial and adaxial cuticles, and to sort them for use in subsequent diffusion experiments.

Furthermore, microscopical observation of the cuticles also revealed some interesting differences in the efficiency of the two isolation methods. Apparently, chemical treatment of the leaves led to the more efficient removal of cell debris as compared to the enzymatic procedure (see the black spots on the micrographs shown in Fig. 1). This finding corresponds well with general differences in cuticle thickness for the two isolation methods as revealed by profilometry, i.e., it was found that the thickness was always greater for enzymatically isolated cuticles (see Table 1). Anyway, both types of cuticles (i.e. chemically and enzymatically isolated ones) were included in the next step of the testing of the proposed methodology, i.e. in the diffusion couple experiments with agarose hydrogels.

Diffusion of lignohumate through the cuticles

The main experimental core of the proposed diffusion methodology is based on our previous studies [60, 61, 65, 66]. Generally, as far as the experimental study of molecular diffusion is concerned, hydrogels represent a highly beneficial material form. In the gel phase, the diffusion flow of a solute is not disturbed by thermal or mechanical convection such as in liquid solution. Furthermore, a hydrogel sample of precisely defined shape and dimensions can be prepared, which enables correct description of the diffusion flow by quantitative parameters such as diffusion coefficients. In the current experiments, a simple diffusion couple arrangement was used [24, 67].

Table 1 Basic morphological characteristics of the isolated cuticles

	Avg. cuticle thickness (μm)	Avg. dimensions of stomata (μm)
Chemically isolated		
Abaxial	4.4 ± 1.2	14 × 7
Adaxial	5.5 ± 0.3	–
Enzymatically isolated		
Abaxial	6.7 ± 2.0	12 × 5
Adaxial	9.2 ± 0.9	–

In order to evaluate this technique, the diffusion of lignohumate—a model artificial humate—was studied using the above-described experimental arrangement. The composition, structure, and physico-chemical properties of lignohumate are discussed in detail elsewhere [63, 68], as well as its biological effects [69, 70]. For our purposes, the main practical benefits of using lignohumate as a model humic biostimulant are its very high water solubility, low molecular size, and reproducible means of preparation, the latter resulting in a stable and standardized structure with standardized properties.

In Fig. 3, the movement of the dark-brown-colored lignohumate through the cuticle and its subsequent diffusion into the optically transparent agarose gel can be observed visually. It is evident how the local concentration of lignohumate and its depth of penetration increases with time and that the adaxial and abaxial cuticles show large differences in their barrier properties. As expected, the rate of diffusion is higher in the case of abaxial cuticles. The explanation is straightforward; isolation of stomateous cuticles results in membranes with freely permeably holes of several microns in size (guard cells which protect stomata against penetration are lost during the isolation). The penetration of lignohumate through these membranes is therefore controlled by the size and density of the holes and by the rate of free diffusion of lignohumate in solution rather than by the barrier properties of the neighbouring lipophilic cuticle area.

In addition, visual evaluation of the concentration of lignohumate in acceptor gels indicates a higher diffusion rate in the case of chemically isolated abaxial cuticles as compared to enzymatically isolated ones. For the adaxial cuticles, the differences were less pronounced. This can

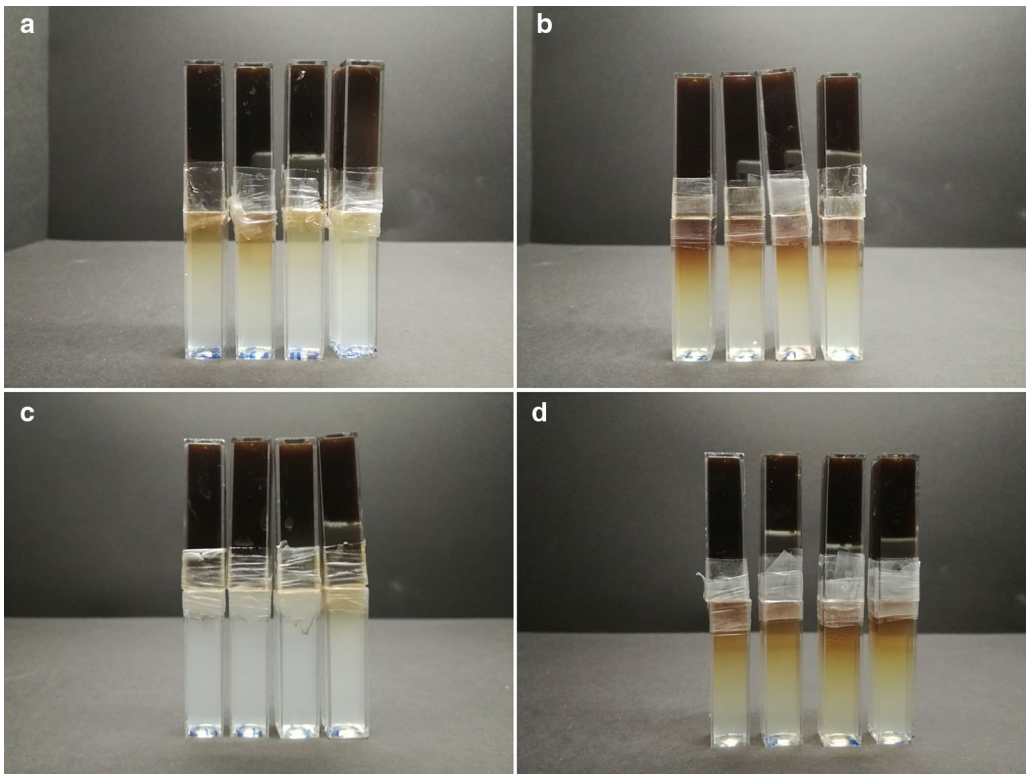

Fig. 3 Diffusion couples after 7 days of experiment. Comparison of diffusion progress for adaxial (**a**, **c**) and abaxial (**b**, **d**) cuticles and for chemical (**a**, **b**) and enzymatical (**c**, **d**) methods of cuticle isolation

be explained by the already mentioned outcomes of the structural analysis of the cuticles. Enzymatically isolated cuticles are thicker and mainly exhibit higher levels of contamination by debris from the leaf. It is likely that in the case of enzymatically isolated cuticles stomata are partially blocked by leaf debris and, consequently, contribute less effectively to the transport of lignohumate.

Quantitative description of the transcuticular transfer of lignohumate

Figure 4 shows example of the set of UV–VIS spectra collected at various positions in acceptor hydrogel that illustrates uneven distribution of lignohumate in the gel. It should be noted that each recorded spectrum (shown as the apparent absorbance vs. wavelength) is actually formed by the combination of two separate contributions—the turbidity of the hydrogel caused by light scattering on the solid agarose matrix and light absorption by the dissolved humate in the aqueous phase of the gel. While the former contribution was homogenous and constant for all the measured gels (i.e. it changed neither with time nor with location in the gel), the latter depended on the actual concentration of the humate at a particular time and at a particular point in the gel. In order to calculate the concentration of lignohumate from the respective UV–VIS spectrum, we also measured the spectra of reference samples of agarose gels in which the exact concentration of homogenously distributed lignohumate was achieved by dispersion of a known amount of lignohumate in the agarose solution before its gelation. It is also evident from Fig. 4 that lignohumate provides a

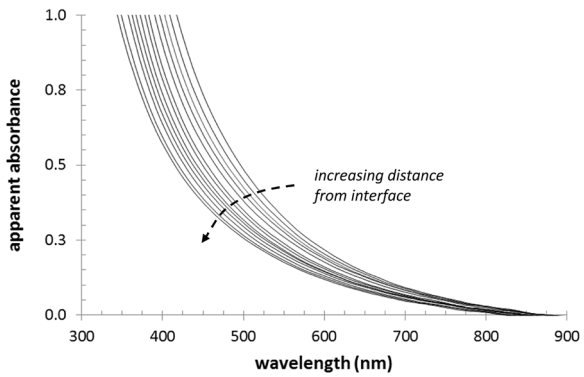

Fig. 4 UV–VIS spectra measured at different positions in the acceptor gel (adaxial chemically isolated cuticle, after 96 h). Spectra were taken in 2 mm increments of distance from the cuticle

continuous absorption spectrum covering a wide range of wavelengths instead of any separate absorption peak. This is a spectroscopic feature typical of humic substances and is the result of their complex structural nature. Therefore, we used a multiple calibration approach in which the concentration of the lignohumate was determined as an average of the values calculated for three different wavelengths (600, 700 and 800 nm). In this way, the concentration profiles of lignohumate in the particular acceptor gels were determined (see Fig. 5).

As can be seen from Fig. 5, the concentration profiles confirmed all above mentioned visual observations. The concentration of lignohumate at a given distance in the acceptor gel was significantly higher when the lignohumate penetrated through an abaxial cuticle. While enzymatically isolated abaxial cuticles had lower penetration rates than chemically isolated ones, no such significant difference was found for adaxial cuticles. The concentration profiles were also subjected to further mathematical processing in order to calculate the total amounts of lignohumate accumulated in the acceptor gels. For this purpose, we fitted the experimentally derived concentration profiles using the following relation

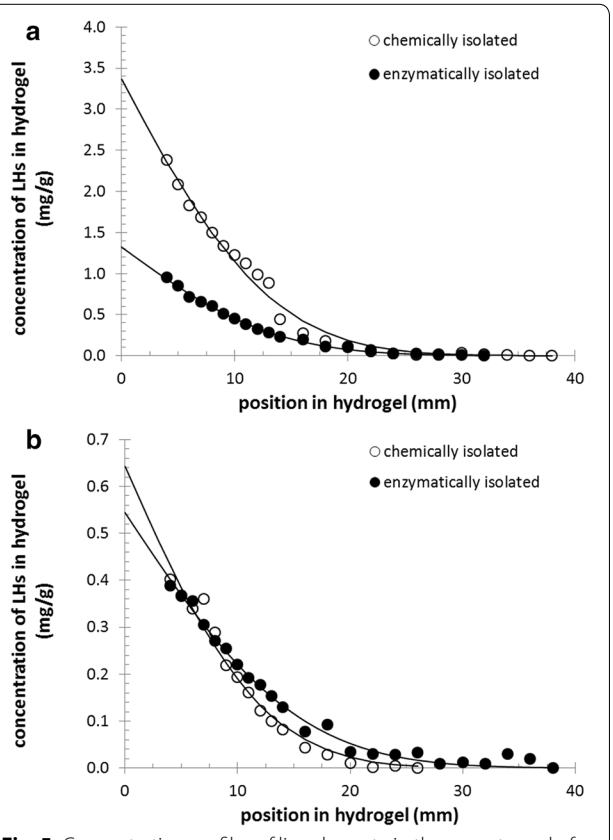

Fig. 5 Concentration profiles of lignohumate in the acceptor gel of the diffusion couple **a** after 96 h of diffusion through abaxial, and **b** after 168 h of diffusion through adaxial cuticles

$$c = \mathrm{A} \cdot \mathrm{erfc}\left(\frac{x}{\mathrm{B}}\right) \tag{1}$$

where c is the concentration of lignohumate in mg_{LH}/g_{gel} at distance x from the gel-cuticle interface, and A and B are the fitting parameters. The complementary error function erfc is a non-elementary function of sigmoid shape that generally occurs in non-stationary diffusion equations [71]. The fitting of experimental data was performed by non-linear least square regression using the Solver tool in Excel (Microsoft). With the known fitting parameters A and B at given time t, the total diffusion flux of lignohumate across unit area n (in g_{LH}/m^2) can easily be determined from the integration of Eq. (1) in the range $x = 0$ to $x = \infty$, which leads to the relation

$$n(t) = \rho_{\mathrm{gel}} \cdot \frac{\mathrm{A} \cdot \mathrm{B}}{\sqrt{\pi}} \tag{2}$$

where the density of the gel (ρ_{gel}) was substituted by the density of pure water for simplicity because of the very low dry matter content of the gels (approximately 1 wt%).

For the non-stationary Fickian diffusion of a solute in a composite medium, the total diffusion flux n increases linearly with the square root of time. As can be seen in Fig. 6, the linearity of this dependency was confirmed for the diffusion of lignohumate through all forms of the tested cuticles (for the comparison, the results of lignohumate diffusion in absence of any cuticle is shown in Fig. 6a as well). In the case of abaxial cuticles, the linear regression of the function $n = f\left(\sqrt{t}\right)$ crosses the origin of coordinates. In other words, lignohumate penetrates abaxial cuticles instantaneously. This confirms that the stomata on the abaxial side of the leaf, after the removal of the guard cells during the isolation process, represent freely penetrable parts of the cuticle. In contrast, the x-axis intercept of the function $n = f\left(\sqrt{t}\right)$ for adaxial cuticles is shifted to significantly higher times. From the intercept, the time needed for lignohumate to penetrate the cuticle (usually called the lag time) was calculated. For both types of adaxial cuticle, quite high lag times were determined. This confirms that in the case of adaxial cuticles molecular transport takes place over a much more tortuous pathway. It is also further evidence that neither of the isolation procedures led to significant mechanical damage to the cuticles in the form of cracks or ruptures.

It was found that while lignohumate needed about 60 h to penetrate enzymatically isolated adaxial cuticles, this lag time increased to about 80 h in the case of chemically isolated ones. Interestingly, after the penetration of the cuticle was complete, the trend was reversed—the amount of lignohumate transported into the acceptor gel increased more rapidly in the case of chemically isolated

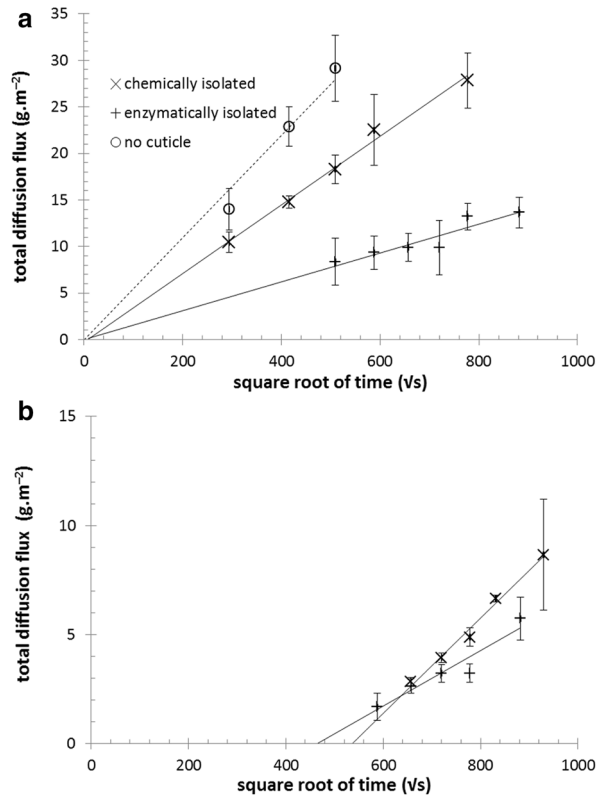

Fig. 6 Confirmation of the Fickian type of diffusion process. Dependence of total diffusion flux on the square root of time for abaxial (**a**) and adaxial (**b**) cuticles

cuticles compared to enzymatically isolated ones. It is not possible to propose a reasonable explanation for this phenomenon just from the basic structural analysis of cuticles performed in this work, a comprehensive chemical assay of the isolated cuticles would be necessary for a detail discussion of these results (see "Discussion" section).

Discussion

The urgent need for an assembly of methods for a systematic study of foliar action of humates was claimed recently [58]. To contribute to this complex task, we hereby propose a simple experimental method for a quantitative description of permeability of plant cuticles for liquid humates. The main aim of the present work was to devise and to verify the usability of the proposed methodology.

We are well aware that the proposed experimental approach suffers several general limitations. First of all, the method is based on isolated plant cuticles. Taking into account that isolation of large-sized cuticular membranes is only successful with few species and that the resulting isolates may differ significantly in their structure and chemical composition [72], even the choice of suitable plant becomes a non-trivial issue. In the current work, we proposed and tested *Prunus laurocerasus* as a source plant. The selected plant may not have any direct agricultural relevance as far as the foliar application of humates is concerned. Rather, its choice was based on specific experimental demands with respect to the universality and reproducibility of the developed methodology. The main requirements were as follows: there had to be adequate availability of the plant (both seasonal and regional); the method of cuticle separation had to be simple and reproducible; and the isolated cuticles had to exhibit suitable mechanical properties. From this viewpoint, *Prunus Laurocerasus* was chosen as a suitable candidate. Nevertheless, a proposal of an alternative plant with a specific relevance in current agricultural use of humic-based foliar formulations is highly welcome.

Another issue, which must be considered, is represented by possible artifacts brought by the process of cuticle isolation. Results of optical microscopy and profilometry confirmed higher efficiency of chemical removal of cell debris as compared to the enzymatic treatment. It can be expected that the presence of residual cell debris on the cuticle surface will negatively influence the accuracy of any experiments mapping barrier properties. From this point of view, the results of the structural characterization of the obtained cuticles support the choice of chemical method of isolation. On the other hand, it is likely that more adverse conditions employed during the chemical isolation treatment will result in more severe alteration of chemical composition of the isolated cuticles. It was suggested by several researchers [4, 73], that the isolation can induce changes in chemical structure of the cuticular membrane which may lead to the results of permeability studies different from those performed with intact leaves. Also our results (different permeability of chemically and enzymatically isolated) are consistent with this suggestion. As far as the importance of polysaccharides in the chemical structure of cuticle has been recently highlighted [74–76], it is likely that the observed differences in the barrier properties of the two types of cuticular isolates may be caused by hydrolysis of the cuticular polysaccharides during the acid treatment. Furthermore, potential influence of the isolation methods on the wax compositions of cuticles cannot be discarded. Therefore, a comprehensive chemical assay of the isolated cuticles is still needed before a definite choice of the most appropriate isolation procedure. Alternatively, a compromise between the two methods could be achieved by supplying the more user-friendly enzymatic method of isolation with a subsequent step of cuticle purification (e.g. treatment with chloroform or another organic solvent [19, 77].

Moreover, it was clearly demonstrated that the relevant information on the in situ barrier performance of the

cuticle is given only when the astomatous cuticular membranes are used. In the case of stomatous membranes, no information is obtained about the stomatal penetration pathway, because the guard cells, which control opening and closing of the stomata in the intact plant, are lost during the isolation process. As far as several authors have stressed the general importance of this entry route [78, 79], stomatal absorption of humic substances remains to be an important issue for the future experimental concern. Nevertheless, since the liquid foliar formulations are usually primarily supplied to astomatous adaxial sides of leaves, we consider the model of transcuticular diffusion using this type of isolated membrane reasonable.

It is worth highlighting that the experimental arrangement of the diffusion experiment (diffusion couple with almost constant concentration of the solute in the donor compartment) has no ambition to simulate the real conditions during the foliar feeding process, where the solute concentration is changing dramatically in time by the evaporation, washing out by rain etc. Its application is aimed to answer the specific research questions concerning penetration of humic-based substances into leaves, such as the characterization and comparison of permeability of cuticles of different species to the single tested humate or the barrier properties of a specific cuticle against humic-based solutes of different size or solubility. It provides information on an upper limit of the rate of diffusional transport through cuticle. As was illustrated on the presented data, the barrier properties can be easily quantified. In this work, we used just the temporal development of the total diffusion flux for the quantification purposes. Nevertheless, if some additional experimental parameters were provided (e.g. the equilibrium amount of solute absorbed by the receptor compartment), it would be possible to calculate also further quantitative transport parameters, such as permeances or diffusion coefficients. The mathematical apparatus for these calculations are well described [71, 80]. On the basis of these parameters, barrier performance of cuticles against humic substances and other solutes (nutrients etc.) can be directly compared. Moreover, this applies also to comparison of the barrier properties of different types of membranes; permeability of a specific humate through a cuticle can hence be compared to the values obtained for different synthetic membranes etc.

Conclusions

The results of the performed diffusion experiments revealed usability of described methodology for the study on the transcuticular transport of humic-based biostimulants. The proposed methodology represents a simple and cheap experimental tool. Nevertheless, the penetration experiments provide only one part of the overall perspective on all processes which take place in a collective manner when the humate penetrates the cuticle from the liquid product into the leaf. One crucial separate process which deserves more detailed description is the adsorption of the humate on the cuticle surface. The assessment of such parameters as the total adsorption capacity and sorption isotherm, or an explanation of the sorption mechanism and kinetics would lead to a better understanding the specific effects and modes of operation of humate-based biostimulants after their application on plants.

Abbreviations

PMMA: polymethylmethacrylate; UV–VIS: ultraviolet and visible spectroscopy.

Acknowledgements

Not applicable.

Authors' contributions

MS performed the major part of experimental work and contributed to preparation of manuscript. JS contributed to the experimental part (diffusion experiments), evaluation of experimental results and preparation of manuscript. MK contributed to the experimental part (characterization of cuticles), evaluation of experimental results and preparation of manuscript. MK supervised the experiments and contributed to discussion of the results of diffusion experiments. PS was responsible for design of experiments, evaluation and discussion of the results and coordination of the manuscript preparation. MP participated in writing the manuscript and its final revision. All authors read and approved the final manuscript.

Funding

This work was supported by the Materials Research Centre at FCH BUT—Sustainability and Development, REG LO1211, with financial support from the National Program for Sustainability I (Ministry of Education, Youth and Sports) and by project COST LD15047.

Availability of data and materials

The datasets used and/or analysed during the current study are available from the corresponding author on reasonable request.

Ethics approval and consent to participate

Not applicable.

Consent for publication

All authors have consented for publication.

Competing interests

The authors declare that they have no competing interests.

Author details

[1] Institute of Physical and Applied Chemistry, Brno University of Technology, Faculty of Chemistry, Purkynova 464/118, 612 00 Brno, Czech Republic. [2] Materials Research Centre, Brno University of Technology, Faculty of Chemistry, Purkynova 464/118, 612 00 Brno, Czech Republic.

Received: 2 April 2019 Accepted: 23 July 2019
Published online: 31 July 2019

References

1. Neshev N, Manolov I. Content and uptake of nutrients with plant biomass of potatoes depending on potassium fertilization. Agric Agric Sci Procedia. 2015. https://doi.org/10.1016/j.aaspro.2015.08.039.
2. Peigne J, Vian JF, Payet V, Saby NPA. Soil fertility after 10 years of conservation tillage in organic farming. Soil Tillage Res. 2018. https://doi.org/10.1016/j.still.2017.09.008.

3. Okuda A, Kawasaki T, Yamada Y. Foliar absorption of nutrients. Soil Sci Plant Nutr. 1960. https://doi.org/10.1080/00380768.1960.10430928.
4. Fernandez V, Eichert T. Uptake of hydrophilic solutes through plant leaves: current state of knowledge and perspectives of foliar fertilization. Crit Rev Plant Sci. 2009. https://doi.org/10.1080/07352680902743069.
5. Fageria NK, Barbosa Filho MP, Moreira A, Guimaraes CM. Foliar fertilization of crop plants. J Plant Nutr. 2009. https://doi.org/10.1080/01904160902872826.
6. Mandic V, Simic A, Krnjaja Z, Bijelic Z, Tomic A, Stanojkovic D, Ruzic Music D. Effect of foliar fertilization on soybean grain yield. Biotechnol Anim Husb. 2015. https://doi.org/10.2298/BAH1501133M.
7. Li M, Wang S, Tian X, Li S, Chen Y, Jia Z, Liu K, Zhai A. Zinc and iron concentrations in grain milling fractions through combined foliar applications of Zn and macronutrients. Field Crop Res. 2016. https://doi.org/10.1016/j.fcr.2015.12.018.
8. Chamel A, Gambonnet B. Sorption and diffusion of an ethoxylated stearic alcohol and an ethoxylated stearic amine into and through isolated plant cuticles. Chemosphere. 1997. https://doi.org/10.1016/S0045-6535(97)00033-7.
9. Liu H, Shao B, Long X, Yao Y, Meng Q. Foliar penetration enhanced by biosurfactant rhamnolipid. Colloid Surf B. 2016. https://doi.org/10.1016/j.colsurfb.2016.05.058.
10. Solel Z, Edgington LV. Transcuticular movement of fungicides. Phytophatology. 1972. https://doi.org/10.1094/Phyto-63-505.
11. Chamel A, Vitton N. Sorption and diffusion of C14-atrazine through isolated plant cuticles. Chemosphere. 1996. https://doi.org/10.1016/0045-6535(96)00241-X.
12. Wang CJ, Liu ZQ. Foliar uptake of pesticides—present status and future challenge. Pestic Biochem Phys. 2007. https://doi.org/10.1016/j.pestbp.2006.04.004.
13. Zelena V, Veverka K. Effect of surfactants and liquid fertilizers on transcuticular penetration of fungicides. Plant Prot Sci. 2007. https://doi.org/10.17221/2236-PPS.
14. Khayet M, Fernandez V. Estimation of the solubility parameters of model plant surfaces and agrochemicals: a valuable tool for understanding plant surface interactions. Theor Biol Med Model. 2012. https://doi.org/10.1186/1742-4682-9-45.
15. Khorram MS, Zhang Q, Lin D, Zheng Y, Fang H, Yu Y. Biochar: a review of its impact on pesticide behavior in soil environments and its potential applications. J Environ Sci. 2016. https://doi.org/10.1016/j.jes.2015.12.027.
16. Martin JT, Juniper BE. The cuticles of plants. New York: St. Martin's Press; 1970.
17. Riederer M, Schreiber L. Protecting against water loss: analysis of the barrier properties of plant cuticles. J Exp Bot. 2001. https://doi.org/10.1093/jexbot/52.363.2023.
18. Barel D. Foliar application of phosphorus compounds. Doctoral thesis, Iowa State University, USA; 1975. p. 1–345.
19. Villena JF, Dominguez E, Heredia A. Monitoring biopolymers present in plant cuticles by FT-IR. J Plant Physiol. 1999. https://doi.org/10.1016/S0176-1617(00)80083-8.
20. Pollard M, Beisson F, Li Y, Ohlrogge JB. Building lipid barriers: biosynthesis of cutin and suberin. Trends Plant Sci. 2008. https://doi.org/10.1016/j.tplants.2008.03.003.
21. Yeats TH, Rose JK. The formation and function of plant cuticles. Plant Physiol. 2013. https://doi.org/10.1104/pp.113.222737.
22. Riederer M, Müller C. Biology of the plant cuticle. Annual plant reviews. Oxford: Blackwell; 2006. https://doi.org/10.1002/9780470988718.
23. Gutschick VP. Biotic and abiotic consequences of differences in leaf structure. New Phytol. 1999. https://doi.org/10.1046/j.1469-8137.1999.00423.x.
24. Zeisler-Diehl V, Migdal B, Schreiber L. Quantitative characterization of cuticular barrier properties: methods, requirements, and problems. J Exp Bot. 2017. https://doi.org/10.1093/jxb/erx282.
25. Orgell WH. The isolation of plant cuticle with pectic enzymes. Plant Physiol. 1955;30:78–80.
26. Holloway PJ, Baker EA. Isolation of plant cuticles with zinc chloride-hydrochloric acid solution (short communication). Plant Physiol. 1968. https://doi.org/10.1104/pp.43.11.1878.
27. Solel Z. The systematic fungicidal effect of benzimidazole derivatives and thiophanate against Cercospora leaf spot of sugar beet. Phytopathology. 1970. https://doi.org/10.1094/Phyto-60-1186.
28. Edgington LV, Buchenauer H, Grossmann F. Bioassay and transcuticular movement of systematic fungicides. Pestic Sci. 1973. https://doi.org/10.1002/ps.2780040517.
29. Schonherr J, Lendzian K. A simple and inexpensive method of measuring water permeability of isolated plant cuticular membranes. Z Pflanzenphysiol. 1981. https://doi.org/10.1016/S0044-328X(81)80203-6.
30. Yamada Y, Wittwer SH, Bukovac MJ. Penetration of organic compounds through isolated cuticular membranes with special reference to C14 urea. Plant Physiol. 1964. https://doi.org/10.1104/pp.40.1.170.
31. Darlington WA, Cirulis N. Permeability of apricot leaf cuticle. Plant Physiol. 1963. https://doi.org/10.1104/pp.38.4.462.
32. Wittwer SH, Lundahl WS. Autoradiography as an acid in determining the grass absorption and utilization of foliar applied nutrients. Plant Physiol. 1951;26:792–7.
33. Eggert R, Kardos LT, Smith RD. The relative absorption of phosphorus by apple trees from foliar sprays and from soil applications of fertilizer using radioactive tracers. Proc Am Soc Hortic Sci. 1952;60:75–86.
34. Tukey HB, Ticknor RL, Hinsvark ON, Wittwer SH. Absorption of nutrients by stems and branches of woody plants. Science. 1952. https://doi.org/10.1126/science.116.3007.167.
35. Bargel H, Koch K, Cerman Z, Neinhuis Ch. Structure-function relationships of the plant cuticle and cuticular waxes—a smart material? Funct Plant Biol. 2006. https://doi.org/10.1071/FP06139.
36. Bukovac MH, Wittwer SH. Absorption and mobility of foliar applied nutrients. Plant Physiol. 1957. https://doi.org/10.1104/pp.32.5.428.
37. Yamada Y, Wittwer SH, Bukovac MJ. Penetration of ions through isolated cuticles. Plant Physiol. 1963. https://doi.org/10.1104/pp.39.1.28.
38. Yu JH, Lim HK, Choi GJ, Cho KY, Kim JH. A new method for assessing foliar uptake of fungicides using Congo Red as a tracer. Pest Manag Sci. 2001. https://doi.org/10.1002/ps.327.
39. Pinton R, Cesco S, Santi S, Varanini Z. Soil humic substances stimulate proton release by intact oat seedling roots. J Plant Nutr. 1997. https://doi.org/10.1080/01904169709365301.
40. Chen Y, Clapp CE, Magen H, Cline VW. Stimulation of plant growth by humic substances: effects on iron availability. In: Ghabbour EA, Davies G, editors. Understanding humic substances: advanced methods, properties and applications. Cambridge: Royal Society of Chemistry; 1999.
41. Russo RO, Berlyn GP. The use of organic biostimulants to help low input sustainable agriculture. J Sustain Agric. 1990. https://doi.org/10.1300/J064v01n02_04.
42. Tan KH. Humic matter in soil and the environment. 2nd ed. New York: Marcel Dekker; 2003.
43. Nardi S, Condheri G, Dell'Agnola G. Biological activity of humus. In: Piccolo A, editor. Humic substances in terrestrial ecosystems. Amsterdam: Elsevier; 1996. p. 361–406.
44. Canellas LP, Olivares FL. Physiological responses to humic substances as plant growth promoter. Chem Biol Technol Agric. 2014. https://doi.org/10.1186/2196-5641-1-3.
45. Nardi S, Pizzeghello D, Schiavon M, Ertani A. Plant biostimulants: physiological responses induced by protein hydrolyzed-based products and humic substances in plant metabolism. Sci Agric. 2016. https://doi.org/10.1590/0103-9016-2015-0006.
46. Tejada M, Gonzalez JL. Influence of foliar fertilization with amino acids and humic acids on productivity and quality of asparagus. Biol Agric Hortic. 2003. https://doi.org/10.1080/01448765.2003.9755270.
47. Pizzeghello D, Nicolini G, Nardi S. Hormone-like activity of humic substances in *Fagus sylvaticae* forests. New Phytol. 2001. https://doi.org/10.1046/j.0028-646x.2001.00223.x.
48. Basiolio ZD, Pasqualoto CL, Facanha AR. Indolacetic and humic acids induce lateral root development through a concerted plasmalemma and tonoplast H^+ pumps activation. Planta. 2007. https://doi.org/10.1007/s00425-006-0454-2.
49. Jackson TA. Effects of clay minerals, oxyhydroxides, and humic matter on microbial communities of soil, sediment, and water. In: Huang PH, et al., editors. Environmental impact of soil component interactions: metals, inorganics and microbial activity. Berlin Heidelberg: CRC Press, Springer; 1995. p. 165–200.
50. Parandian F, Samavat S. Effects of fulvic and humic acid on anthocyanin, soluble sugar, α-amylase enzyme and some micronutrient elements in Lilium. Int Res J Appl Basic Sci. 2012;3:924–9.

51. Dorer SP, Peacock CH. The effect of humate and organic fertilizer on establishment and nutrient of creeping bent putting greens. Int Turfgrass Soc. 1997;78:437–43.
52. Liu C, Cooper RJ, Bowman DC. Humic acid application affects photosynthesis, root development, and nutrient content of creeping bentgrass. HortScience. 1998;33:1023–5.
53. Fernandez-Escobar R, Benlloch M. Response of olive trees to foliar application of humic substances extracted from leonardite. Sci Hortic. 1996. https://doi.org/10.1016/S0304-4238(96)00914-4.
54. Maibodi NDH, Kafi M, Nikbakht A, Rejali F. Effect of foliar applications of humic acid on growth, visual quality, nutrients content and root parameters of perennial ryegrass (*Lolium perenne* L.). J Plant Nutr. 2014. https://doi.org/10.1080/01904167.2014.939759.
55. Bettoni MM, Mogor AF, Pauletti V, Goicoechea N, Aranjuelo I, Germendia I. Nutritional quality and yield of onion as affected by different application methods and doses of humic substances. J Food Compos Anal. 2016. https://doi.org/10.1016/j.jfca.2016.06.008.
56. Olk DC, Dinnes DL, Rene Scoresby J, Callaway CR, Darlington JW. Humic products in agriculture: potential benefits and research challenges–a review. J Soils Sediments. 2018. https://doi.org/10.1007/s11368-018-1916-4.
57. Rose MT, Patti AF, Little KR, Brown AL, Roy Jackson W, Cavagnaro TR. A meta-analysis and review of plant-growth response to humic substances: practical implications for agriculture. Adv Agron. 2014. https://doi.org/10.1016/B978-0-12-800138-7.00002-4.
58. Lyons G, Genc Y. Commercial humates in agriculture: real substance or smoke and mirrors? Agronomy. 2016. https://doi.org/10.3390/agronomy6040050.
59. Kulikova NA, Abroskin DP, Badun G, Chernysheva MG, Korobkov VI, Beer AS, Tsvetkova EA, Senik SV, Klein OI, Perminova IV. Label distribution in tissues of wheat seedlings cultivated with tritium-labeled leonardite humic acid. Sci Rep. 2016. https://doi.org/10.1038/srep28869.
60. Sedlacek P, Smilek J, Klucakova M. How the interactions with humic acids affect the mobility of ionic dyes in hydrogels—2. Non-stationary diffusion experiments. React Funct Polym. 2014. https://doi.org/10.1016/j.reactfunctpolym.2013.12.002.
61. Smilek J, Sedlacek P, Klucakova M. On the role of humic acids' carboxyl groups in the binding of charged organic compounds. Chemosphere. 2015. https://doi.org/10.1016/j.chemosphere.2015.06.093.
62. Gladkov OA. U.S. Patent 7198805B2, Method for producing humic acid salts, Sankt-Peterburg (RU), chemical abstract (57). 2007.
63. Novak F, Sestauberova M, Hrabal R. Structural features of lignohumic acids. J Mol Struct. 2015. https://doi.org/10.1016/j.molstruc.2015.03.054.
64. Sedlacek P, Smilek J, Klucakova M. How the interactions with humic acids affect the mobility of ionic dyes in hydrogels—results from diffusion cells. React Funct Polym. 2013. https://doi.org/10.1016/j.reactfunctpolym.2013.07.008.
65. Sedlacek P, Smilek J, Kalina M, Lastuvkova M, Klucakova M. Hydrogels: invaluable experimental tool for demonstrating diffusion phenomena in physical chemistry laboratory courses. J Mater Educ. 2017;39:59–90.
66. Smilek J, Sedlacek P, Lastuvkova M, Kalina M, Klucakova M. Transport of organic compounds through porous systems containing humic acids. Bull Environ Contam Toxicol. 2017. https://doi.org/10.1007/s00128-016-1926-0.
67. Cussler EL. Diffusion: mass transfer in fluid systems. 2nd ed. London: Cambridge University Press; 1997.
68. Enev V, Pospisilova L, Klucakova M, Liptaj T, Doskocil L. Spectral characterization of selected humic substances. Soil Water Res. 2014. https://doi.org/10.17221/39/2013-SWR.
69. Prochazka P, Stranc P, Pzderu K, Strnc J, Jedlickova M. The possibilities of increasing the production abilities of soya vegetation by seed treatment with biologically active compounds. Plant Soil Environ. 2015. https://doi.org/10.17221/225/2015-PSE.
70. Prochazka P, Stranc P, Pazderu K, Stranc J. The influence of pre-sowing seed treatment by biologically active compounds on soybean seed quality and yield. Plant Soil Environ. 2016. https://doi.org/10.17221/570/2016-PSE.
71. Crank J. The mathematics of diffusion. 2nd ed. Oxford: Clarendon Press; 1956.
72. Guzman P, Fernandez V, Khayet M, Garcia ML, Fernandez A, Gil L. Ultrastructure of plant lead cuticles in relation to sample preparation as observed transmission electron microscopy. Sci World J. 2014. https://doi.org/10.1155/2014/963921.
73. Tyree MT, Scherbatskoy D, Tabor CA. Leaf cuticles behave as asymmetric membranes: evidence from the measurement of diffusion potentials. Plant Physiol. 1990. https://doi.org/10.1104/pp.92.1.103.
74. Guzman P, Fernandez V, Garcia ML, Khayet M, Fernandez A, Gil L. Localization of polysaccharides in isolated and intact cuticles of eucalypt, poplar and pear leaves by enzyme-gold labelling. Plant Physiol Biochem. 2014. https://doi.org/10.1016/j.plaphy.2013.12.023.
75. Guzman P, Fernandez V, Garcia J, Cabral V, Hayali N, Khayet M, Gil L. Chemical and structural analysis of *Eucalyptus globulus* and *E. camaldulensis* leaf cuticles: a lipidized cell wall region. Front Plant Sci. 2014. https://doi.org/10.3389/fpls.2014.00481.
76. Fernandez V, Guzman-Delgado P, Graca J, Santos S, Gil L. Cuticles structure in relation to chemical composition: re-assessing the prevailing model. Front Plant Sci. 2016. https://doi.org/10.3389/fpls.2016.00427.
77. Riederer M, Schönherr J. Accumulation and transport of (2,4-dichlorophenoxy)acetic acid in plant cuticles. 1. Sorption in the cuticular membrane and its components. Ecotoxicol Environ Saf. 1984. https://doi.org/10.1016/0147-6513(85)90022-3.
78. Eichert T, Burkhardt J. Quantification of stomatal uptake of ionic solutes using a new model system. J Exp Bot. 2001. https://doi.org/10.1093/jexbot/52.357.771.
79. Burkhardt J, Basi S, Pariyar S, Hunsche M. Stomatal penetration by aqueous solutions—an update involving leaf surface particles. New Phytol. 2012. https://doi.org/10.1111/j.1469-8137.2012.04307.x.
80. Schreiber L, Schonherr J. Water and solute permeability of plant cuticles. 1st ed. Berlin: Springer; 2009.

Publisher's Note

Colloids and Surfaces A 557 (2018) 116–122

Contents lists available at ScienceDirect

Colloids and Surfaces A

journal homepage: www.elsevier.com/locate/colsurfa

The transport of metal ions in hydrogels containing humic acids as active complexation agent

Martina Klučáková*, Michal Kalina, Jiří Smilek, Marcela Laštůvková

Brno University of Technology, Faculty of Chemistry, Materials Research Centre, Purkynova 464/118, 612 00 Brno, Czech Republic

GRAPHICAL ABSTRACT

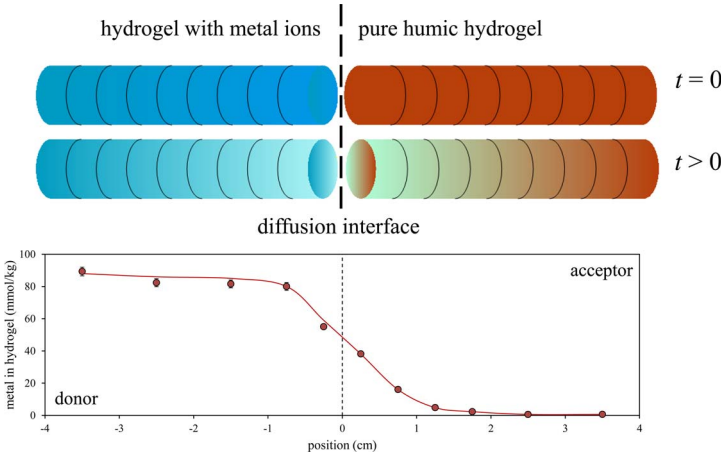

ARTICLE INFO

Keywords:
Humic acid
Diffusion
Complexation
Metal ions
Hydrogel

ABSTRACT

The complexation and transport/immobilization abilities of humic acids are the most important environmental qualities of these substances. Therefore, the study of these properties is important for understanding their role both in natural systems and in human-driven applications. This contribution is focused on the diffusion of metal ions (Co, Cu and Ni) studied by means of a diffusion couple, and their immobilization in humic hydrogels. It was found that the diffusion characteristics of metal ions are strongly affected by their reactivity and their initial concentrations. The concentration dependence of Cu diffusivity exhibited a different trend when compared to Co and Ni, which the result of the high affinity of Cu to humic acids. When a metal ion is first complexed by humic acids it is bound in an exchangeable mode, which can be transferred to a nonexchangeable one. Our results indicate that the dynamic equilibrium established in the diffusion process includes mainly Cu ions in an exchangeable mode as a result of their high affinity and the high amount of bound Cu. Their transformation of bound Cu ions in strong Cu-humic complexes is very slow. In contrast, Co and Ni have much lower affinities to humic acids, thus their diffusivities are less affected by their reaction with humic acids.

* Corresponding author.
E-mail address: klucakova@fch.vutbr.cz (M. Klučáková).

https://doi.org/10.1016/j.colsurfa.2018.02.042
Received 29 November 2017; Received in revised form 16 February 2018; Accepted 16 February 2018
Available online 15 March 2018

1. Introduction

The incorporation of potentially toxic metals into natural systems through industrial activities, such as metal mining, smelting and refining, fossil fuel combustion, atmospheric deposition, the land application of sewage sludge and industrial by-products, gasoline processing, and fertilization pose a great threat to the environment and human health. After combining with soil particles, heavy metals can persist in soils, resulting in harmful effects on biota. Such metals may be accumulated in the food chain, leach out of soils to pollute groundwater supplies or accumulate in plants, shrubs and trees [1–4]. A better understanding of soil and water pollution, as well as the factors controlling the retention and release of metal ions in nature is required. Many pollution problems involve such simultaneous processes as water flow, multicomponent solute transport, heat transport and biogeochemical processes and reactions. Models integrating various processes can be valuable tools for investigating the mobility of a wide range of inorganic and organic contaminants subject to different hydrologic and geochemical conditions [5]. The important process affecting the behavior of metal ions in natural systems is their complexation with soil components, which can involve the sorption of metal ions from the liquid phase (e.g. soil solution) onto solid particles, the immobilization of metals in the solid phase, and the complexation of metal ions with dissolved organic matter. The mobility of metal ions in soils is related to the partitioning between the soil solid phase and the solution phase, defined usually as the distribution coefficient [4,6]. Therefore, the sorption of metal ions on solid humic particles has been extensively studied by many authors (e.g. [7–10]).

Martyniuk and Wieckowska [7] compared the ion exchange capacities of solid and gel forms of humic acids. They showed that the binding of metal ions by the gel form was higher in comparison with the adsorption on solid humic particles. This finding was later supported by our previous results, which showed the presence of significant amounts of free mobile metal ions and weakly-bonded metal ions in ion-exchangeable mode, these contributing to an increase in the total amount of bonded metals [11–13]. In contrast, metal ions adsorbed on solid humic particles are mainly in form of stable metal-humic complexes and their amount is lower [14]. Similarly, Cao et al. [15] and Garcia-Mina [16] obtained a negative relationship between the stability constant of metal-humic complexes and the binding capacity of active sites and the metal humic ratio. Alvarez-Puebla et al. [8] studied the retention mechanism of Co(II), Cu(II) and Ni(II) ions. Their results showed that 2:1 complexes were formed at low concentrations. This structural coordination was energetically favored due to the chelate effect. The increase in metal concentrations caused an increase in the metal:humic ratio and metals occupied most of the surface active sites. In addition, the authors stated that high concentrations of metals preserved the 3D structure of humic acids. Our results confirmed that only a portion of metal ions are bonded with humic acids through carboxylic or phenolic groups and that other binding sites contributed to the total amounts of adsorbed metals [9]. Antonelli et al. [17] distinguished between specific binding sites (carboxylic and phenolic ones) and non-specific binding sites in humic substances. Baker and Khalili [18] identified four binding sites for chemical interactions between metal ions and humic acids. Shaker and Albishri [10] indicated three types of binding sites with different adsorption capacities. In contrast to other works, they presumed mainly the existence of physical adsorption which was diffusion controlled.

The mobility of metal ions in soils depends on the combination of several factors, including the nature of the metal, its concentration, environmental factors, and soil components. These factors determine the soil solution-solid phase equilibrium of metals through the mechanisms of sorption-desorption and dissolution-precipitation [19–21]. Bryan et al. [22] stated that metal ions in a non-exchangeable mode had a significantly higher mobility than those in an exchangeable mode. Metal ions in an exchangeable mode are strongly bound, but they may dissociate from the humic substance and be immobilized by a stronger binding site on the surface. The sorption may significantly reduce the mobility. Lippold et al. [23] assessed the mobility of contaminant metals in transport systems with humic substances. They emphasized the influence of kinetic effects on stabilization processes leading to an increase in strongly humic-bonded metals. Chakraborty et al. [24] studied the dynamics of metal complexes and their diffusion in the presence of humic substances. They discovered that the interactions of Cu and Ni with humic acids are stronger than their interactions with fulvic acids and natural organic matter. They indicated that labile complexes were formed with different binding sites with diverse binding energies in humic substances. Labile Ni complexes were small [24,25] with very fast diffusion rates which corresponded with Ni bioavailability. The diffusion coefficients of labile Ni complexes were very similar to those of free Ni(II) ions. In contrast, the diffusion coefficients of Cu complexes were similar to those of humic substances or natural organic matter presented in studied systems and their diffusion rates were lower [24]. Comparing these findings with our previous work [26], we can see that the diffusion coefficient of Cu(II) ions in humic hydrogels was higher than the diffusion coefficients of Ni(II) and Co(II). Differences can be explained by the much higher content of diffusing metal ions in humic hydrogels (an excess concentration in relation to humic binding sites) resulting in high amount of free mobile ions. Kostic et al. [27] determined the binding strength of heavy metals bound to humic acids. Their results confirmed the high stability of metal humic complexes in the order Cu(II) > Ni(II) > Co(II), which indicated that in conditions of increased amounts of metal ions in the natural environment, these metal ions may be preferred and can thus indirectly increase the mobility and bioavailability of other metal ions. Furukawa and Takahashi [28] investigated the effect of complexation with humic substances on the diffusion of metal ions in aqueous solutions. Their results showed that the diffusion of each ion lost its characteristics by complexation with humic substances due to their large molecular weight. This is incompatible with results published in [24], which indicated that the diffusivities of Ni complexes were very similar to those of free Ni(II) ions.

The diffusion behavior of metal ions described above was studied by different authors using different methods. In general, diffusion can be sensitive to the concentration of diffusing particles, the properties of the diffusion medium, and (potential) chemical interactions. Therefore, the obtained discrepancies are not surprising. They are a result of differences in many factors concerning the realized diffusion experiments. We decided to study the transport of metal ions in humic hydrogels by means of the diffusion couple method [29–32]. In order to determine the concentration dependence of the diffusion coefficient, experiments were performed using three different initial contents of metal ions.

2. Material and methods

2.1. Humic acids

Humic acids were isolated from lignite mined in the Czech Republic (South Moravia). The sample was extracted in the ratio of 30 g of lignite to 1 dm^3 of extraction agent - a mixture of 0.5 M NaOH and 0.1 M $Na_4P_2O_7$ (1:1). The obtained suspension was stirred at laboratory temperature (25 °C) overnight. The solid part was removed by centrifugation and extracted again for 60 min. Both leaches were mixed, acidified using concentrated HCl up to a pH value close to 1, and left in the refrigerator overnight. Precipitated humic acids were centrifuged (4000 rpm, 15 °C), washed repeatedly with deionized water until free of chlorides, and dried in an oven at 50 °C.

The ash and moisture contents of the prepared humic sample, measured by means of thermogravimetry (TGA Q5000), were equal to 11.0% wt. (ash) and 5.7% wt. (moisture).

The elemental composition of humic acids was determined by means of Euro EA CHNO Elemental analyser. The total acidity of the

Table 1
Elemental composition and total acidity of humic acids (normalized on dry ash-free sample).

C (at.%)	H (at.%)	N (at.%)	O (at.%)	total acidity (mmol g^{-1})
39.1 ± 0.5	38.4 ± 0.4	1.1 ± 0.5	21.4 ± 0.4	9.0 ± 0.4

extracted humic sample was determined by the standard titration method [9,12,33–35]. These traditional characteristics are listed in Table 1. More details on their chemical structure can be found in our previous works [11,14,21,33,35,36].

2.2. Humic hydrogels

The powdered humic sample (8 g) was dissolved in 0.5 M NaOH (1 dm^3) and then acidified with concentrated HCl up to a pH value close to 1. The precipitated humic hydrogel was repeatedly centrifuged (4000 rpm, 15 °C) and washed with deionized water until free of chlorides. The dry matter of the prepared hydrogel was 10.1% wt. The pH value of prepared hydrogel was 3.81 ± 0.07.

2.3. Diffusion experiments

A diffusion couple was created by connecting cylindrical glass tubes filled with humic hydrogel containing metal ions and pure humic hydrogel without metal ions (see Fig. 1). The left side of the humic couple was the source of metal ions diffunding through the diffusion interface into the right side representing their acceptor.

The hydrogel was gently packed into the individual tubes in order to fill their entire volume. First, metal ions were incorporated into the humic hydrogel. Tubes 1–5 were placed into the stock solution of metal ions until the achievement of equilibrium and a homogeneous distribution of metal ions in the hydrogel (3 days). Solutions of $CoCl_2$, $CuCl_2$ and $NiCl_2$ were used. Their initial concentrations were 0.05, 0.1 and 1 mol dm^{-3}, respectively. The total amount of metal ions in the diffusion source was determined on the basis of the decrease in the concentration of the stock solution.

Then, the tubes were connected together. Due to the sufficiently strong consistency of the hydrogel, no deformations of the interfaces in the diffusion couples were observed. The connected tubes were stopped with parafilm and aluminium foil to prevent the hydrogel drying. The durations of the diffusion experiments were 10, 24 and 72 h. After the given time the tubes were disconnected and metal ions were extracted separately in 1 M HCl solution. This procedure was developed in our previous studies and is described in detail there e.g. [26,32,37].

The concentration of metal ions in leaches was determined by means of UV/VIS spectroscopy (Hitachi U3900H). The obtained data were used to compute the concentration profiles of metal ions in the tubes and diffusion fluxes (the total amounts diffused in the acceptor part of the couple at given times).

All experiments were performed at laboratory temperature (25 ± 1 °C) and in triplicate. Data are presented as average values with standard deviation bars.

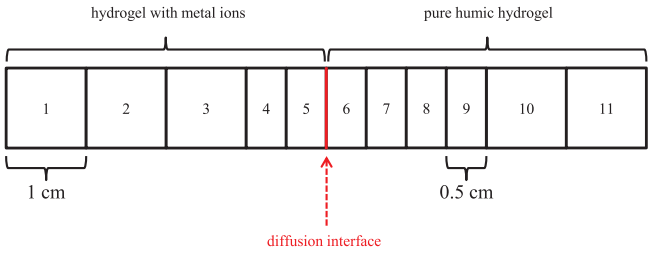

Fig. 1. Scheme of diffusion couple.

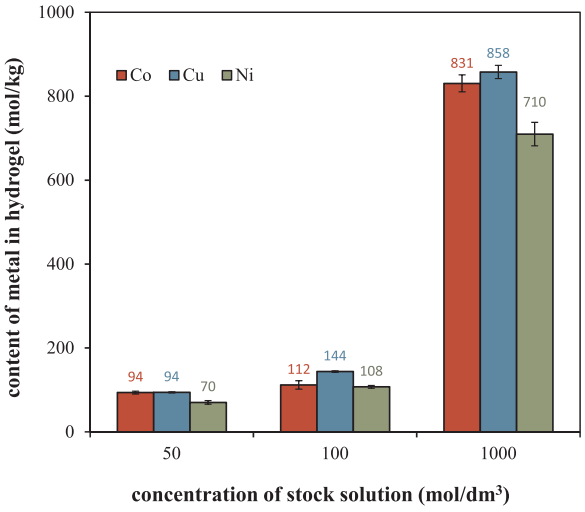

Fig. 2. The initial concentrations of metal ions in humic hydrogel (the donor part of the diffusion couple).

3. Results and discussion

Differences in the diffusion behavior of metal ions were observed already in the preparation of the donor parts of the diffusion couples. The donor part was doped with metal ions by means of their diffusion from the stock solution into the humic hydrogel in the glass tubes. Three different initial concentrations of stock solution were used. As we can see in Fig. 2, the initial concentrations of metal ions in the hydrogels differed, the differences increasing with the increasing concentration of the stock solution. The lowest initial concentrations were determined in the case of Ni ions. Cu ions exhibited the highest concentrations. We used the same humic hydrogel for all metal ions. Therefore, the differences were caused by their properties and behavior. It seems that the initial concentrations were connected with the affinity of metal ions to humic acids as well as their diffusivity. The observed differences were related to differences in the diffusion and reactivity of the used metal ions described below.

The concentration profiles in the diffusion couple are shown in Fig. 3. The characteristic sigmoidal curves intersecting at diffusion interface were obtained. Their development over time was used for the determination of total amounts diffused in the acceptor part of the hydrogel at given times and for the calculation of effective diffusion

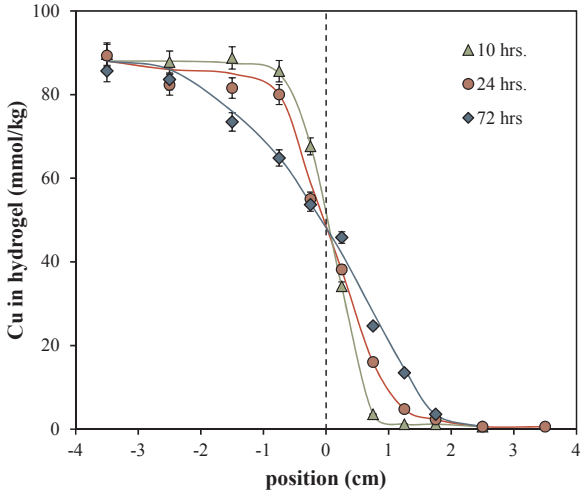

Fig. 3. Concentration profiles of Cu ions in the diffusion couple at different times. The donor part of the diffusion couple was doped by Cu ions from 0.05M stock solution. Experimental data were fitted using Eq. (10).

coefficients.

The mathematical procedure used in this work was based on Fick's equation describing one-dimensional non-stationary diffusion [29,30]:

$$\frac{\partial c}{\partial t} = D_{\text{eff}} \frac{\partial^2 c}{\partial x^2}, \tag{1}$$

where c represents the concentration of the diffusing compound (metal ions) at time t and position x (the distance from the diffusion interface). The diffusion coefficient D_{eff} is the main parameter characterizing the rate of the transport. In general, the diffusion coefficient is an "effective" characteristic reflecting the pore structure of the hydrogel [12,13,38,39] and the influence of chemical interactions between metal ions and humic acids in their transport through the hydrogel [12,13,29,32,37].

If the diffusing particles are transported through an unreactive medium, the effective diffusion coefficient is the medium's affected only by the medium's pore structure and is given by:

$$D_{\text{eff}} = D^* = \frac{\phi}{\tau} D = \mu D^0, \tag{2}$$

where the diffusion coefficient in hydrogel D^* is dependent on its porosity (ϕ) and tortuosity (τ) expressed by the structural factor μ and D°, which is the diffusion coefficient in water.

The effects of the chemical reaction can be described mathematically by the following equation based on the conservation of mass:

$$\frac{\partial c}{\partial t} = D^* \frac{\partial^2 c}{\partial x^2} - \dot{r}, \tag{3}$$

where $\dot{r}$ is rate of chemical reaction.

It is well known that humic acids have a relative high affinity to metal ions (e.g. [7–10]). This can be considered as a sufficient assumption for relatively fast chemical reaction between diffunding metal ions and humic acids homogeneously distributed in hydrogel. Bryan et al. [22] reported that if a metal ion is first complexed by humic acids, it is bound in an "exchangeable" mode. According to their results the metal ion in this fraction is bound, however, over time, "exchangeably-bound" metal may transfer to a "non-exchangeable" mode. The interactions between metal ions and humic acids are very complex, mainly due to the presence of many different humic active sites and complicated reaction mechanisms. On the other hand, if we consider that the first reaction step between metal ions and humic acids is fast, we can assume the presence of local equilibrium between free unbound metal ions (c) and metals bound to humic acids (c_b) [29,32,37], given by:

$$c_b = K_{\text{app}} c, \tag{4}$$

where K_{app} is the apparent equilibrium constant. It should be noted that the equilibrium constant is an "alternative" parameter characterizing the simple reaction "metal ion ↔ bound metal". It is, in fact, the ratio between the concentration of bound metals and the concentration of free metal ions.

Eq. (3) can be written as

$$\frac{\partial c}{\partial t} = D^* \frac{\partial^2 c}{\partial x^2} - K_{\text{app}} \frac{\partial c}{\partial t}, \tag{5}$$

and, consequently,

$$\frac{\partial c}{\partial t} = \frac{D^*}{1 + K_{\text{app}}} \frac{\partial^2 c}{\partial x^2} = D_{\text{eff}} \frac{\partial^2 c}{\partial x^2}. \tag{6}$$

The effective diffusion coefficient D_{eff} can thus be defined by the following equation

$$D_{\text{eff}} = \frac{D^*}{1 + K_{\text{app}}} = \frac{\mu D^0}{1 + K_{\text{app}}}, \tag{7}$$

in which the effects of the tortuous movement of diffusing metal ions in humic hydrogel and their chemical interaction are involved.

The mathematical description of diffusion in a diffusion couple formed from the same hydrogel and differing only in the metal concentrations in the donor and acceptor parts is relatively easy. Before the start of diffusion, the donor part of the couple has a constant concentration of metal ions c_0 along its whole length whereas, the concentration of metal ions in the acceptor part of the couple is zero; therefore the initial conditions are

$$c = c_0, \quad x < 0, \quad t = 0, \tag{8}$$

and

$$c = 0, \quad x > 0, \quad t = 0, \tag{9}$$

and the solution to the second Fick law (Eq. (1)) is [29–32]:

$$c\,(x, t) = \frac{1}{2} c_0 \, erfc \, \frac{x}{\sqrt{4 D_{\text{eff}} t}}. \tag{10}$$

It can be seen that the concentration of the diffused component at the interface is time independent and equal to $c_0/2$.

The total diffusion flux m_t which goes through the diffusion interface between the donor and acceptor parts of the diffusion couple ($x = 0$) at time t can be calculated as [29–32]:

$$m_t = c_0 \sqrt{\frac{D_{\text{eff}} t}{\pi}}. \tag{11}$$

In our study, the diffusion coefficients D_{eff} were calculated on the basis of Eq. (11). Examples of data fitting are shown in Fig. 4. We can see that the highest total fluxes were determined for Co ions, the lowest ones for Ni ions. The total diffusion fluxes were affected not only by the diffusivities of the used metal ions (D_{eff} values) but also by their initial contents in the donor parts of diffusion couples (c_0). The slopes obtained on the basis of linear regression were proportional to c_0 and $\sqrt{D_{\text{eff}}}$. The values of D_{eff} are listed in Table 2 and displayed schematically in Fig. 5. The highest values of D_{eff} were obtained for Ni ions, the lowest for Cu ions. The obtained effective diffusion coefficients are strongly affected by the reactivity of humic acids conditioned mainly by the acidic functional groups and by the affinity of metal ions to humic acids. Our previous work [13] was focused on the diffusion of cupric ions as a model metal with high affinity to humic acids in order to investigate the effect of selective blocking of humic functional groups. In the present study, we used only one type of humic hydrogel with the same content of binding sites for metal ions with different affinities to humic acids. In comparison of values of D_{eff} of Co and Ni with their total diffusion fluxes in Fig. 4 can be seen that the amount of Ni ions diffusing through unit area of diffusion interface was lower than that of Co ions. The reason for this discrepancy was the lower initial concentration

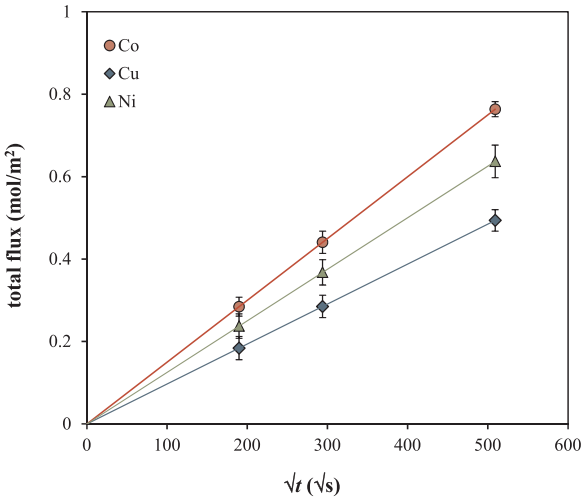

Fig. 4. The dependence of total flux of metal ions through the diffusion interface on the square root of time. The donor part of diffusion couple was doped with metal ions from 0.05M stock solution. Experimental data were fitted by Eq. (11).

Table 2
D_{eff} values obtained for the transport of metal ions in humic hydrogels on the basis of Eq. (11).

concentration of stock solution (mol/m^3)	10^{-10} D_{eff} (m^2/s)		
	Co	Cu	Ni
50	8.04 ± 0.16	3.32 ± 0.09	9.93 ± 0.14
100	7.85 ± 0.19	5.24 ± 0.05	9.54 ± 0.15
1000	7.13 ± 0.21	6.42 ± 0.22	8.46 ± 0.13

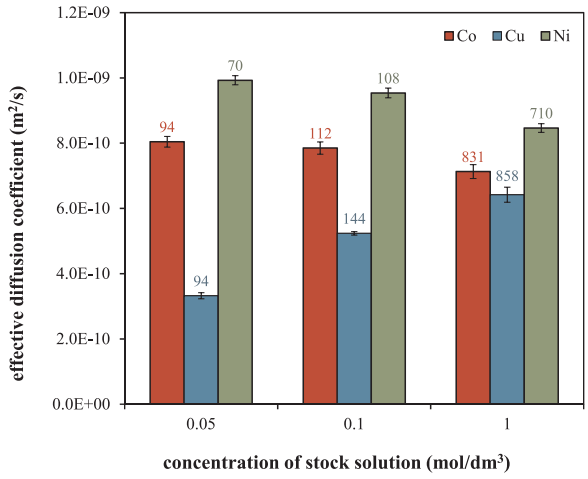

Fig. 5. D_{eff} values obtained for the transport of metal ions in humic hydrogels on the basis of Eq. (11). Values above columns are initial contents of metal ions in the donor parts of diffusion couples.

of Ni ions in the humic hydrogel (i.e. in the donor part of diffusion couple).

In general, the diffusion coefficient is dependent on the concentration of diffusing particles. Such concentration dependence exists in most systems, but often, e.g. in dilute solutions, the dependence is slight and the diffusion coefficient can be assumed to be constant for practical purposes [29,30]. It was found that the obtained values of D_{eff} were relatively strongly affected by the initial content of metal ions in donor part of the diffusion couple. As we can see, the effective diffusion coefficient decreased with increasing concentration in the case of Co and Ni ions, while the concentration dependence of D_{eff} determined for Cu ions exhibited the opposite trend (Table 2). The reason was the high affinity of Cu ions to humic acids in comparison with other metals (e.g. [7–10,27]), this resulting in their different diffusion behavior in systems containing humic substances [24,25]. Furukawa and Takahashi [28] showed that metal mobility is also strongly affected by the size of humic or fulvic particles contained in the studied system. Some metal-humic and metal-fulvic complexes can remain mobile with changed diffusion characteristics [22,24,25,28,41].

The different affinities of metal ions were also observed to have an effect on their mobilities in their diffusion through hydrogels containing chitosan as a reactive biopolymer [42].

The values of D_{eff} were used for the calculation of numerical concentration profiles using Eq. (10) in order to compare them with experimental data. The examples in Fig. 3 show that the experimental and numerical concentration profiles were in very good agreement. This means that the mathematical model was suitable for our experiments and that initial and boundary conditions were kept. The influence of hydrogel reactivity on the diffusion of metal ions was studied in detail in our previous work [12]. The value of the structural parameter μ was determined as 0.79. If we assume that our humic hydrogel is very similar (prepared from humic acids extracted from the same lignite), we can calculate the diffusion coefficient D^* affected only by the pore structure of the hydrogel according to Eq. (2) with the use of D° values

Table 3
D^* values obtained for the transport of metal ions in humic hydrogels on the basis of Eq. (2) using structural parameter μ determined in [12] and D° values published in [40].

	Co	Cu	Ni
D^* 10^{-9} (m^2/s)	1.15 ± 0.06	1.13 ± 0.06	1.04 ± 0.05
D° 10^{-9} (m^2/s)	1.46	1.43	1.32

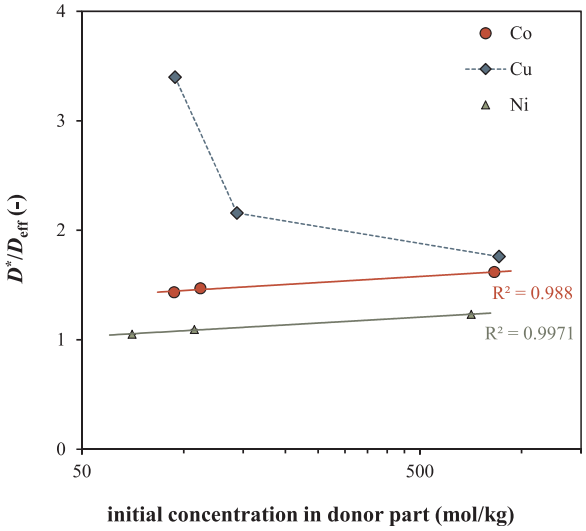

Fig. 6. The D^*/D_{eff} ratio in the dependence of the initial content of metal ions in the donor part of the diffusion couple.

published in [40]. The values of D^* and D° are listed in Table 3. It is logical that D^* is highest for Co and lowest for Ni ions similarly as in the case of D°, because, in this case, the value of D^* is 79% of the value of D°. In contrast, the ratio D^*/D_{eff} is highest for Cu ions and its concentration dependence exhibits the opposite trend to that for Co and Ni (Fig. 6). It was found that the dependence of the ratio D^*/D_{eff} on the initial content of metal ions in the donor part of the diffusion couple was linear in logarithmic coordinates and increased slightly with the increasing content of metal ions in the hydrogel. In contrast, the ratio D^*/D_{eff} decreased with the increasing content of Cu ions in the hydrogel and the decrease was greater for lower concentrations. The D^*/D_{eff} ratios corresponded with the values of the apparent equilibrium constant K_{app} defined by Eq. (7). The K_{app} values demonstrated the high affinity of Cu ions to humic acids in comparison with Co and Ni (Table 4). K_{app} is according to this definition the ratio between bound and free metals It is not the stability constant and cannot be directly comparable with data published in literature. On the other hand, our approach can include interactions between metal ions and humic acids directly in Fick's law and solve the transport of metal ions simultaneously with their interactions during this transport. Our apparent equilibrium constant K_{app} is involved in the effective diffusion coefficient D_{eff} together with the effects of the tortuous movement of diffusing metal ions in humic hydrogel. The value of K_{app} represents an alternative parameter characterizing the affinity of metals to humic acids.

Table 4
K_{app} values obtained for the transport of metal ions in humic hydrogels on the basis of Eq. (7).

concentration of stock solution (mol/m^3)	K_{app} (−)		
	Co	Cu	Ni
50	0.43 ± 0.01	2.40 ± 0.07	0.05 ± 0.01
100	0.47 ± 0.01	1.16 ± 0.01	0.09 ± 0.01
1000	0.62 ± 0.02	0.76 ± 0.03	0.23 ± 0.01

As we can see, the apparent equilibrium constant K_{app} is concentration-dependent mainly in the case of Cu (Table 4). The K_{app} values decreased with the increasing concentration of Cu. In contrast, the concentration dependencies of K_{app} for Co and Ni were not pronounced. Their values decreased slightly with increasing concentration. The amount of bound Co was around 50% in comparison with free mobile ions. The apparent equilibrium constants obtained for Ni ions were very low. This means that their bound portion in humic gel was minimal and the effective diffusion coefficient was near to the value of D^*. In this case, the pore structure of the hydrogel had the decisive influence. Our results are in agreement with the finding of Chakraborty et al. [24] and Hassan et al. [25], which showed very fast diffusion rates for Ni complexes, these corresponding with Ni bioavailability.

The apparent equilibrium constants obtained for Cu ions were much higher. The portion of bound metals predominated over free mobile ions at low concentrations and decreased with increasing total metal content. Alvarez-Puebla et al. [8] assumed humic acids to have a 3D structure at high metal concentrations and the presence of energetically favored 2:1 complexes at low concentrations. The reaction mechanism and structure of formed complex can significantly influence the equilibrium between bound and free mobile metal ions expressed by their ratio K_{app}. Lower value of D_{eff} was the consequence of the binding of Cu by humic acids described similarly in [24] and [28].

The ifferences the values of the parameters obtained in this study show that the mobility of metal ions in systems containing humic acids (or organic matter) is strongly affected by their reciprocal interactions. Although, the diffusion coefficients in water (D°) differed only slightly, their values changed significantly, when they diffused through the reactive humic hydrogel. This decrease in the diffusion rate is partly the result of the pore structure of the hydrogel. The existence of the solid network comprising the porous medium results in diffusion pathways that are more tortuous (meandering) than those that exist in the absence of the porous medium [39]. Our assumption is that this effect is the same or very similar for the diffusion of all the metal ions studied in this work. Therefore, this reduction effect was likely to be the same in all realized experiments. The most important effect of the reactive humic hydrogel and the distinctive differences between the used metals can be characterized by the values of the effective diffusion coefficients D_{eff} and the resulting values of the apparent equilibrium constants K_{app}.

4. Conclusions

In conclusion, we showed that the diffusion characteristics of metal ions in humic hydrogels are strongly affected by their reactivity. Comparing the diffusion characteristics of Co, Cu and Ni, the differences characterizing the affinity of the metals to humic acids in dynamic conditions can be obtained. It was found that the most mobile metal was Ni whose mobility was impaired by humic acids only slightly. In contrast, the high affinity of Cu to humic acids resulted in the lowest effective diffusion coefficient. In this case, the low value of D_{eff} was not directly connected with the diffusion rate. The diffusion rate can be defined as “how fast particles spontaneously move through unit area”. The diffusivity or mobility of Cu in water, characterized by D°, was comparable with that of Co and Ni. Frequent interactions between Cu and humic acids caused a decrease in the value of D_{eff} as a consequence of K_{app} being in the denominator in Eq. (7). However, the driving force of diffusion was the concentration gradient (or more exactly the gradient of chemical potential). The immobilization of Cu in humic hydrogel thus caused a decrease in free mobile metal and (as a result of this decrease) an increase in the concentration gradient.

The diffusion experiments presented in this work can be used to characterize the mobility, reactivity, and bioavailability of metals in systems containing humic acids or organic matter. They can be used to resolve issues directly related to specific environmental problems or in studies concerning the development of hydro-gels for the controlled transport of plant nutrients.

Acknowledgments

The Materials Research Centre at the Faculty of Chemistry, Brno University of Technology is supported by Project No. LO1211 from the Czech Ministry of Education, National Sustainability Program I.

References

[1] L. Hongyan, W. Jinsbeng, W. Zhenyu, Study on the mechanism of transport of heavy metals in soil in western suburh of Beijing, Chin. J. Geochem. 25 (2006) 173–177.
[2] S. Hermle, M.S. Gunthardt-Goerg, R. Schulin, Effects of metal-contaminated soil on the performance of young trees growing in model ecosystems under field conditions, Environ. Pollut. 144 (2006) 703–714.
[3] S. Montinaro, A. Concas, M. Pisu, G. Cao, Rationale of lead immobilization by ball milling in synthetic soils and remediation of heavy metals contaminated tailings, Chem. Eng. J. 155 (2009) 123–131.
[4] J. Lee, K. Sung, Effects of chelates on soil microbial properties, plant growth and heavy metal accumulation in plants, Ecol. Eng. 73 (2014) 386–394.
[5] D. Jacques, J. Simunek, D. Mallants, M.Th. van Genuchten, Modelling coupled water flow, solute transport and geochemical reactions affecting heavy metal migration in a podzol soil, Geoderma 145 (2008) 449–461.
[6] A.L. Perez, K.A. Anderson, Soil-diffusive gradient in thin films partition coefficients estimate metal bioavailability to crops at fertilized field sites, Environ. Toxicol. Chem. 28 (2009) 2030–2037.
[7] H. Martyniuk, J. Wieckowska, Adsorption of metal ions on humic acids extracted from brown coal, Fuel Process. Technol. 84 (2003) 23–36.
[8] R.A. Alvarez-Puebla, C. Valenzuela-Calahorro, J.J. Garrido, Retention of Co(II), Ni (II), and Cu(II) on a purified brown humic acid. Modeling and characterization of the sorption process, Langmuir 24 (2004) 3657–3664.
[9] M. Klucakova, M. Pekar, New model for equilibrium sorption of metal ions on solid humic acids, Colloids Surf. A 286 (2006) 126–133.
[10] M.H. Shaker, M.A. Hassan, Dynamics and thermodynamics of toxic metals adsorption onto soil-extracted humic acid, Chemosphere 111 (2014) 587–595.
[11] M. Kalina, M. Klucakova, P. Sedlacek, Utilization of fractional extraction for characterization of the interactions between humic acids and metals, Geoderma 207–208 (2013) 92–98.
[12] M. Klucakova, M. Kalina, P. Sedlacek, L. Grasset, Reactivity and transport mapping of Cu(II) ions in humic hydrogels, J. Soils Sediments 14 (2014) 368–376.
[13] M. Klucakova, M. Kalina, Diffusivity of Cu(II) ions in humic gels - influence of reactive functional groups of humic acids, Colloids Surf. A 483 (2015) 162–170.
[14] M. Klucakova, M. Pavlikova, Lignitic humic acids as environmental friendly adsorbent for heavy metals, J. Chem. 2017 (2017) 1–5.
[15] J. Cao, K.C. Lam, R.W. Dawson, W.X. Liu, S. Tao, The effect of pH, ion strength and reactant content on the complexation of Cu^{2+} by various natural organic ligands from water and soil in Hong Kong, Chemosphere 54 (2004) 507–514.
[16] J.M. Garcia-Mina, Stability, solubility and maximum metal binding capacity in metal-humic complexes involving humic substances extracted from peat and organic compost, Org. Geochem. 37 (2006) 1960–1972.
[17] M.L. Antonelli, N. Calace, D. Centioli, B.M. Petronio, M. Pietroletti, Complexing capacity of different molecular weight fractions of sedimentary humic substances, Anal. Lett. 34 (2001) 989–1002.
[18] H. Baker, F. Khalili, Comparative study of binding strengths and thermodynamic aspects of Cu(II) and Ni(II) with humic acid by Schubert’s ion-exchange method, Anal. Chim. Acta 497 (2003) 235–248.
[19] F.A. Vega, M.L. Andrade, E.F. Covelo, Influence of soil properties on the sorption and retention of cadmium, copper and lead, separately and together, by 20 soil horizons: comparison of linear regression and tree regression analyses, J. Hazard. Mater. 174 (2010) 522–533.
[20] A. de Santiago-Martin, I. Valverde-Asenjo, J.R. Quintana, C. Gonzalez-Huecas, A.L. Lafuente, Soil properties affecting metal extractability patterns in periurban calcareous agricultural soils in the Mediterranean area, Int. J. Environ. Res. 7 (2013) 831–840.
[21] M. Klucakova, Complexation of metal ions with solid humic acids, humic colloidal solutions, and humic hydrogel, Environ. Eng. Sci. 31 (2014) 612–620.
[22] N.D. Bryan, D.L.M. Jones, R.E. Keepax, D.H. Farrelly, L.G. Abrahamsen, A. Pitois, P. Ivanov, P. Warwick, N. Evans, The role of humic non-exchangeable binding in the promotion of metal ion transport in groundwaters in the environment, J. Environ. Monit. 9 (2007) 329–347.
[23] H. Lippold, S. Eidner, M.U. Kumke, J. Lippmann-Pipke, Diffusion, degradation or on-site stabilisation - Identifying causes of kinetic processes involved in metal-humate complexation, Appl. Geochem. 27 (2012) 250–256.
[24] P. Chakraborty, A. Manek, S. Niyogi, J. Hudson, Determination of dynamic metal complexes and their diffusion coefficients in the presence of different humic substances by combining two analytical techniques, Anal. Lett. 47 (2014) 1224–1241.
[25] N.M. Hassan, J.D. Murimboh, A.L. Sekaly, R. Mandal, C.L. Chakraborti, D.C. Gregoire, Cascade ultrafiltration and competing ligand exchange for kinetic speciation of aluminium, iron, and nickel in fresh water, Anal. Bioanal. Chem. 384 (2006) 1558–1566.
[26] M. Klucakova, M. Pekar, Study of diffusion of metal cations in humic gels, in: E.A. Ghabbour, G. Davies (Eds.), Humic Substances: Nature`s Most Versatile Materials, Taylor & Francis, New York, 2004, pp. 263–273.
[27] I.S. Kostic, T.D. Andelkovic, R.S. Nikolic, T.P. Cvetkovic, D.D. Pavlovic, A.L. Bojic, Comparative study of binding strengths of heavy metals with humic acid, Hem. Ind.

67 (2013) 773–779.
[28] K. Furukawa, Y. Takahashi, Effect of complexation with humic substances on diffusion of metal ions in water, Chemosphere 73 (2008) 1272–1278.
[29] J. Crank, The Mathematics of Diffusion, Clarendon Press, Oxford, 1956.
[30] E.L. Cussler, Diffusion Mass: Transfer in Fluid Systems, Cambridge University Press, Cambridge, 1984.
[31] M. Klucakova, M. Pekar, Transport of copper(II) ions in humic gel – new results from diffusion couple, Colloids Surf. A 349 (2009) 96–101.
[32] P. Sedlacek, M. Klucakova, Diffusion experiments as a new approach to the evaluation of copper transport in humics-containing systems, Collect. Czech. Chem. C. 74 (2009) 1323–1340.
[33] M. Klucakova, R. Kolajova, Dissociation ability of humic acids: spectroscopic determination of pK_a and comparison with multi-step mechanism, React. Funct. Polym. 78 (2014) 1–6.
[34] S.L. Khilko, A.I. Kovtun, V.I. Rybachenko, Potentiometric titration of humic acids, Solid Fuel Chem. 45 (2011) 337–348.
[35] M. Kurkova, Z. Klika, C. Klikova, J. Havel, Humic acids from oxidized coals I. Elemental composition, titration curves, heavy metals in HA samples, nuclear magnetic resonance spectra of HAs and infrared spectroscopy, Chemosphere 54 (2004) 1237–1245.
[36] J. Peuravuouri, P. Zbankova, K. Pihlaja, Aspects of structural features in lignite and lignite humic acids, Fuel Process. Technol. 87 (2006) 829–839.
[37] M. Klucakova, M. Pekar, Study of structure and properties of humic and fulvic acids. IV. Study of interactions of Cu^{2+} ions with humic gels and final comparison, J. Polym. Mater. 20 (2003) 155–162.
[38] F.A.L. Dullien, Porous Media. Fluid Transport and Pore Structure, Academic, San Diego, 1992.
[39] C.D. Shackelford, S.M. Moore, Fickian diffusion of radionuclides for engineered containment barriers: diffusion coefficients, porosities, and complicating issues, Eng. Geol. 152 (2013) 133–147.
[40] W.M. Haynes, D.R. Lide, T.J. Bruno, CRC Handbook of Chemistry and Physics, CRC Press, London, 2012.
[41] M. Paradelo, P. Perez-Rodriguez, D. Fernandez-Calvino, M. Arias-Estevez, J.E. Lopez-Periago, Coupled transport of humic acids and copper through saturated porous media, Eur. J. Soil Sci. 63 (2012) 708–716.
[42] B. Krajewska, Diffusion of metal ions through gel chitosan membranes, React. Funct. Polym. 47 (2001) 37–47.

Bull Environ Contam Toxicol (2017) 98:373–377
DOI 10.1007/s00128-016-1926-0

Transport of Organic Compounds Through Porous Systems Containing Humic Acids

Jiri Smilek[1] · Petr Sedlacek[1] · Marcela Lastuvkova[1] · Michal Kalina[1] · Martina Klucakova[1]

Received: 11 January 2016 / Accepted: 15 September 2016 / Published online: 22 September 2016

Abstract Soil pollution by the presence of different contaminants (e.g. heavy metal ions or pesticides) is one of the biggest problems worldwide. The positive affinity of natural humic acids towards these contaminants might contribute to the soil and ground water protection; therefore it is necessary to study the reactivity and barrier properties of humic acids. An original reactivity-mapping tool based on diffusion techniques designed to study the reactivity and barrier properties of polyelectrolytes was developed and tested on humic acids. The results of diffusion experiments demonstrate that the electrostatic interactions between humic acids functioning as a polyelectrolyte interpenetrated in a supporting hydrogel matrix (agarose) and cationic dye (methylene blue) as a model solute have a crucial impact on the rate of diffusion processes and on the barrier properties of hydrogels. The intensity of interactions was evaluated by fundamental diffusion parameters (effective diffusion coefficients and breakthrough time). The impact of modification of humic acids was also studied by means of diffusion experiments conducted on two types of standard humic acids (Leonardite 1S104H) and humic acids with selectively methylated carboxylic groups.

Keywords Humic acids · Reactivity-mapping tool · Diffusion · Hydrogel · Transport properties

✉ Jiri Smilek
xcsmilek@fch.vutbr.cz

[1] Faculty of Chemistry, Materials Research Centre, Brno University of Technology, Purkynova 118/464, 612 00 Brno, Czech Republic

Humic acids (HAs) are complex substances which are a crucial component of soil. Their role in the natural environment is indisputable, especially in the case of pollutant binding. The most important aspect of humic acids in the natural environment (i.e. in soil) is their capacity for pollutant complexation. Humic acids have a relatively high affinity towards common pollutants (i.e. heavy metal ions, pesticides, etc.). This capacity has been reported in several publications (Schnitzer and Khan 1972; Kördel et al. 1997; Tipping 2002; Sachs and Bernhard 2011; Lishtvan et al. 2012). Interactions between humic acids and pollutants are mostly given by carboxylic and phenolic functional groups. The complex structure of humic acids and the presence of diverse functional groups such as carboxylic groups and phenolic groups have been widely reported (Ritchie and Perdue 2003; Fukushima and Nakayasu 1995).

From another perspective, the positive affinity and sorption ability of humic acids to common pollutants may also be given by the presence of hydrophobic centres (De Paolis and Kukkonen 1997; Ran et al. 2007), which are predominantly responsible for these interactions while the presence of acidic functional groups has only a minor influence. Verification of the role of acidic functional groups in comparison with that of hydrophobic centres in interactions between humic acids and pollutants was one of the main goals of this study.

Humic acids belong to the extensive group of natural biocolloids. Chemistry of humic acids is relatively well known and very well described in literature (Stevenson 1994). One of the most important gaps in the knowledge of humic acids (generally biocolloids or polyelectrolytes) is their reactivity. This is mostly studied by classical sorption experiments (Martyniuk and Wieckowska 2003; Bradl and Acikel 2004) but such experiments have several deficiencies. Firstly, sorption experiments are mostly conducted on humic acids

in solid form; however in the natural environment, humic acids are mostly in the colloid or hydrogel form. Further, the sorption of active compounds (i.e. heavy metal ions) is mostly realized on the surface of humic acids; i.e. that only the surface reactivity of humic acids can be studied by classical sorption experiments. Therefore, simple diffusion techniques for studying the reactivity of humic acids have been developed. These methods are based on the assumption that humic acids are homogeneously distributed in the agarose hydrogel used for diffusion experiments. In several works (Klucakova and Pekar 2003, 2006, 2009; Klucakova et al. 2013), the reactivity of humic acids was studied by means of their interaction with heavy metal ions (Cu^{2+}) and the effective diffusion coefficients (diffusion coefficients where the tortuous movement of diffusing matter and the chemical interactions between humic acids and heavy metal ions are involved), and sorption capacities of humic-like hydrogels were determined as the main transport parameters of diffusion processes.

The aim of this paper is to offer a new approach to studying the reactivity of HAs, namely the use of unconventional diffusion techniques (non-stationary diffusion in cuvettes and diffusion cell technique) in hydrogel media. For the routine determination of basic diffusion parameters, such as diffusion coefficients, lag time, and sorption capacity in semi-solid samples (e.g. gels), the presented method employing diffusion cells represents one of the best choices for these experiments. A diffusion cell method is based on measurement of the time needed by the solute to penetrate through the porous hydrogel and, after penetration, for its flux to achieve a steady state (Sedlacek et al. 2013; Smilek et al. 2015). A diffusion cell technique is mainly used for the routine determination of diffusion parameters through the human dermis (Ibrahim and Kasting 2012) or the penetration of drugs through synthetic membranes (Mustapha et al. 2011). However, the diffusion cell technique also seems to be of value for studying the reactivity of active compounds in supporting porous media (e.g. hydrogels).

Materials and Methods

Agarose (routine use class, <10 wt% moisture content) and Methylene Blue hydrate (MB, CI Basic Blue 9, dye content, ≥95 wt%) were purchased from Sigma–Aldrich and were used without further purification.

Standard samples of humic acids (IHSS) were obtained from the International Humic Substances Society (Leonardite 1S104H). Modified humic acids were prepared via methylation using trimethylsilyl-diazomethan. The procedure of modification is described in detail in literature (Klucakova et al. 2013). The modification procedure adjusts the amount of acidic carboxylic groups. Carboxylic groups are covered by methyl- groups during modification; therefore the influence of carboxylic acidity on the reactivity of humic acids is eliminated. The presence of carboxylic groups in the structure of humic acids was tested by FTIR (Klucakova et al. 2013).

Diffusion experiments described in this paper were conducted in a supporting hydrogel matrix based on linear polysaccharide agarose. The preparation of interpenetrating polymer network (IPN) from humic acids in a supporting hydrogel-forming polymer based on agarose was achieved via thermoreversible processes. The network of agarose chains is interpenetrated by molecules of humic acids at higher temperatures –in our study the mixture dissolved at 85°C and was then poured into a pre-heated mould. The used concentrations of humic acids were 0.002 wt%, 0.005 wt% and 0.010 wt%. The fourth sample was a pure agarose hydrogel without the addition of HAs, used as a reference. Each agarose solution with/without humic acids was poured into a pre-heated PTFE mould, and glass slides (also pre-heated) were placed on the opposite sides of the mould. A mixture of agarose with humic acids gradually solidified into a cylindrical hydrogel plate sample (40 mm in diameter and 5 mm thick).

The hydrogel in the PTFE mould was placed between the two chambers of the diffusion cell. The first chamber of diffusion cell was filled with 0.01 g dm^{-3} Methylene Blue (Sigma–Aldrich, purity >95 wt%) and the second chamber was filled with deionized water. Both chambers of the diffusion cell were filled simultaneously with 60 cm^3 of solutions. A circulating water bath was used in order to keep the experiments at constant temperature (30°C). The change in concentration of the diffusion probe was determined by USB 2000+ ultraviolet–visible fibre spectrometer (Ocean Optics, Inc.) in the acceptor part of diffusion cell as a function of time. The ultraviolet–visible spectra were collected continuously at given time intervals. After termination of diffusion experiments, the absorbance in the donor part of the diffusion cell was measured, and the concentration of solute in the hydrogel was calculated as from the difference of concentration at the beginning and the end of the experiment. The water-jacketed side-by-side diffusion cell was purchased from Permegear Inc. (Fig. 1).

Results and Discussion

The diffusion process in the diffusion cell can be divided into two discrete steps: (1) sorption, (2) steady state flux. During the first stage, the concentration of the diffusion probe does not change in the acceptor compartment of the diffusion cell. The diffusion probe (a simple organic dye) may interact with humic acids until all functional groups (or hydrophobic centres) are occupied by dye molecules. After that,

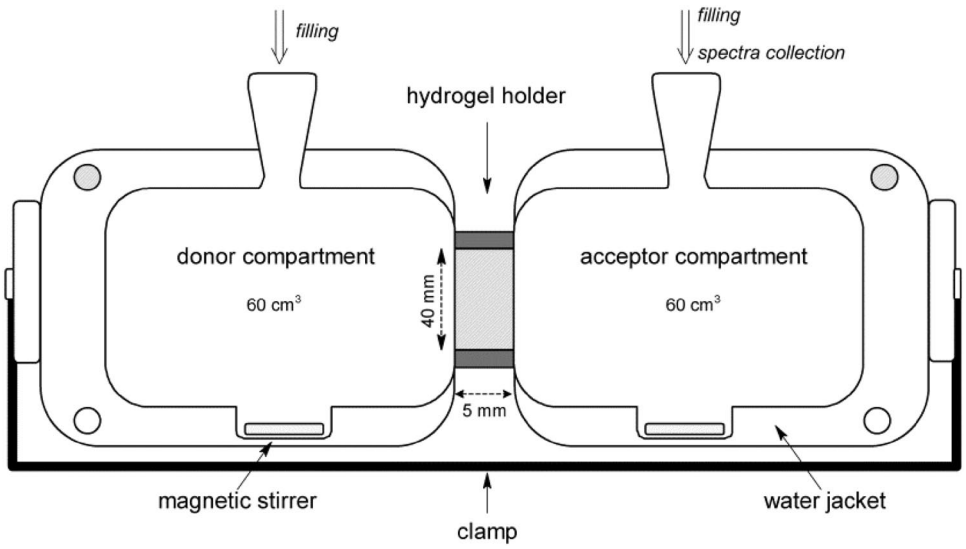

Fig. 1 Schematic drawing of the diffusion cell apparatus

the concentration of the diffusion probe will begin to change in the acceptor compartment and the steady state stage will occur. The steady state flux can be determined by fitting the linear part of the break-through curve (steady-state stage), while the break-through time (lag time) is calculated from the x-axis intercept (Fig. 2) the time when the first molecule of organic dye penetrated through the porous agarose hydrogel with/without addition of humic acids. From the steady state flux, the effective diffusion coefficient as one of the most important parameter can be calculated according to Eq. 1.

$$D_{\text{eff}} = \left(\frac{\mathrm{d}n}{\mathrm{d}t}\right)\left(\frac{l}{\Delta c}\right) \quad (1)$$

where D_{eff} is effective diffusion coefficient, $\mathrm{d}n/\mathrm{d}t$ is the change of moles of organic dye with time, l is thickness of the porous agarose hydrogel and Δc is the difference of concentration of organic dye in donor and acceptor part of diffusion cell at the beginning of the experiment.

A detailed description of mathematical apparatus used for calculation of diffusion parameters is described in our previous work (Sedlacek et al. 2013).

It is obvious that the increasing concentration of humic acids in the agarose hydrogel sample slowed down the rate of diffusion processes. This finding is supported by the increasing lag time (the time needed for the penetration of the dye through the hydrogel sample) and by the decreasing slope of the linear part of the curve with the increasing content of humic acids in the agarose hydrogel. The effective diffusion coefficients were calculated from the linear parts of the break-through curves (Fig. 2). The calculated values of the effective diffusion coefficients for agarose hydrogels with or without the addition of humic acids are shown in Fig. 3.

The values of the effective diffusion coefficients decreased with the increasing concentration of humic acids for both tested humic acids (native and methylated). It should be noted that the effective diffusion coefficients for methylated IHSS humic acids were lower in comparison with the effective

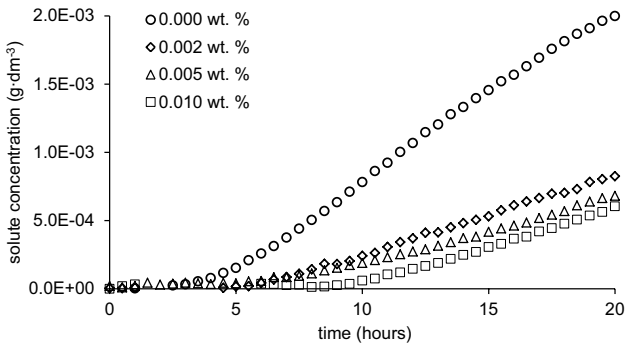

Fig. 2 The change of concentration of methylene blue in acceptor part of diffusion cell as a function of time for 1 wt% agarose hydrogel with increasing concentrations of native IHSS humic acids

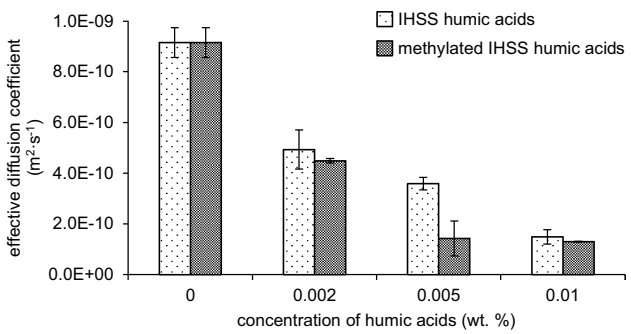

Fig. 3 The effective diffusion coefficients of methylene blue in 1 wt% hydrogels with increasing concentrations of native IHSS humic acids in hydrogel in comparison with methylated IHSS humic acids

diffusion coefficients for native IHSS humic acids. Therefore we can believe that the effective diffusion coefficients (which reflect the rate of positive interactions between anionic humic acids and cationic methylene blue) would be lower for native humic acids with non-blocked carboxylic groups. Such groups are available for interaction with cationic methylene blue because according to theoretical assumptions, the positive affinity or rate of interactions of humic acids with cationic compounds is given mainly by the presence of acidic functional groups in the structure of humic acids (Guo-Ping et al. 2009). From the comparison of effective diffusion coefficients for native and methylated IHSS humic acids (Fig. 3), it is obvious that the presence of carboxylic groups in the structure of humic acids is not as important as we expected. This represents a very interesting finding regarding the transport and barrier properties of humic acids. Interactions between humic acids and cationic compounds are much more complex and are given not only by acidic functional groups but also by other effects in complex structure of humic acids such as non-electrostatic binding (Zanini et al. 2006) or the hydrophobicity of humic acids (Murphy et al. 1994).

Diffusion coefficients, calculated from the linearly increasing concentration of methylene blue in the acceptor cell, are one of the most important parameters illustrating the interaction between the methylene blue and humic content in the studied hydrogels. Another important parameter providing useful information about the reactivity, transport and barrier properties of humic acids in hydrogel media is the break-through time or so-called lag time (the time needed for the first molecule of methylene blue to penetrate through the hydrogel into the acceptor cell). From Fig. 4, it is evident from the increasing lag times that increasing the amount of humic acids in the hydrogel slows down the diffusion of the dye breaking through the hydrogel in comparison with pure agarose hydrogel without addition of humic acids because the lag time distinctly increases with increasing the concentration of humic acids in agarose hydrogels. In the case of addition of 0.010 wt% of humic acids (without modification) to the same agarose hydrogel, the penetration time increases to more than 14 h for native humic acids and more than 10 h for methylated humic acids. This is given by specific interactions between humic acids and the cationic organic dye.

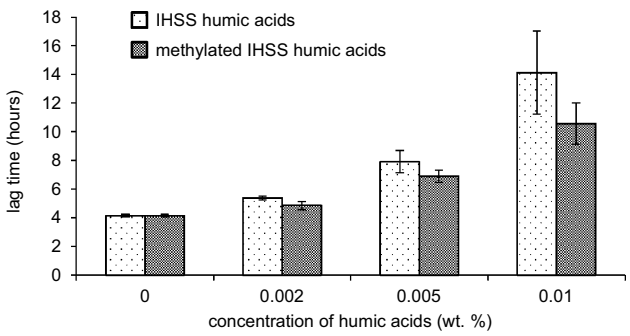

Fig. 4 The break-through time (lag time) for 1 wt% agarose hydrogels with different concentrations of humic acids (native and methylated)

The modification of humic acids –in particular, the selective blocking of carboxylic groups has a minor influence on the reactivity and barrier properties of standard humic acids because the differences in the two main diffusion parameters (effective diffusion coefficients and break-through time) are not so significant. Changes of absolute values of lag time for both studied humic acids are at the level of error bars. One of the most important findings is that the presence of acidic functional groups in the structure of humic acids is not as significant as we expected. The positive affinity of humic acids to cationic compounds, especially organic dyes is given not only by specific functional groups, but also by other effects such as hydrophobicity or non-covalent interactions (Simpson et al. 2004).

The unconventional diffusion techniques presented in this paper represent a very challenging and useful tool for mapping the reactivity, barrier, and transport properties of biocolloids or biopolymers. Innovative diffusion approaches seem to give much more information about the reactivity of humic acids in their natural environment than classical sorption experiments because the results obtained from sorption experiments are strongly dependent on the particle size of the humic acids and the level of homogeneity. These disadvantages are eliminated when experiments are conducted in hydrogel media. Hydrogel contains a high percentage of water; therefore it is able to simulate the real environment of humic acids. From an experimental point of view, hydrogel is easy to be prepared in exact shapes and thicknesses, and knowledge of these parameters is necessary for the mathematical description of diffusion processes. These methods also seem to be suitable for experiments running under different conditions (e.g. the use of different temperatures, different ionic strengths, and different values of pH), which can be in these methods easily controlled. Diffusion experiments based on the presented diffusion techniques could also become a universal method applicable for studying the reactivity of different compounds under different conditions.

Acknowledgments This work was supported by the project "Materials Research Centre at FCH BUT—Sustainability and Development" No. LO1211 of the Ministry of Education, Youth and Sports of the Czech Republic and by project "Multiscale study on the structure–transport–flow relationship in the behavior of biopolymer–based hydrogels" COST LD15047.

References

Bradl HB, Acikel YS (2004) Adsorption of heavy metal ions on soils and soils constituents. J Colloid Interface Sci 277:183–223. doi:10.1016/j.jcis.2004.04.005

De Paolis F, Kukkonen J (1997) Binding of organic pollutants to humic and fulvic acids: influence of pH and the structure of humic material. Chemosphere 34:1693–1704. doi:10.1016/S0045-6535(97)00026-X

Fukushima M, Nakayasu K (1995) Chromium (III) binding abilities of humic acids. Anal Chim Acta 317:195–206. doi:10.1016/0003-2670(95)00410-6

Guo-Ping S, Meng-Lin Z, Han-Qing Y (2009) Quantification of the interactions between a cationic dye and humic substances in aqueous solutions. J Colloid Interface Sci 331:15–20. doi:10.1016/j.jcis.2008.11.006

Ibrahim R, Kasting GB (2012) Partitioning and diffusion of parathion in human dermis. Int J Pharm 435:33–37. doi:10.1016/j.ijpharm.2012.03.023

Klucakova M, Pekar M (2003) Study of structure and properties of humic and fulvic acids. IV. Study of interactions of Cu^{2+} ions with humic gels and final comparison. J Polym Mater 20:155–162. doi:10.1016/j.colsurfa.2009.08.001

Klucakova M, Pekar M (2006) New model for equilibrium sorption of metal ions on solid humic acids. Colloid Surf A 286:126–133. doi:10.1016/j.colsurfa.2006.03.013

Klucakova M, Pekar M (2009) Transport of copper(II) ionts in humic gel—new results from diffusion couple. Colloid Surf A 349:96–101. doi:10.1016/j.colsurfa.2009.08.001

Klucakova M, Kalina M, Sedlacek P, Grasset L (2013) Reactivity and transport of Cu(II) ions in humic hydrogels. J Soils Sediments 14:579–583. doi:10.1007/s11368-013-0730-2

Kördel W, Dassenakis M, Lintalmann J, Padberg S (1997) The importance of natural organic material for environmental processes in waters and soils. Pure Appl Chem 69:1571–1600. doi:10.1351/pac199769071571

Lishtvan II, Yanuta YG, Abramets AM, Monich GS, Glukhova NS, Aleinikova VN (2012) Interaction of humic acids with metal ions in the water medium. J Water Chem Technol 34:211–217. doi:10.3103/S1063455X12050013

Martyniuk H, Wieckowska J (2003) Adsorption of metal ions on humic acids extracted from brown coals. Fuel Proces Technol 84:23–36. doi:10.1016/S0378-3820(02)00246-1

Murphy EM, Zachara JM, Smith SC, Phillips JL, Wietsma TW (1994) Interaction of hydrophobic organic compounds with mineral-bound humic substances. Envrion Sci Technol 28:1291–1299. doi:10.1021/es00056a017

Mustapha RB, Lafforgue C, Fenina N, Marty JP (2011) Influence of drug concentration on the diffusion parameters of caffeine. Indian J Pharmacol 43:157–162. doi:10.4103/0253-7613.77351

Ran Y, Sun K, Yang Y, Xing B, Zeng E (2007) Strong sorption of phenanthrene by condensed organic matter in soils and sediments. Environ Sci Technol 41:3952–3958. doi:10.1021/es062928i

Ritchie JD, Perdue EM (2003) Proton-binding study of standard and reference fulvic acids, and natural organic matter. Geochim Cosmochim Acta 67:85–88. doi:10.1016/S0016-7037(02)01044-X

Sachs S, Bernhard G (2011) Humic acid model substances pronounced redox functionality for the study of environmentally relevant interaction processes of metal ions in the presence of humic acid. Geoderma 162:132–140. doi:10.1016/j.geoderma.2011.01.012

Schnitzer J, Khan SU (1972) Humic subtances in the environment. Marcel Dekker Inc, New York

Sedlacek P, Smilek J, Klucakova M (2013) How the interactions with humic acids affect the mobility of ionic dyes in hydrogels—1. Results from diffusion cells. React Funct Polym 73:1500–1509. doi:10.1016/j.reactfunctpolym.2013.07.008

Simpson MJ, Simpson AJ, Hatcher PG (2004) Noncovalent interactions between aromatic compounds and dissolved humic acid examined by nuclear magnetic resonance spectroscopy. Environ Toxicol Chem 23:355–362. doi:10.1897/03-217

Smilek J, Sedlacek P, Kalina M, Klucakova M (2015) On the role of humic acids' carboxyl groups in the binding of charged organic compounds. Chemosphere 138:503–510. doi:10.1016/j.chemosphere.2015.06.093

Stevenson F (1994) Humus chemistry: genesis, composition, reactions. Wiley, London

Tipping E (2002) Cation binding by humic substances. Cambridge University Press, Cambridge

Zanini GP, Avena MJ, Fiol S, Arce F (2006) Effects of pH and electrolyte concentration on the binding between a humic acid and an oxazine dye. Chemosphere 63:430–439. doi:10.1016/j.chemosphere.2005.08.053

Journal of Materials Education Vol. 39 (1-2): 59 – 90 (2017)

HYDROGELS: INVALUABLE EXPERIMENTAL TOOL FOR DEMONSTRATING DIFFUSION PHENOMENA IN PHYSICAL CHEMISTRY LABORATORY COURSES

Petr Sedláček*, Jiří Smilek, Marcela Laštůvková, Michal Kalina and Martina Klučáková

Faculty of Chemistry, Brno University of Technology, Purkynova 118, 612 00 Brno, Czech Republic
* *Corresponding author: sedlacek-p@fch.vut.cz*

ABSTRACT

An original experimental methodology, which provides both qualitative and quantitative insights into fundamental diffusion processes, is described and proposed for use in a variety of laboratory courses, e.g., chemical-biological engineering, materials science and physical chemistry.

In the proposed experiments, transient and stationary diffusion flow of a colored solute is studied in an aqueous solution entrapped in an agarose gel matrix. Furthermore, the demonstration of the effect of the reaction between the solute and the gel matrix is illustrated through the addition of a reactive polyelectrolyte component into the gel structure. The proposed methodology is intended for higher-level undergraduate physical chemistry laboratory classes. It also has applications at many levels of materials science and engineering education, as it allows for direct and timely observation, as well as practical experience in data acquisition and analysis of basic diffusion concepts.

INTRODUCTION

Apart from comprehensive theoretical knowledge of specific physical and chemical phenomena, outcomes for students studying physical chemistry at a university require also the ability to apply such knowledge to practical experience and to the problems of everyday life. These attributes are especially important to students majoring in materials science and engineering (MSE) where the fundamental paradigm is learning how to predict and control the changes that occur due to reaction of various materials with their environment. The phenomena may involve many states of matter, but the essential mechanisms of change commonly depend on mass transport by diffusion. In general, diffusion represents an interesting example of an area of overlap between Chemistry and Materials Science and Engineering (other examples can be found elsewhere[1,2]). The understanding of diffusion through planned observation, data acquisition and analysis represents a solid example of how the teaching and learning of physical chemistry through well-structured laboratory experiments contributes to such fundamental behavior of materials. On one hand, as a ubiquitous

phenomenon affecting both the natural and synthetic world as well as the vast majority of technological procedures of various kinds, diffusion is undoubtedly seen as an essential topic in theoretical courses on physical chemistry, where it usually poses a difficulty for students due to its complicated and often incomprehensible mathematical formalism, e.g., the "error function" concept (for details on the mathematics of diffusion, see e.g. Cranck[3]). On the other hand, rarely do students get practical familiarization with diffusion phenomena, e.g. in laboratory courses in physical chemistry as well as in MSE courses.

Experimental demonstration of a diffusion process is usually performed either in liquids or gases, where the typical diffusion rates are high enough to be observable in a reasonably available timeframe i.e., minutes, hours, or days. Hence, diffusion phenomena are often demonstrated in simple experiments like placing a few crystals of a colored substance (e.g. copper sulphate) at the bottom of a water-filled beaker and observing as the color consequently gently spreads throughout the bottle. Unfortunately, such experiments always entail some inevitable interference processes such as the convective flow of the liquid caused by the inhomogeneity in temperature or the density of the solution. Furthermore, these experiments usually provide little opportunity for the investigating the diffusion in a quantitative way and thus confront the experimental analysis/interpretation with hard to apply knowledge of diffusion mathematics. Several attempts have been made to optimize solution diffusion experiments for under-graduate chemistry courses. For instance, King et al.[4] proposed a simple laser refraction technique for the measuring the diffusion coefficients of liquids. The method is quick, accurate and offers a good visualization of the diffusion process.

In this report, we will demonstrate that the frequent serious drawbacks of the above-mentioned demonstrations can be circumvented by carrying out the diffusion experiments in a hydrogel medium instead of a liquid. Hydrogels[5,6] combine their solid (continuous network of polymer molecules or colloidal particles) and liquid fraction (aqueous solution) into a unique composite structure which possesses beneficial properties from the diffusion-related point of view. Because the greater part of gels by weight is made up of an aqueous solution, the corresponding diffusion rate is almost as high as in the solution alone. Nevertheless, in comparison with the solution, convective flow is markedly suppressed by the continuous solid network, or matrix, of the gel.

Hydrogel media are already commonly applied in demonstrations of some special diffusion-related phenomena such as those presented in Figure 1[†]. Chemical gardens, a phenomenon discovered more than three centuries ago[7], represent not only a popular chemical experiment for middle-school chemistry lessons, but nowadays there is also a growing interest in them in disciplines as varied as chemistry, physics, nonlinear dynamics and materials science[8,9]. Liesegang rings, periodical bands or ring patterns formed by inorganic precipitation in a polymer gel medium, have attracted the attention of chemists, geologists and biologists, in experiments in order to understand natural patterning. Although numerous qualitative and mathematically formulated models have been suggested, we still lack a complete explanation of both phenomena[10].

[†] Preparation of the 'chemical garden' shown in Fig. 1: the glass container was filled up by waterglass (sodium silicate). On the bottom of the container the solid crystals of multivalent ions of metals (cobalt chloride, copper chloride, nickel chloride, magnesium chloride or ferric sulphate) were added.
Preparation of Liesegang rings shown in Fig. 1: 2 wt. % agarose hydrogel with addition of 0.002 M potassium dichromate (C) or 0.2 M cobalt chloride (D) was prepared in glass tubes. On the top of the glass tubes, 0.1 M silver nitrate (C) or concentrated ammonia (D) was poured. As the ions diffuse from the respective solution into the hydrogel, sharp concentric rings of insoluble hexa-amine-cobalt (II) ions (C) or silver chromate (D) are formed wherever concentration of the produced salt exceeds the respective solubility product constant.

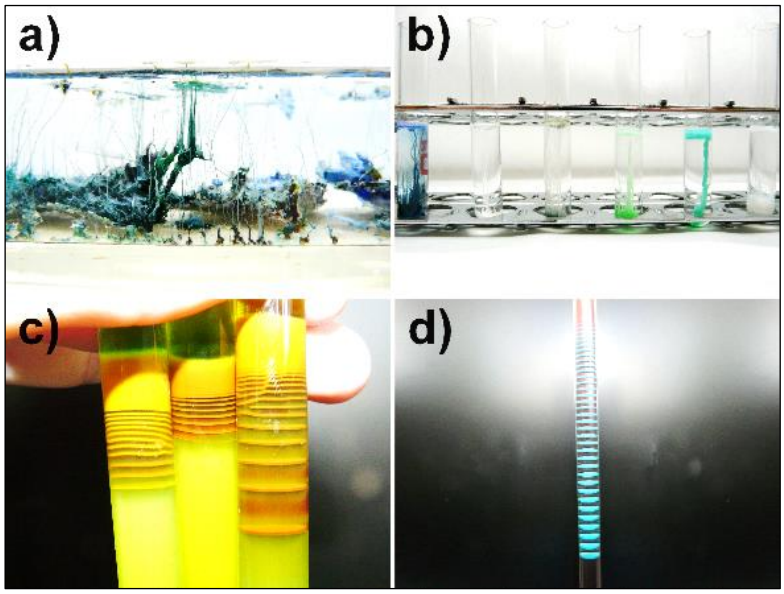

Figure 1. Common practical demonstrations of diffusion-related phenomena in hydrogels: chemical gardens (a, b), Liesegang rings (c, d). The characteristic fibrous pattern of the chemical gardens is a consequence of the specific permeability of metal silicate colloidal gel, which forms around a crystal of a dissolving metal salt in the water-glass solution. On the other hand, periodic patterning of a weakly soluble salt in the Liesegang phenomenon is well observable in gels where the patterns are not destroyed by convection or sedimentation.

In the current paper, we extend the traditional use of hydrogel in educational diffusion demonstrations by introducing a simple experimental methodology which provides both a qualitative and a quantitative insight into two fundamental diffusion processes: transient and steady-state diffusion flow of a colored solute in aqueous solution entrapped in an agarose gel matrix. Furthermore, it involves a demonstration of the effect of the reaction between the solute and the gel matrix by the addition of a reactive component into the gel structure. The proposed methodology is intended for use in higher-level undergraduate laboratory classes of physical chemistry and is adaptable to instruction in related disciplines, such as materials science and engineering. In the Experimental section, we present a general experimental procedure, which allows for adaptation to the particular requirements of the laboratory course supervisor in such things as the selection of chemicals used. The proposed methodology was tested and optimized with students employing agarose hydrogels as a diffusion media, cationic organic dyes as diffusing compounds and model synthetic and natural polymers as the reactive components of the gel. Selected experimental data as determined for these systems are presented in Results and Discussion.

THEORY

Hydrogels

The term hydrogel describes a three-dimensional network structure obtained from a class of synthetic/natural polymers, which can absorb and retain significant amount of water. Hydrogels are defined as substantially diluted cross-linked systems formed by three-dimensional polymeric networks[11]. Hydrogel is a colloid dispersion system, in which the dispersion phase (solid) combines with the dispersion medium (liquid) to produce a semisolid material. Hydrogels can be prepared by changing the physical conditions of

solutions (temperature, pH, and level of electrolyte); covalent hydrogels can be prepared by means of chemical reactions. Covalently cross-linked hydrogels have better mechanical properties than physically cross-linked ones. Another method of hydrogel preparation is swelling[12] (the addition of dispersion medium to a compact xerogel – the dispersion phase without the dispersion medium). Despite the majority of the hydrogel volume being made up of water, it has the properties of the solid state (mechanical properties, diffusivity)[13].

Diffusion

Diffusion is a molecular transport process caused by random Brownian motion of molecules. The rate of transport of molecules is related to the diffusion coefficient (*D*, in $m^2 \cdot s^{-1}$), a parameter dependent on the nature of the substance, defined by Fick's First Law

$$J = Aj = -AD\frac{\partial c}{\partial x} \quad (1)$$

where *J* is the total flux of molecules ($mol \cdot s^{-1}$) along the distance *x* (m), *A* is the area across which the diffusion occurs (m^2), *j* is the flux per unit area ($mol \cdot s^{-1} \cdot m^{-2}$) and *c* is the concentration ($mol \cdot m^{-3}$) of the solute[14]. Note that the form of Fick's First Law, shown in Equation 1 is valid only when the diffusive flow is one-dimensional and *D* is constant.

Depending on whether the gradient of concentration along the dimension of diffusive flux of the compound is constant, we differentiate between steady-state and non-stationary (transient) diffusion. Diffusive flux is time-variable for the non-stationary diffusion which is governed by the Fick's Second Law in the form (valid for the above-mentioned assumptions):

$$\frac{\partial c}{\partial t} = D\left(\frac{\partial^2 c}{\partial x^2}\right) \quad (2)$$

According to exact initial and boundary conditions, which correspond to the particular system, the solution of this partial differential equation provides the time-spatial dependence of the concentration of diffusing solute in the medium. Comprehensive literature sources, providing these solutions, are available[3, 14, 15].

If the diffusion proceeds in a porous medium, e.g. in hydrogel, it is complicated by two inevitable effects: (i) a reduced cross-sectional area, available for the diffusive flux compared to the macroscopic cross-sectional area (assuming that the compound cannot penetrate the solid phase), and (ii) a more tortuous transport of the compound into the pores of medium (see Fig. 2). As a result, the modified Fick's equations describe the transport of solute through the porous specimen. Furthermore, the diffusing compound may also interact with or even bind to the solid phase of the porous medium (e.g. with the polymer network in the hydrogel). The appropriate mathematical model for the description of diffusion in porous media, including both above mentioned effects, is discussed in detail by Shackelford and Moore[16] and summarized in our previous papers[17–20].

EXPERIMENTAL SECTION

Preparation of hydrogels for the diffusion experiments

The model hydrogels proposed here for the diffusion experiments are prepared from agarose, a commercially available polysaccharide extracted from sea algae. From the chemical point of view, agarose is made up of repeating units of agarobiose, disaccharide consisting of galactose and 3,6-anhydrogalactose (see Fig. 3). Nevertheless, alternative hydrogel systems which meet the requirements of the proposed methodology (optical transparency, ability to interpenetrate a reactive polymer additive, dimensional stability in utilized diffusion apparatuses) can be easily found in the literature (e.g. gelatin[21], chitosan gels[22], waterglass gels[23]). The particular experimental procedure of the thermoreversible gelation of agarose is exceedingly simple[24] as described in the next section (and summarized in Table 1). To prepare the hydrogel with an improved binding affinity to the diffusing

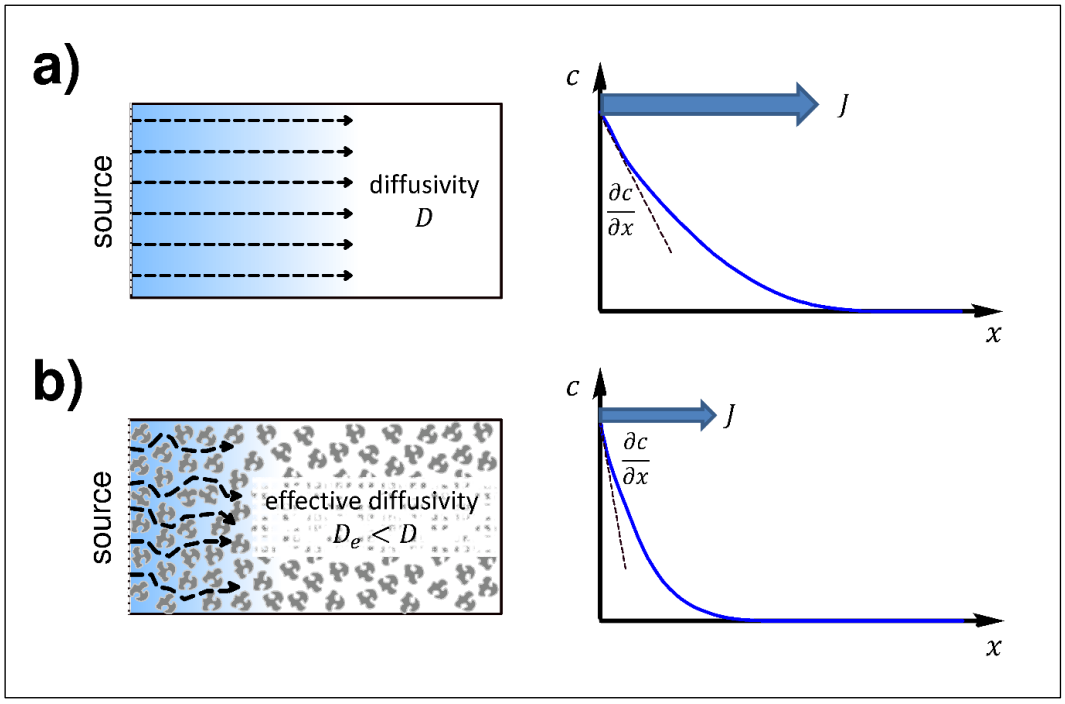

Figure 2. Schematic illustration of the non-stationary diffusion of a solute into non-porous (a) and porous medium (b), respectively. The lower volume fraction available to the diffusion of the solute and the more tortuous trajectory of the diffusion transport in the porous medium results in the decreased total diffusion flux *J*.

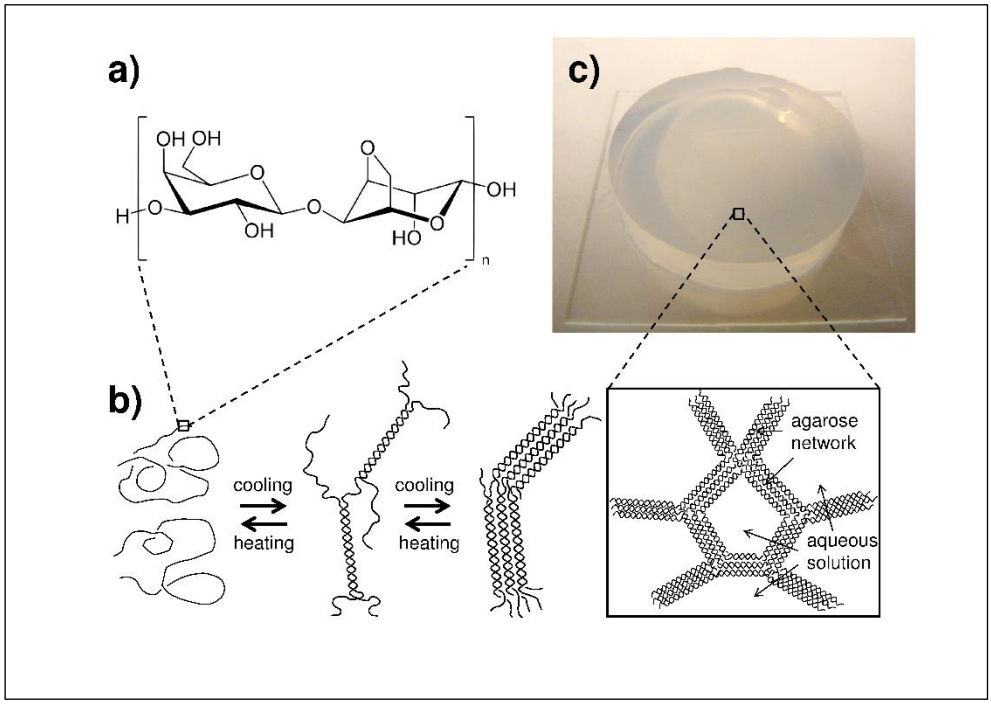

Figure 3. Molecular structure of agarose (a) and the schematic illustration of the macromolecular aggregation processes (b) which take place during the thermoreversible agarose gelatinization leading to the final agarose hydrogel (c).

Table 1. Detailed work-flow of individual 1 wt.% agarose gel samples preparation procedure (*both reference agarose gels as well as the improved binding capacity agarose gels with addition of 0.01 wt. % of individual polyelectrolytes*)

step no.	procedure	reference agarose gel	polyelectrolyte/ agarose gel
1	source materials	agarose powder and distilled water	agarose powder, distilled water and 0.1 wt. % water solutions of individual polyelectrolytes
2	mixing of source materials	disperse solid agarose powder in distilled water (use ratio 0.1 g of agarose to 10 ml of distilled water)	disperse solid agarose powder in distilled water (use ratio 0.1 g of agarose to 1 ml of appropriate polyelectrolytes solution and 9 ml of distilled water)
3	agarose dissolution	under continuous stirring slowly heat the dispersion to 80 °C	
4	sample degassing	rinse vessel with dissolved agarose solution or agarose – polyelectrolyte mixture in ultrasonic bath for 1 minute	
5	final gel shape adjusting	transfer the dissolved gel sample into a form holder according to its subsequent utilization in diffusion experiments (e.g. cylindrical rings for diffusion cells experiment, standard spectrophotometric cuvettes for in-diffusion experiment)	
6	cooling down	cool the form with the gel sample down to the ambient laboratory temperature	

compound, small amounts of a water-soluble polymer carrying appropriate functional groups are dissolved in water prior to the addition of solid agarose. The remaining steps of the gelation are left unchanged. The proper polymer functionality is selected with respect to the chemical nature of the diffusing compound, i.e. according to the charge of ionic compounds, H-bond donor/acceptor character and so forth. A sufficiently low concentration of added polymer compared to the agarose matrix is used to ensure that major mechanical and structural parameters of the gel are not affected by the polymer component so that the observed differences in determined diffusion parameters can be attributed unambiguously to the effect of the binding of the diffusing compound to the reactive additive. The molecular weight of the reactive polymer needs to be high enough to keep the polymer molecules immobilized in the hydrogel network. Any possible release of the polymer from the gel during the diffusion experiments should be verified experimentally as a part of the implementation and optimization of the diffusion methodology.

Selection of the diffusing solute

In the proposed methodology, the concentration of diffusing solute within the gel (in-diffusion/transient experiments) and in the diffusion-cells apparatus (through-diffusion/ steady-state experiments), respectively, is measured by means of spectrophotometry (see the trial laboratory experiments). Therefore, a colored substance with high solubility in water represents a suitable candidate for the diffusing compound. As far as the molecular structure of the solute is concerned, ionic compounds additionally possess great binding affinity towards polyelectrolytes, which can be employed in the demonstration of an effect of binding on the diffusion process. Moreover, because the anion-active polyelectrolytes are much more common than the cation-active ones, positively charged low-molecular-weight

compounds are better utilizable for this purpose. Both inorganic and organic cations with a high molar absorption coefficient in aqueous solution can be used, for instance copper (absorption maximum 810 nm), nickel (390 and 720 nm) or cobalt (510 nm) ions as inorganic ions[25] and methylene blue (665 nm), rhodamine 6G (525 nm) or other basic dyes from organic solutes[18].

Through-diffusion/steady-state experiments in diffusion cells

The method of a diffusion cell[17, 26] (alternatively referred to as a "Franz cell" or the "through-diffusion method")] represents one easy way to study the diffusion experimentally. The experimental principle of the method is straightforward. As the solute diffuses through a studied sample (e.g. a membrane, solid or semi-solid sample like hydrogel, etc.) positioned between two compartments (i.e. cells) of the apparatus, its concentration is continuously measured either in one or both cells. When the diffusing solute is colored, its penetration through the sample can be easily observed even visually. However, the process can be easily studied in a quantitative way by employing spectrophotometry as an available analytical tool routinely used in basic courses of physical and analytical chemistry.

The through-diffusion/steady-state experiment proposed here for undergraduate laboratory classes of physical chemistry proceeds as follows: agarose gel is prepared by *in-situ* gelation in a ring holder like that shown in Figure S1 in the Supplementary Material. After complete solidification of the gel, the holder is fixed in the middle of the diffusion cells apparatus. A schematic drawing of the horizontal diffusion cell apparatus used in the trial experiments (see the next section) is shown in Figure 4. At the same time, the cells of the apparatus are filled with the same volume of a source solution of the diffusing substance and deionized water, respectively. The single-wavelength absorbance or whole absorption spectra of the acceptor solution (water initially) is recorded on the spectrophotometer either after the manual sampling or by means of an optical-fibre dip probe.

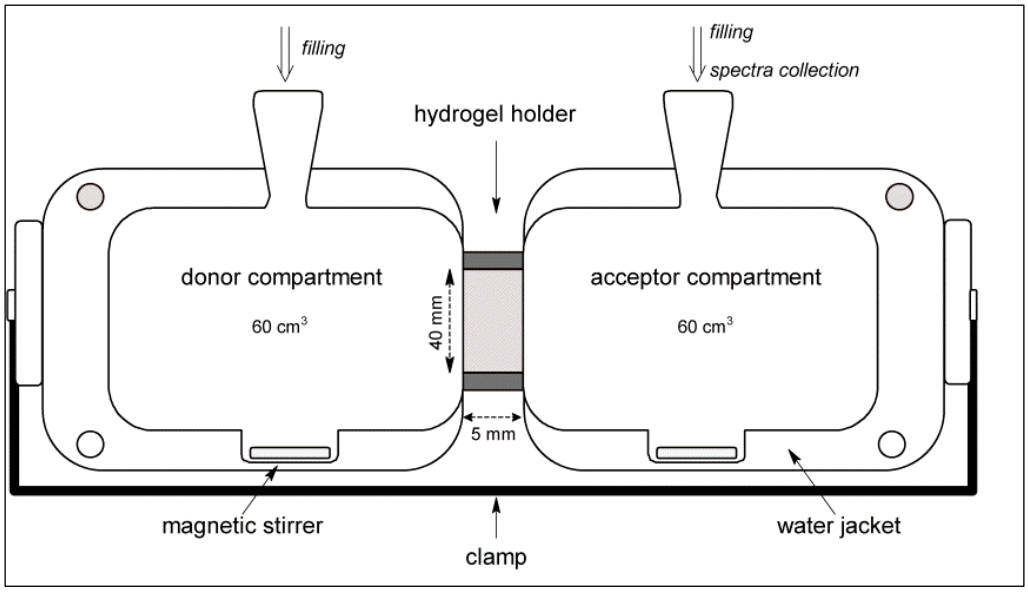

Figure 4. Schematic drawing of the commercial diffusion cells apparatus used in the through-diffusion experiments (not to scale). Diffusion of a solute proceeds from the solution placed in the donor compartment (higher concentration of the solute) into the solution in the acceptor compartment (lower concentration of the solute) through the studied hydrogel sample. The concentration of the solute in the acceptor compartment is continuously measured.

The evaluation of experimental data is based on the linear regression of the increasing part of the time dependency of the concentration of the solute into the "acceptor" cell of the apparatus (breakthrough curve). The *x*-axis intercept of the line provides the time, needed by the solute to break through the gel (i.e. the lag time). From the slope of the line, the steady-state diffusion flux j_d (in $mol.m^{-2}.s^{-1}$) is calculated. This parameter represents the molar amount of solute transported through the unit area of gel sample per second and it depends on the gel thickness L (in m) and the effective diffusivity D_e of the solute in the gel according to the equation

$$j_d = D_e \frac{\Delta c_{gel}}{L} \quad (3)$$

The effective diffusivity of solute provides interesting information about the gel structure as it embraces the effects of gel porosity and tortuosity of the solute flow in gel. The porous nature of the gel results in the fact that only a specific volume fraction is available to the diffusion of solute. Tortuosity is a factor that describes how the trajectory of the solute flow is tortuous because of the presence of dispersed solid content. Both effects decrease the effective diffusivity of the solute (see Fig. 2). A detailed mathematical description of the two effects is provided elsewhere[16, 27].

In-diffusion/transient experiments in cuvettes

Because the diffusion-cell experiments describe quantitatively mainly the later step of the diffusion process when the whole gel sample has already been permeated by the diffusing solute, it is reasonable to combine this experiment with an additional one that focuses on the initial stage of the penetration of the solute into the sample. For this purpose, a simple study can be performed where the gel is prepared via the in-situ gelation in the cuvettes for ultraviolet-visible (UV-VIS) spectrometry. The gel-filled cuvettes are then immersed in the source solution of diffusing solute. To maximally simplify the mathematical description of the diffusion process by using the model for diffusion from a constant source[3, 14], the volume of the solution is kept high enough to maintain the concentration of solute at an approximately constant value during the diffusion experiment. During the diffusion experiment, the cuvettes are taken from the solution at selected time intervals and the UV-VIS spectra are recorded at different positions from the edge of the cuvette. For this purpose, a vertical positioner of the cuvette (i.e. the cuvette holder equipped with finely controlled vertical movement) is needed. An example of such an accessory (made by the authors) is shown in Figure S2 in the Supplementary Material. This leads to the determination of the solute concentration profiles in gel at different time intervals. The calculation of the apparent diffusion coefficient D_a is allowed by comparing of these profiles with the corresponding solution of the Fick's Second Law in the following form

$$c = c_s \cdot \mathrm{erfc} \frac{x}{\sqrt{4 D_a t}} \quad (4)$$

where c represents the concentration of basic organic dye at various distances from the boundary, c_s is the concentration on the hydrogel-solution interface, erfc is the Complementary error function[28] (a non-elementary function of sigmoid shape that often occurs in probability, statistics or in diffusion equations), and t is the time from the beginning of the diffusion process. In comparison with the effective diffusion coefficient, the apparent diffusion coefficient involves also any effect of interactions between the diffusing solute and the gel medium.

Testing the methodology in trial laboratory experiments

The methodology as generally described in the previous section was implemented in trial laboratory experiments performed by undergraduate students as a part of the colloidal chemistry laboratory course at the Brno University of Technology, Faculty of Chemistry. For these experiments, agarose (AG, routine use class, < 10 wt.% moisture

content), methylene blue hydrate (MB, CI Basic blue 9, dye content ≥ 95 wt.%), poly (sodium 4-styrenesulfonate) (PSS, purity > 99 wt.%) and alginate (ALG, purity >99 wt.%) were purchased from Sigma-Aldrich. Leonardite Humic Acid Standard (HA, 1S104H) were purchased from International Humic Substances Society (*www.humicsubstances.org*). All compounds were used without further purification. Agarose was selected as a standard gel-forming agent, methylene blue as a model positively charged low molecular solute and other compounds as anionic polymers of natural (ALG and HA) and synthetic (PSS) origin.

Reference agarose hydrogel was gelatinized from 1 wt.% solution of AG in water (see Table 1). In this process, an accurately weighted amount of solid agarose was dispersed in water and the dispersion was slowly heated under continuous stirring to 80 °C. Then, the mixture was maintained at this temperature until it turned clear and transparent as the agarose dissolved. The solution was then degassed (e.g. in an ultrasonic bath) as the temperature was still kept at 80°C. The hydrogel was formed from this solution during cooling to ambient temperature.

Gels with their binding capacity improved by the addition of polyelectrolyte component were prepared as follows: specific amounts of solid AG and respective polyelectrolyte (PSS, ALG or HA) were dissolved in water in order to prepare the solutions of 1 wt.% content and 0.01 wt.% content of AG and the poly-electrolyte, respectively. The solutions were then gelatinized via the same method as described above.

For the diffusion experiments, warm solutions of AG or AG – polyelectrolyte mixture were poured into appropriate containers to prepare the gels in required proportions. In the case of experiments in diffusion cells, the container was constituted from the plastic ring holder placed between two glass plates (see Figure S3 in the Supplementary Material). Cylindrical gels (40 mm in diameter and 5 mm thick) were prepared by this procedure. For the in-diffusion experiments, the solution was left gelatinizing in standard cuvettes for spectrophotometry (inner dimensions: 10 × 10 × 45 mm), covered by glass to prevent the evaporation and shrinking of the sample during the gelation.

Through-diffusion/steady-state experiments were performed in standard diffusion cells purchased from PermeGear, Inc. (see Figure 4 and Figure S4 in the Supplementary Material). The gel sample in the plastic ring holder was fixed between the donor and acceptor cell of the apparatus. The donor cell was filled with 60 cm^3 of 0.01g.dm^{-3} aqueous solution of methylene blue and the acceptor cell with the same volume of deionized water. VIS absorption spectra were collected automatically in the acceptor solution by USB 2000+ fibre spectrometer (Ocean Optics, Inc.) equipped with an optical fibre dip probe. No samples were taken from the cells and the total volumes of the solutions thus stayed constant during the diffusion experiment. After the termination of the diffusion experiment, the absorbance was measured in both cells. For every measurement, the values of steady-state diffusion flux and time lag were derived from the linear regression of linear part of the break-through curve. Furthermore, the total mass of methylene blue absorbed in the hydrogel specimen was determined from the mass balance in the diffusion cell compartments at the initial and final stage.

In-diffusion experiments with hydrogels were performed as follows: the hydrogel samples in transparent cuvettes were immersed in horizontal positions in 0.01 g dm^{-3} aqueous solution of methylene blue in a container filled with 250 cm^3 of the dye solution. The dye solution was stirred continuously by a magnetic stirrer and the dye was left to diffuse from the solution into the gel samples through the square orifices of the cuvettes. At selected time intervals (24, 48 and 72 hours), the cuvettes were taken out of the solution and the UV–VIS spectra were measured at various distances from the orifice on the Varian Cary 50 UV–VIS spectrophotometer equipped with a special accessory providing controlled fine vertical

movement of the cuvette in the spectrophotometer (see Fig. S2 in the Supplementary Material). From the collected UV–VIS spectra, the concentration profile of the dye was determined along the gel (spectra were taken at 1mm increments at a distance from the gel/solution interface).

After the trial laboratory experiments had been completed, the undergraduate students involved were asked to answer an anonymous survey prepared in the Google forms tool. The survey focused on students' subjective evaluation of the implemented methodology mainly in terms of its contribution to understanding the related theoretical phenomena (transport/diffusion processes, binding of solute to polymer), defining the experimental pros and cons of the particular diffusion techniques and providing the supervisor with feedback on his explanation of the fundamental theory and experimental procedure.

Results and discussion

The general concept for implementing the proposed experiments into undergraduate laboratory courses is to provide students with a practical demonstration of diffusion phenomena. The main emphasis is placed on the illustrative nature of the experiments, the easy transfer of observations into practice and the low technical demands on the experimental design. Therefore, only instrumentation widely available in a common university/commercial lab is used. Furthermore, the diffusion cell apparatus represents a standard analytical tool routinely used in practice e.g. for skin-penetration experiments in pharmacy or cosmetics. From the viewpoint of the desired level of illustration, the combination of transparent hydrogel medium and colored diffusing substances results in the diffusion of the solute being observable even visually (see Figure 5)

.

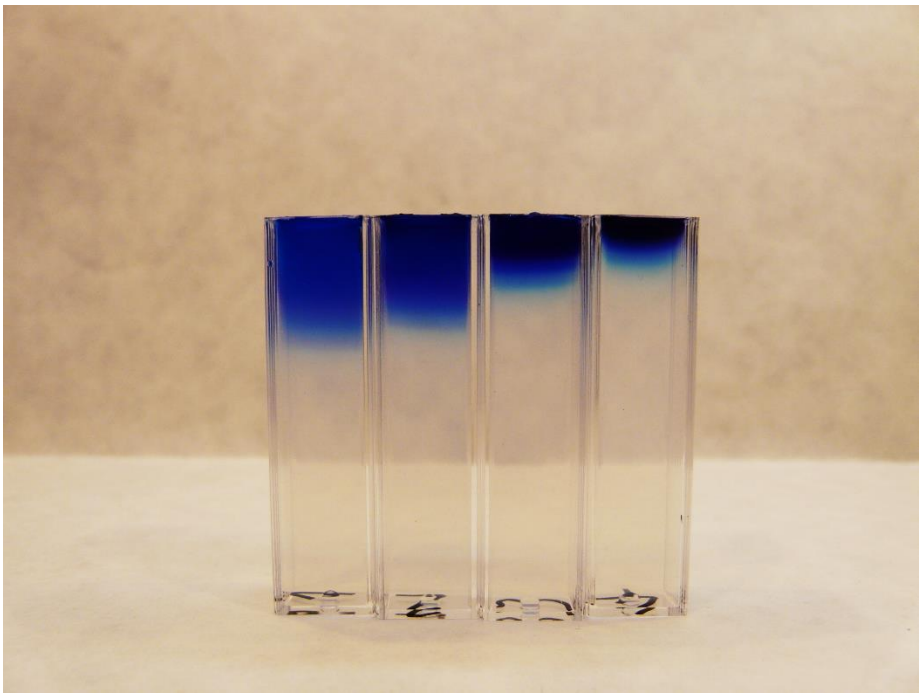

Figure 5. Photo of the gel samples with different content of PSS after 72 hours of diffusion of Methylene Blue (from left to right: 0 wt.%, 0.002 wt.%, 0.005 wt.% and 0.010 wt.% PSS in 1 wt.% AG gel). The decrease of the depth of the dye penetration with increasing concentration of PSS in the gel is obvious.

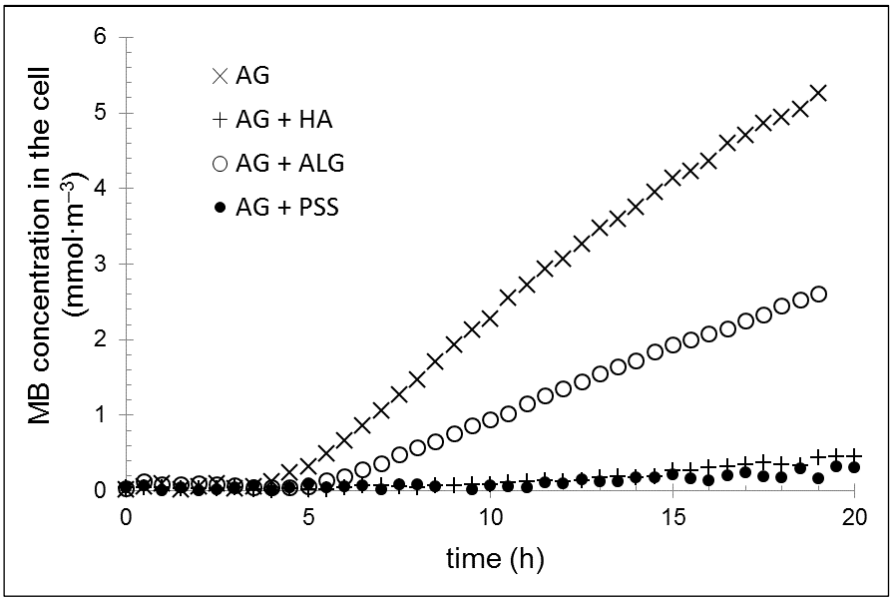

Figure 6. Results of the through-diffusion experiments; breakthrough curves of MB for reference agarose hydrogel (AG) and for gels with respective polyelectrolyte component (ALG, HA and PSS).

Figure 6 shows the results of through-diffusion experiments performed in the diffusion cells. The breakthrough curves (the time dependencies of diffusing solute concentration in the acceptor cell) are shown for the reference agarose gel as well as for the gels with added content of reactive polyelectrolyte. It is evident how the improved binding capacity of gel for the diffusing compound affects the penetration of the compound through the gel. The lag time is increased for all tested polyelectrolyte components of the gel in comparison with the reference agarose gel, while the steady-state diffusion flux is decreased correspondingly (see Table 2). Although a detailed explanation of these results is outside the scope of this paper (a corresponding discussion including mathematical evaluation of data is presented elsewhere[14]), this general finding represents a clear illustration of the way that the binding of solute affects its mobility within the gel. Hence, a small addition of the polyelectrolyte component (note that the dry weight of agarose in the gel is 100× higher than that of polyelectrolyte) can result in a more than 100% increase in the lag time. The effect is qualitatively similar for all tested polyelectrolytes – humic acids as an important reactive compound from non-living nature (soil, sediments), alginate as a model biopolymer and poly(styrenesulphonate) as a representative of synthetic polymers. Obviously, a wide variety of solute-polyelectrolyte combinations is available for the demonstration of this effect and a particular choice can be made with respect to the specific focus of the study program, etc. From the mass balance in the diffusion cell compartments at the initial and final stage the total concentration of methylene blue absorbed in the hydrogel specimen was determined. It can be seen that ALG deviates from the general rule that a polyelectrolyte component enhances the absorption of solute within the gel (see Table 1).

The primary experimental outcome of the in-diffusion/transient experiments is illustrated in Figure 7. Here, the experimental concentration profiles of gels (scattered points) are shown together with the theoretical ones (solid lines), which were determined by the least-square fitting of experimental data with Equation 4 using the Solver tool in Microsoft Excel. The main results of this regression (apparent

Table 2. Main experimental parameters calculated for the diffusion of Methylene Blue in reference agarose gels (AG) and in gels with respective polyelectrolyte component (ALG, HA and PSS) from through-diffusion and in-diffusion experiments. It is evident that the binding of MB on the polyelectrolytes affects the values for both diffusion (j_d, t_{LT}, D_a) and concentration (n, c_S). For details on the way these parameters are determined, see the Supplementary Material (Student Sheets).

through-diffusion experiments			
hydrogel composition	steady state diffusion flux $j_d \times 10^9$ ($mol \cdot m^{-2} \cdot s^{-1}$)	absorbed amount of MB in gel $n \times 10^7$ (mol)	lag time t_{LT} (h)
AG	5.39 ± 0.09	3.8 ± 0.4	3.9 ± 0.6
AG + ALG	2.50 ± 0.02	3.8 ± 0.4	4.9 ± 0.1
AG + HA	0.560 ± 0.001	16.6 ± 0.1	9.3 ± 0.1
AG + PSS	0.240 ± 0.002	24.5 ± 1.5	9.0 ± 0.5
in-diffusion experiments			
hydrogel composition	apparent diffusion coefficient D_a ($m^2 \cdot s^{-1}$)	boundary concentration c_s ($mol \cdot m^{-3}$)	
AG	3.5 ± 0.3	33 ± 8	
AG + ALG	1.6 ± 0.2	14 ± 4	
AG + HA	1.71 ± 0.01	55 ± 4	
AG + PSS	0.18 ± 0.04	622 ± 64	

diffusion coefficient and boundary concentrations of the solute) are listed in Table 2. Again, binding of the solute with the polyelectrolyte component strongly affects the experimental data. The decrease in the rate of diffusion resulting from this binding is characterized by a lower apparent diffusion coefficient in gels with added polyelectrolyte, contrary to the reference agarose gel. Qualitatively, this effect can be observed visually as a lower depth of sample penetration by the colored substance at given time (see Figure 5). Furthermore, the addition of a reactive component often affects also the solution – gel partitioning of the diffusing solute and corresponding boundary concentration of the solute within the gel (for the details, see Sedlacek et al.[18]). A substantial increase in the boundary concentration was confirmed for PSS and HA in comparison with reference AG gels, while the boundary concentration of MB was reduced significantly

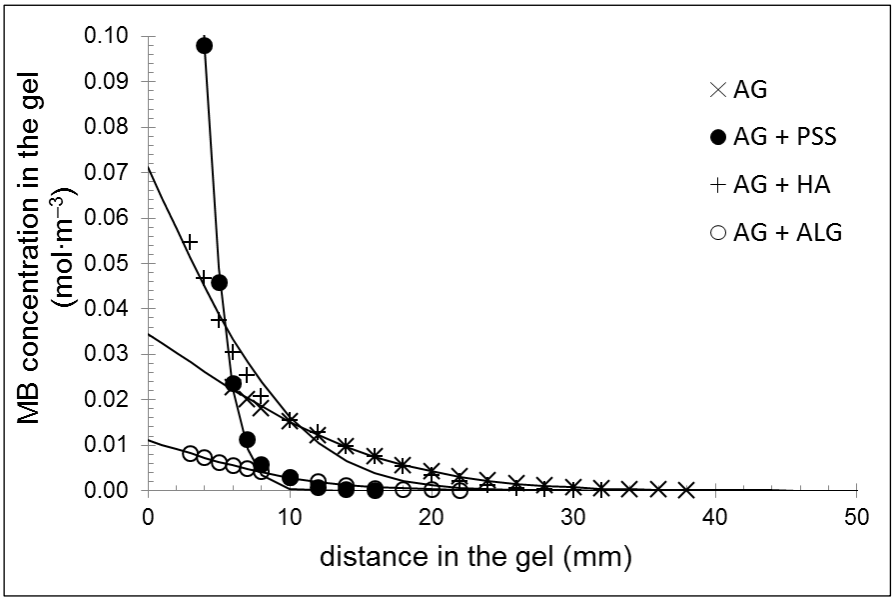

Figure 7. Results of the in-diffusion experiments; experimental (scattered points) and theoretical (solid lines) concentration profiles of MB in reference agarose hydrogel (AG) and in gels with the respective polyelectrolyte component (ALG, HA and PSS).

in hydrogels with added ALG (note the analogy with the results from the through-diffusion experiments). This difference in the behavior of different polyelectrolytes illustrates the complex character of the solution – gel partitioning as another important physico-chemical phenomena involved in the performed experiments. It also shows the wide scope of these experiments in terms of students applying their theoretical knowledge from various areas of physical chemistry.

That the proposed methodology could make an educational contribution was confirmed also by the feedback from students involved in the trial experiments (the voluntary and anonymous questionnaire was answered by 15 students in total). From the practical point of view, the students pointed out the crucial experimental steps and some procedural difficulties of the experiments (mainly the risk of the formation of air bubbles in the gel and leaks in the diffusion cells apparatus caused by the careless preparation of the gel sample). Nevertheless, all the students unanimously appreciated these experiments as a practical illustration of diffusion processes in general and of the effects of specific interactions on diffusion in particular.

CONCLUSIONS

From an educational point of view, the proposed methodology allows the undergraduate students to support their theoretical knowledge of diffusion and related physico-chemical phenomena with highly-illustrative practical demonstrations. The attractiveness of the experiments is supported also by the preparation of hydrogels being involved, as this is a procedure with great practical applicability in everyday life. The evaluation of experimental data provides an opportunity to employ diffusion mathematics in a less complex and practical way. Since the complete duration of these experiments is in the order of days, it is better suited for block-taught laboratory courses. Nevertheless, they can be implemented also in standard weekly-taught courses e.g. by dividing the workflow into two subsequent steps.

From a scientific point of view, this paper clearly shows that the proposed diffusion techniques provides an innovative approach to the study of binding and barrier properties of diverse natural or synthetic compounds. The diffusion techniques can be utilized as an interesting alternative to traditional reactivity mapping methods such as batch sorption experiments[29].The diffusion cell technique should be a universal method for the study of reactivity or barrier properties of various systems, especially biopolymers in hydrogel form. Furthermore, the proposed methodology enables broadening the experimental scope of the study by involving binding-affecting parameters such as pH, ionic strength or temperature.

ACKNOWLEDGEMENTS

This work was supported by the Materials Research Centre at Faculty of Chemistry of the Brno University of Technology – Sustainability and Development, REG LO1211, with financial support from the National Program for Sustainability I (Ministry of Education, Youth and Sports) and by project COST LD15047. Furthermore, authors gratefully appreciate the enthusiastic help of all involved students.

REFERENCES

1. W. Chang, K. Zong and B.J. Ahn, 'Development of Lecture/lab Materials for Nanotechnology and Chemistry' session of the Astore Program in Korea, *J. Mater. Ed.* **31**, 265 (2009).
2. J. Hill, R.K. Verma and D.D. Kumar, Challenges for Chemical Education: Traversing the Chemical Sciences/Materials Science Interface, *J. Mater. Ed.* **35**, 1 (2013).
3. J. Crank, *The Mathematics of Diffusion*, 2nd Ed., Oxford University Press, Oxford, United Kingdom (1979).
4. E. M. King, E. W. Pitha and S. F. Sontum, A laser refraction method for measuring liquid diffusion coefficients, *J. Chem. Ed.*, **66**, 787 (1989).
5. S. K. H. Gulrez, S. Al-Assaf and G. O Phillips, Hydrogels: Methods of Preparation, Characterisation and Applications, in *Progress in Molecular and Environmental Bioengineering - From Analysis and Modeling to Technology Applications*, Angelo Carpi (Ed.), InTech (2011)
6. W. Brostow and H.E. Hagg Lobland, *Materials: Introduction and Applications*, John Wiley & Sons, New York (2017).
7. J. R. Glauber, *Furni novi philosophici*, Amsterdam, Netherlands: Johan Jansson (1658).
8. J. H. E. Cartwright, J. M. García-Ruiz, M. L. Novella and F. Otálora, Formation of Chemical Gardens, *J. Colloid Interface Sci.*, **256** , 351 (2002).
9. F. Glaab, M. Kellermeier, W. Kunz, E. Morallon and J. M. Garcia-Ruiz, Formation and evolution of chemical gradients and potential differences across self-assembling inorganic membranes, *Angew. Chem. Int. Ed.*, **51**, 4317 (2012).
10. J. Kopinsky, A. Rutherford and E. L. Cussler, Theories of precipitation induced by dissolution, *AICHE. J.*, **34**, 2005 (1988).
11. A. Lyon and M. J. Serpe, *Hydrogel micro and nanoparticles*, Wiley-VCH, Weinheim, Germany (2012).
12. F. Ganji, S. Vasheghani-Farahani, E. Vasheghani-Farahani, Theoretical Description of Hydrogel Swelling: A Review. *Iran. Polym. J.*, **19**, 375 (2010).
13. K. S. Anseth, C. N. Bowman, and L. Brannon-Peppas, Mechanical properties of hydrogels and their experimental determination, *Biomaterials*, **17**, 1647 (1996).
14. E. L. Cussler, *Diffusion mass transfer in fluid systems*, Cambridge University Press, Cambridge, United Kingdom (2009).
15. R. K. M. Thambynayagam, *The Diffusion*

Handbook: Applied Solutions for Engineers, McGraw Hill Professional, New York (2011).

16. C. D. Shackelford and S. M. Moore, Fickian diffusion of radionuclides for engineered containment barriers: diffusion coefficients, porosities, and complicating issues, *Eng. Geol.*, **152**, 133 (2013).
17. P. Sedlacek, J. Smilek and M. Klucakova, How the interactions with humic acids affect the mobility of ionic dyes in hydrogels – results from diffusion cells, *React. Funct. Polym.*, **73**, 1500 (2013).
18. P. Sedlacek, J. Smilek and M. Klucakova, How the interactions with humic acids affect the mobility of ionic dyes in hydrogels – 2. Non-stationary diffusion experiments, *React. Funct. Polym.*, **75**, 41 (2014).
19. J. Smilek, P. Sedlacek, M. Kalina and M. Klucakova, On the role of humic acids‘ carboxyl groups in the binding of charged organic compounds, *Chemosphere*, **138**, 503 (2015).
20. J. Smilek, P. Sedlacek, M. Lastuvkova, M. Kalina and M. Klucakova, Transport of organic compounds through porous systems containing humic acids, *Bull. Environ. Contam. Toxicol*. **98**, 3 (2016).
21. A. S. Hoffman, Hydrogels for biomedical applications, *Adv. Drug. Deliver. Rev.*, **64**, 18 (2012).
22. B. Falk, S. Garamone, and S. Shivkumar, Diffusion coefficient of paracetamol in a chitosan hydrogel, *Mater. Lett.*, **58**, 3261 (2004).
23. B. Knoblich and T. Gerber, Aggregation in SiO_2 sols from sodium silicate solutions, *J. Non-Cryst. Solids.*, **283**, 109-113 (2001).
24. P. Y. Lee, J. Costumbrado, C. Y. Hsu and Y. H. Kim, Agarose gel electrophoresis for the separation of DNA fragments, *J. Vis. Exp.*, **20**, 3923 (2012).
25. M. Klučáková, Complexation of Metal Ions with Solid Humic Acids, Humic Colloidal Solutions, and Humic Hydrogel, *Environ. Eng. Sci.*, **31**, 612 (2014).
26. R.H. Stokes, Integral Diffusion Coefficients of Potassium Chloride Solutions for Calibration of Diaphragm Cells, *J. Am. Chem. Soc.*, **73**, 3527 (1951).
27. L. Shen, Z. Chen, Critical review of the impact of tortuosity on diffusion, *Chem. Eng. Sci.*, **62**, 3748 (2007).
28. M. Abramowitz, and I. A. Stegun, (Eds.), Repeated Integrals of the Error Function, in *Handbook of Mathematical Functions with Formulas, Graphs, and Mathematical Tables*, 9th printing. Dover, New York, (1972) pp. 299-300.
29. W.S. Wan Ngah, L.C. Teong, M.A.K.M. Hanafiah, Adsorption of dyes and heavy metal ions by chitosan composites: A review, *Carbohydr. Polym.* **83**, 1446 (2011).

SUPPLEMENTARY MATERIAL

for the paper:

Hydrogels: Invaluable Experimental Tool for Demonstrating Diffusion Phenomena in Physical Chemistry Laboratory Courses

---

Figure S1. Plastic ring holder filled with in-situ gelatinized AG (left) and AG – HA (right) hydrogels, respectively.

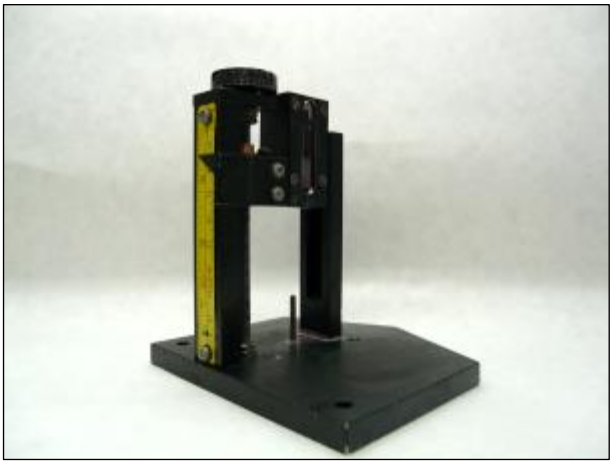

Figure S2. Cuvette holder equipped with fine controlled vertical movement designed and manufactured for the in-diffusion experiments.

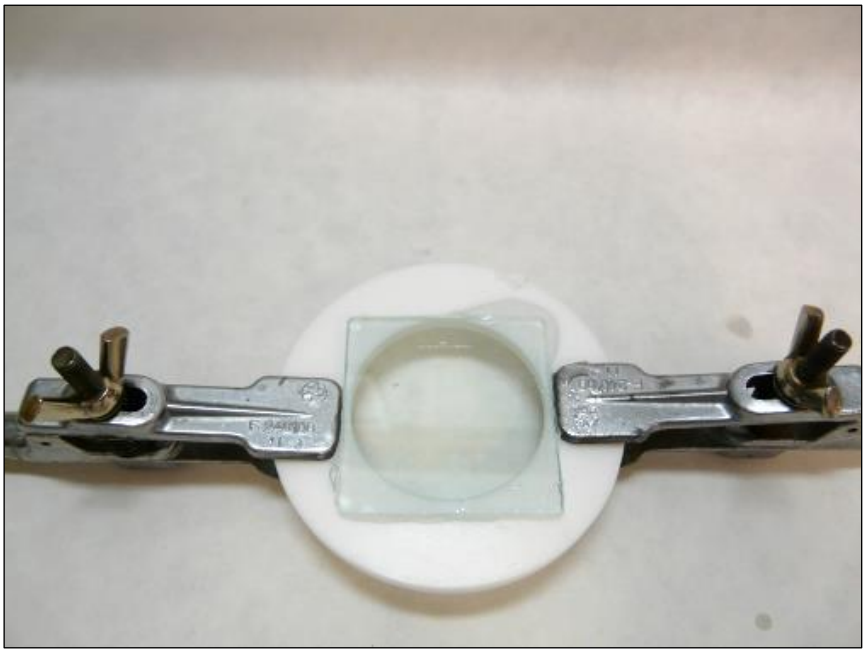

Figure S3. In situ preparation of the AG hydrogel

Figure S4**.** Side-by-side diffusion cells (PermeGear, Inc.)

STUDENT SHEET

THROUGH-DIFFUSION/STEADY STATE DIFFUSION EXPERIMENTS

Instrumentation:

- side-by-side diffusion cell (PermeGear, Inc.)
- fiber spectrophotometer USB 2000+ (Ocean Optics, Inc.)
- software SpectraSuite, data processing software (e.g. OriginPro, MS Excel)

Chemicals:

- agarose (AG, routine use class, Sigma-Aldrich)
- methylene blue hydrate (MB, Sigma-Aldrich)
- poly(sodium 4-styrenesulfonate) (PSS, Sigma-Aldrich)
- alginate (ALG, Sigma-Aldrich)
- Leonardite Humic Acid Standard (HA, 1S104H, International Humic Substances Society)
- deionized water (ELGA Purelab)

Aims of the work:

- to determine a calibration curve for UV-VIS detection of methylene blue in aqueous solutions
- to determine steady-state diffusion parameters (lag time, diffusion flux) of methylene blue in 1 wt.% agarose hydrogel
- to determine steady-state diffusion parameters (lag time, diffusion flux) of methylene blue in 1 wt.% agarose hydrogel with an addition of 0.01 wt.% of selected polyelectrolyte

Laboratory instructions:

1. Calibration curve of methylene blue

- prepare a set of 5 calibration solutions of MB in the concentration range 0.001– 0.01 $g \cdot dm^{-3}$
- measure UV-VIS spectra of the calibration solutions on USB2000+ fiber spectrometer in the range 300 – 800 nm (see the operation manual for the spectrometer)

2. Steady-state diffusion of methylene blue in 1 wt. % agarose hydrogel

- prepare 100 cm^3 of the stock solution of MB (concentration 0.01 $g \cdot dm^{-3}$)

- prepare the agarose hydrogel via the following procedure:
    - put 10 cm^3 of deionized water into a beaker
    - add 0.1 g agarose powder to the water
    - under continuous stirring slowly heat the dispersion to 80°C,
    - keep stirring at 80°C until all the agarose dissolves
    - pre-heat the mold and glass at 80°C in the oven
    - put the agarose solution in an ultrasonic bath at 80°C for 1 minute
    - pour the warm solution of agarose into the mold, cover the solution with the pre-heated glass
    - let the solution solidify for at least 45 minutes at laboratory temperature
    - place the mold between the two chambers of the diffusion cell apparatus
    - simultaneously fill one compartment (donor) of the diffusion cell with 60 cm^3 of the stock solution of MB and the second compartment (acceptor) with the same volume of deionized water
    - immerse the spectrophotometric probe in the acceptor compartment of the diffusion cell and record the baseline for deionized water
    - set the spectra to be recorded every 30 minutes (see the operation manual for the spectrometer)
    - terminate the measurements after 24 hours and measure the concentration of the diffusion probe in the donor compartment of the diffusion cell

3. Steady-state diffusion of methylene blue in in 1 wt.% agarose hydrogel with an addition of 0.01 wt.% polyelectrolyte

- prepare 100 cm^3 of the stock solution of MB (concentration 0.01 $g \cdot dm^{-3}$)
- prepare 10 cm^3 of the stock solution of selected polyelectrolyte (concentration 1 $g \cdot dm^{-3}$)
- prepare the agarose/polyelectrolyte (PE) hydrogel via the following procedure:
    - put 1 cm^3 of the stock solution of polyelectrolyte into a beaker
    - add 0.1 g agarose powder to the water
    - put 9 cm^3 of deionized water into a beaker
    - under continuous stirring slowly heat the dispersion to 80°C
    - keep stirring at 80°C until all the agarose dissolves
    - pre-heat the mold and glass at 80°C in the oven
    - put the agarose/PE solution in an ultrasonic bath at 80°C for 1 minute

- pour the warm agarose/PE solution into the mold, cover the solution with the pre-heated glass
- let the solution solidify for at least 45 minutes at laboratory temperature
- place the mold between the two chambers of the diffusion cell apparatus
- simultaneously fill one compartment of the diffusion cell with 60 cm^3 of the stock solution of MB and the second compartment with the same volume of deionized water
- immerse the spectrophotometric probe in the acceptor compartment of the diffusion cell and record the baseline for deionized water
- set the spectra to be recorded every 30 minutes (see the operation manual for the spectrometer)
- terminate the measurements after 24 hours and measure the concentration of the diffusion probe in the donor compartment of the diffusion cell

Data processing:

1. Calibration curve of methylene blue

- plot a dependency of absorbance at 665 nm on the concentration of MB solution
- from the linear regression of the data (e.g. in MS Excel), calculate the mass extinction coefficient $\mu_{\mathrm{MB,665\ nm}}$ according to Lambert Beer equation

$$A(665\ \mathrm{nm}) = \mu_{\mathrm{MB,665\ nm}} \cdot l \cdot c_{\mathrm{MB}},$$

where c_{MB} is concentration of MB in g·dm^{-3}, A is the absorbance and l represents optical path of the fiber dip probe

2. Steady-state diffusion of methylene blue in 1 wt. % agarose hydrogel

- using the determined value of $\mu_{\mathrm{MB,665\ nm}}$, calculate from the recorded UV-VIS spectra corresponding values of the concentration of MB in the acceptor cell
- plot the dependency of the concentration of MB on time
- from the linear regression of the steady-state phase of the diffusion experiment (see picture below), determine a lag time t_{LT} (from the time-axis interception) and a steady-state diffusion flux j_d from the equation

$$j_d = \left(\frac{\mathrm{d}c_{MB}}{\mathrm{d}t}\right)_{\mathrm{ss}} \cdot \frac{V_{\mathrm{cell}}}{A_{\mathrm{gel}}},$$

where $\left(\frac{\mathrm{d}c_{MB}}{\mathrm{d}t}\right)_{\mathrm{ss}}$ represents the slope of the linear regression, V_{cell} is a volume of the acceptor cell and A_{gel} represents an area of the gel sample in contact with the source and acceptor solution

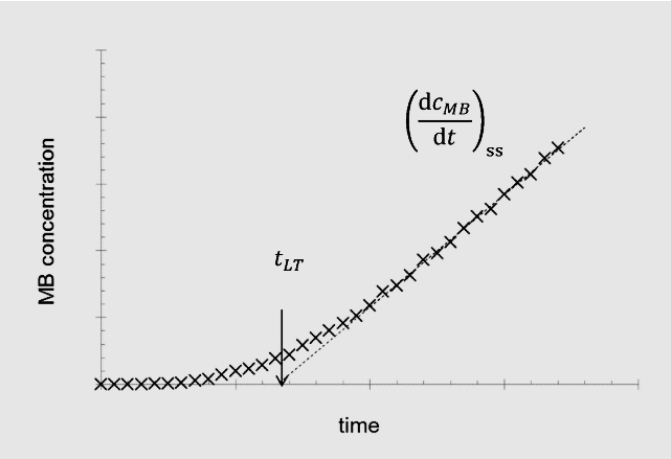

- from the final concentration of MB in the donor and acceptor cell, calculate the absorbed amount of MB in the gel according to equation

$$n = V_{cell} \cdot \left(c_{don,0} - c_{don,\infty} - c_{acc,\infty}\right),$$

where $c_{don,0}$ and $c_{don,\infty}$ represents initial and final concentration of MB in the donor cell and $c_{acc,\infty}$ represents the final concentration of MB in the acceptor cell

3. Steady-state diffusion of methylene blue in in 1 wt.% agarose hydrogel with an addition of 0.01 wt.% polyelectrolyte

- use the same data processing method as in the previous case in order to determine t_{LT}, j_d and n

STUDENT SHEET

IN-DIFFUSION/TRANSIENT DIFFUSION EXPERIMENTS

Instrumentation:

- disposable PMMA spectrophotometric cuvettes
- Cary 50 UV-VIS spectrometer (Varian, Inc.) with a controlled fine vertical movement accessory
- software Cary WinUV, data processing software (OriginPro 8.0, MS Excel)

Chemicals:

- agarose (AG, routine use class, Sigma-Aldrich)
- methylene blue hydrate (MB, Sigma-Aldrich)
- poly(sodium 4-styrenesulfonate) (PSS, Sigma-Aldrich)
- alginate (ALG, Sigma-Aldrich)
- Leonardite Humic Acid Standard (HA, 1S104H, International Humic Substances Society)
- deionized water (ELGA Purelab)

Aims of the work:

- to determine a calibration curve for UV-VIS detection of methylene blue in 1 wt.% agarose hydrogel
- to determine a calibration curve for UV-VIS detection of methylene blue in 1 wt.% agarose hydrogel with an addition of 0.01 wt.% of selected polyelectrolyte
- to determine transient diffusion parameters (apparent diffusion coefficient, boundary concentration) of methylene blue in 1 wt.% agarose hydrogel
- to determine transient diffusion parameters (apparent diffusion coefficient, boundary concentration) of methylene blue in 1 wt.% agarose hydrogel with an addition of 0.01 wt.% of selected polyelectrolyte

Laboratory instructions:

1. **Calibration of methylene blue in 1 wt. % agarose hydrogel and in 1 wt.% agarose hydrogel with the addition of 0.01 wt.% polyelectrolyte**

- prepare 50 cm^3 of the stock solution of MB (concentration 0.01 $g \cdot dm^{-3}$)

- prepare 10 cm^3 of the stock solution of selected polyelectrolyte (concentration 1 $g \cdot dm^{-3}$)
- prepare a set of 5 calibration agarose/MB hydrogels via the following procedure:
    - put a selected volume of MB stock solution (in a range from 0 to 10 cm^3) into a beaker
    - add deionized water to set the total volume of the solution to 10 cm^3
    - add 0.1 g agarose powder to the water
    - under continuous stirring slowly heat the dispersion to 80°C
    - keep stirring at 80°C until all the agarose dissolves
    - put the agarose solution in an ultrasonic bath at 80°C for 1 minute
    - pour the warm solution of agarose into classical cuvettes for spectrophotometry
    - let the solution in cuvettes solidify for at least 45 minutes at laboratory temperature
- measure UV-VIS spectra of the set of individual calibration hydrogel samples on Varian Cary 50 spectrometer in the range 300–800 nm (see the operation manual for the spectrometer)
- prepare the same set of 5 calibration samples of MB in standard cuvettes for UV-VIS spectrophotometry containing 1 wt.% agarose hydrogels with addition of 0.01 wt.% of individual polyelectrolyte (add 1 ml of the polyelectrolyte to the agarose/MB solution during the gel preparation)

2. Transient diffusion of methylene blue in 1 wt. % agarose hydrogel

- prepare 1000 cm^3 of the stock solution of MB (concentration 0.01 $g \cdot dm^{-3}$)
- prepare the agarose hydrogel via the following procedure:
    - put 10 cm^3 of deionized water into a beaker
    - add 0.1 g agarose powder to the water
    - under continuous stirring slowly heat the dispersion to 80°C
    - keep stirring at 80°C until all the agarose dissolves
    - put the agarose solution in an ultrasonic bath at 80°C for 1 minute
    - pour the warm solution of agarose into classical cuvettes for spectrophotometry
    - let the solution in cuvettes solidify for at least 45 minutes at laboratory temperature
    - on the opened side of cuvette cut the excess of hydrogel to create sharp and flat interface
    - immerse the cuvettes with 1 wt. % agarose hydrogel into vessel with 250 cm^3 of stock solution of MB
    - cover the diffusion vessel with a lid

- to prevent evaporation of MB solution seal the space between lid and vessel with parafilm
- at selected time intervals (24, 48) take the cuvettes out from diffusion solution and measure by using of the holder with vertically adjustable measuring position UV-VIS spectra of MB in cuvettes at different position from the edge of cuvette (=solution/hydrogel interface)
- immerse the cuvettes back to the diffusion solution after the measurement
- terminate the diffusion experiments after 72 hours

3. Transient diffusion of methylene blue in in 1 wt.% agarose hydrogel with the addition of 0.01 wt.% polyelectrolyte

- prepare 1000 cm^3 of the stock solution of MB (concentration 0.01 $g \cdot dm^{-3}$)
- prepare 10 cm^3 of the stock solution of selected polyelectrolyte (concentration 1 $g \cdot dm^{-3}$)
- prepare the agarose/polyelectrolyte (PE) hydrogel via the following procedure:
  - put 1 cm^3 of the stock solution of polyelectrolyte into a beaker
  - add 0.1 g agarose powder to the water
  - put 9 cm^3 of deionized water into a beaker
  - under continuous stirring slowly heat the dispersion to 80°C
  - keep stirring at 80°C until all the agarose dissolves
  - put the agarose/PE solution in an ultrasonic bath at 80°C for 1 minute
  - pour the warm solution of agarose/PE into classical cuvettes for spectrophotometry
  - let the solution in cuvettes solidify for at least 45 minutes at laboratory temperature
  - on the opened side of cuvette cut the excess of hydrogel to create sharp and flat interface
  - immerse the cuvettes with 1 wt. % agarose hydrogel with addition of 0.01 wt.% of selected polyelectrolyte into vessel with 250 cm^3 of stock solution of MB
  - cover the diffusion vessel with a lid
  - to prevent evaporation of MB solution seal the space between lid and vessel with parafilm
  - at selected time intervals (24, 48) take the cuvettes out from diffusion solution and measure by using of the holder with vertically adjustable measuring position UV-VIS spectra of MB in cuvettes at different position from the edge of cuvette (=solution/hydrogel interface)
  - immerse the cuvettes back to the diffusion solution after the measurement
  - terminate the diffusion experiments after 72 hours

Data processing:

1. Calibration curve of methylene blue in 1 wt. % agarose hydrogel and in 1 wt.% agarose hydrogel with the addition of 0.01 wt.% polyelectrolyte

- open a recorded UV-VIS spectrum of a 1 wt. % agarose hydrogel with a known concentration of MB in a data processing software OriginPro 8.0
- in order to correct the spectrum form the light scattering effects, set the baseline (light scattering signal) of the spectrum (in Analysis\Spectroscopy\Baseline and Peaks) according to the picture below

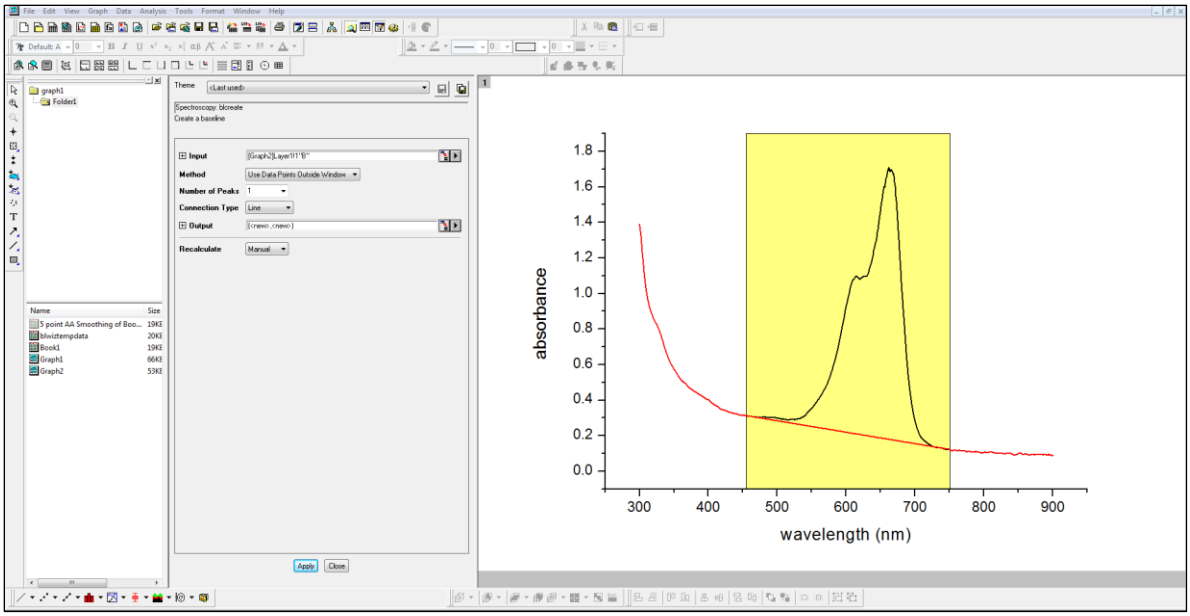

- subtract the determined baseline from the UV-VIS spectrum (in Analysis\Data Manipulation\Subtract Reference Data)

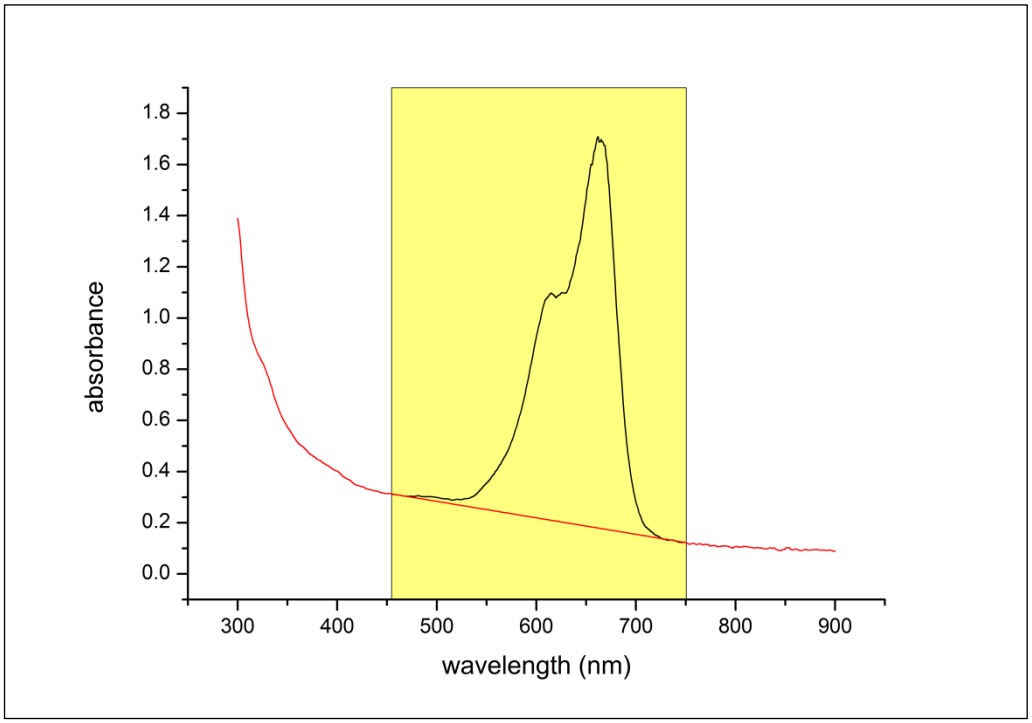
absorbance
wavelength (nm)
0.0
0.2
0.4
0.6
0.8
1.0
1.2
1.4
1.6
1.8
300
400
500
600
700
800
900

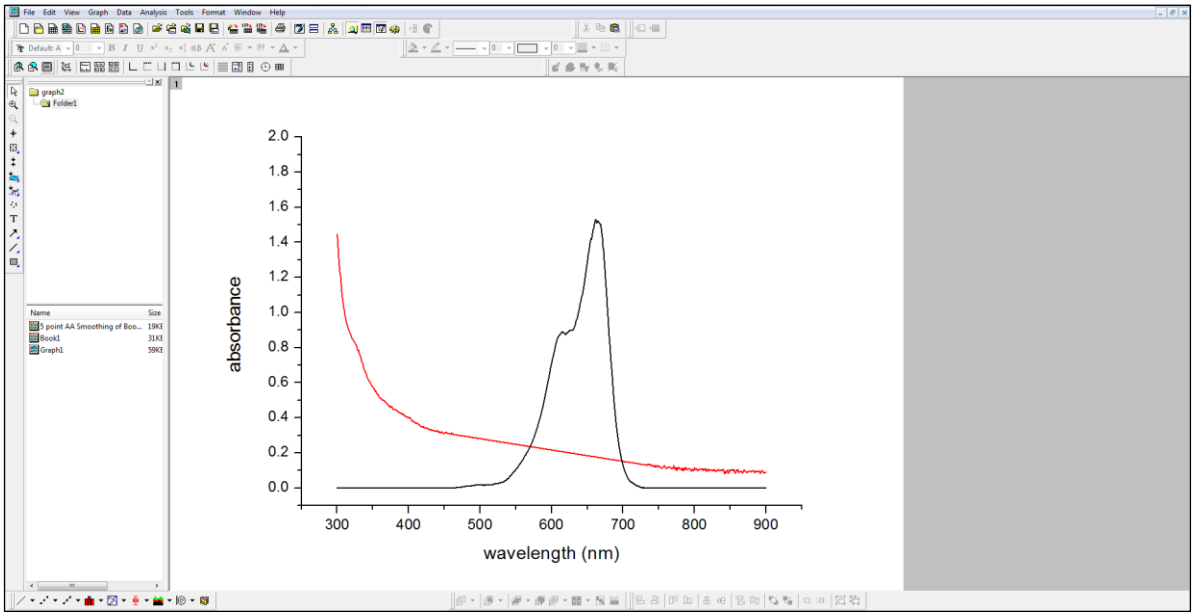
absorbance
wavelength (nm)
0.0
0.2
0.4
0.6
0.8
1.0
1.2
1.4
1.6
1.8
2.0
300
400
500
600
700
800
900

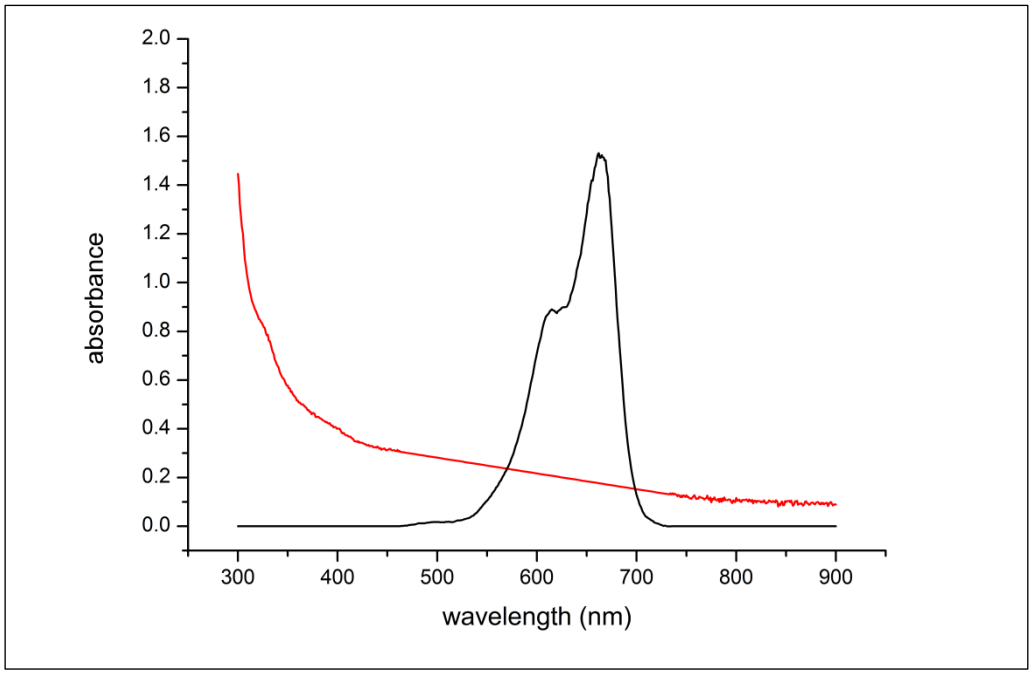

- from the corrected spectrum, determine the corrected absorbance at 665 nm ($A_{\mathrm{cor}}(665\ \mathrm{nm})$)
- plot a dependency of corrected absorbance at 665 nm on the concentration of MB solution
- from the linear regression of the data (e.g. in MS Excel), calculate the mass extinction coefficient of MB in the agarose gel $\mu_{\mathrm{AG\ gel,665\ nm}}$ according to Lambert-Beer equation

$$A_{\mathrm{cor}}(665\ \mathrm{nm}) = \mu_{\mathrm{AG\ gel,665\ nm}} \cdot l \cdot c_{\mathrm{MB}},$$

where c_{MB} is concentration of MB in g·dm^{-3}, A is the absorbance and l represents optical path in the cuvette

- use the same data processing method as in the previous case in order to determine a value of mass extinction coefficient of MB in the agarose/PE gel $\mu_{\mathrm{AG/PE\ gel,665\ nm}} \cdot l \cdot c_{\mathrm{MB}},$

2. Transient diffusion of methylene blue in 1 wt. % agarose hydrogel

- correct the recorded UV-VIS spectra (measured at different positions of the gels) by the correction procedure described above (subtraction of the light-scattering baseline)
- using the determined value of $\mu_{\mathrm{AG\ gel,665\ nm}}$, calculate from the corrected UV-VIS spectra corresponding values of the concentration of MB at specific distances from the gel/solution boundary

- plot the concentration profiles of MB in the gel (dependency of MB concentration on the distance from boundary)
- use the least-square method to fit the experimental concentration profile of MB in the gel by the theoretical equation

$$c_{\mathrm{MB}} = c_s \cdot \mathrm{erfc}\frac{x}{\sqrt{4D_a t}},$$

where c_s is the concentration on the hydrogel-solution interface, erfc is the complementary error function and t is the time from the beginning of the diffusion process. For the fitting purpose, use a selected data processing software, e.g. MS Excel (use a procedure described below, see the demonstration excel workbook):

  - in the table processor, plot the measured concentration profiles (for all times of the spectra recording)

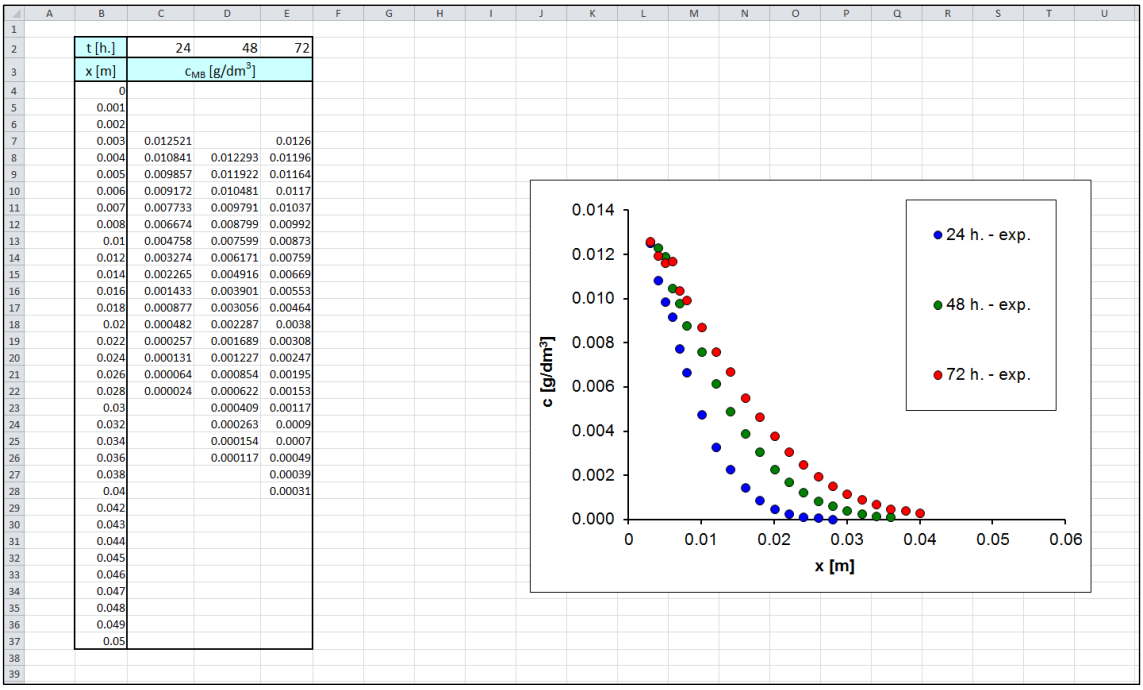

t [h.]	24	48	72
x [m]	c_{MB} [g/dm^3]		
0			
0.001			
0.002			
0.003	0.012521		0.0126
0.004	0.010841	0.012293	0.01196
0.005	0.009857	0.011922	0.01164
0.006	0.009172	0.010481	0.0117
0.007	0.007733	0.009791	0.01037
0.008	0.006674	0.008799	0.00992
0.01	0.004758	0.007599	0.00873
0.012	0.003274	0.006171	0.00759
0.014	0.002265	0.004916	0.00669
0.016	0.001433	0.003901	0.00553
0.018	0.000877	0.003056	0.00464
0.02	0.000482	0.002287	0.0038
0.022	0.000257	0.001689	0.00308
0.024	0.000131	0.001227	0.00247
0.026	0.000064	0.000854	0.00195
0.028	0.000024	0.000622	0.00153
0.03		0.000409	0.00117
0.032		0.000263	0.0009
0.034		0.000154	0.0007
0.036		0.000117	0.00049
0.038			0.00039
0.04			0.00031
0.042			
0.043			
0.044			
0.045			
0.046			
0.047			
0.048			
0.049			
0.05			

  - calculate the theoretical concentration profiles with an initial guess of the parameters c_s, D_a. Plot the theoretical concentration profiles

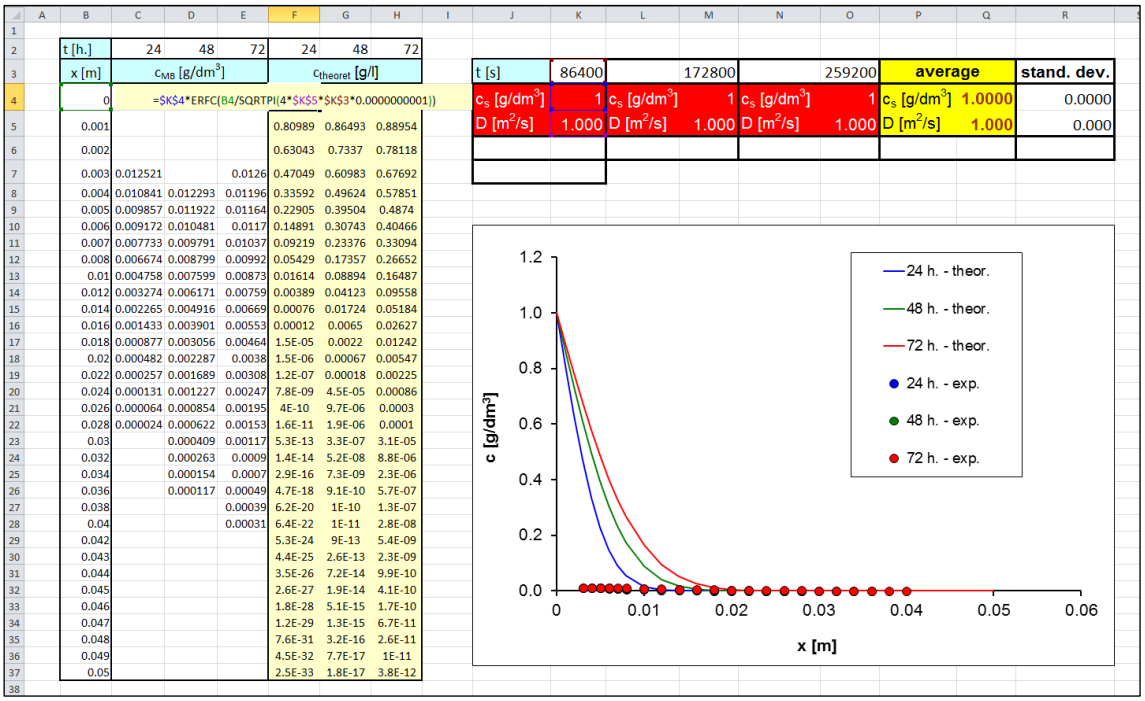

- use MS Excel function SUMXMY2 to calculate the sum of the squares of differences between corresponding experimental and theoretical profiles

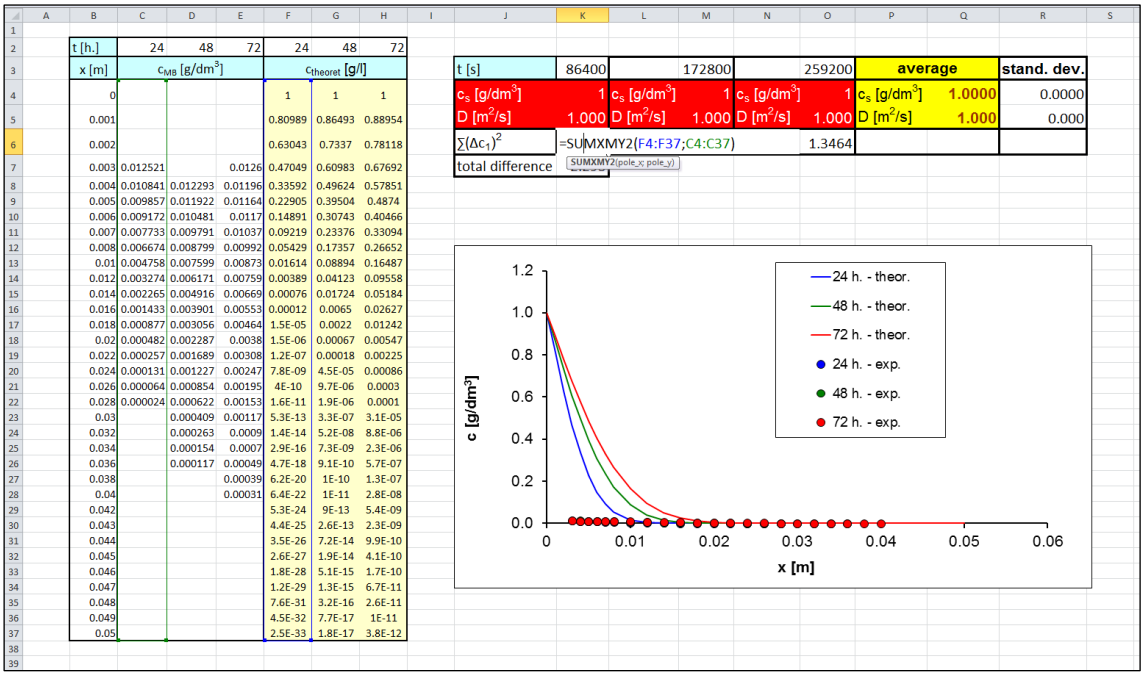

- calculate the total difference as the sum of the squares of differences for the three recorded profiles

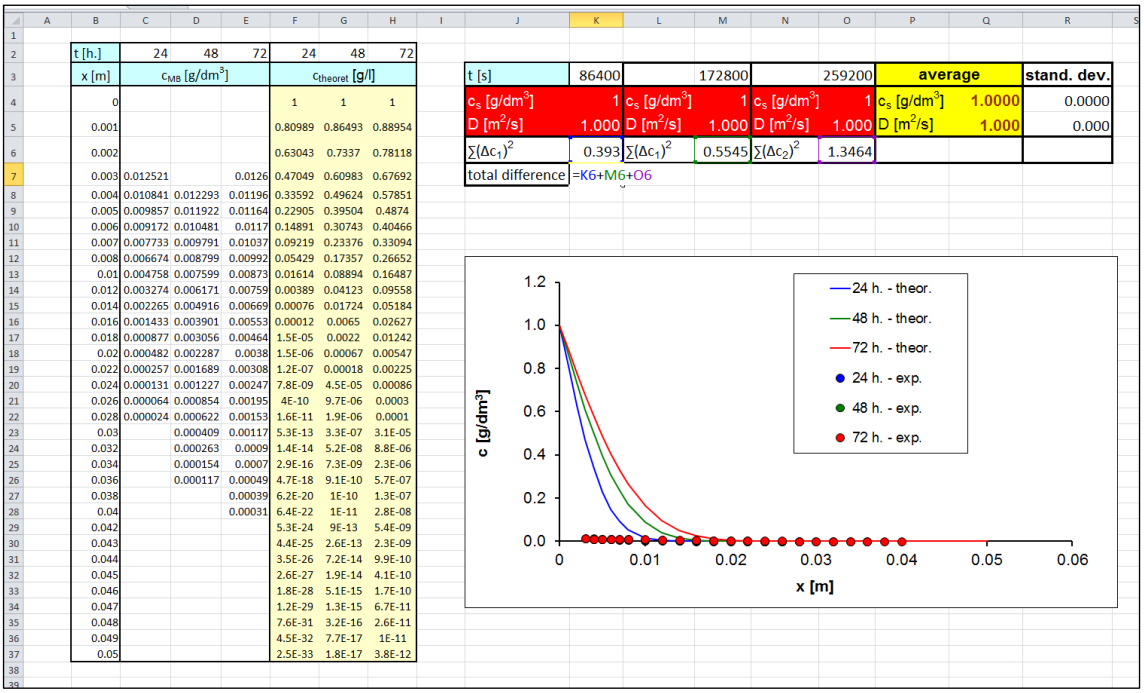

t [h.]	24	48	72	24	48	72
x [m]	c_{MB} [g/dm^3]			$c_{theoret}$ [g/l]		
0				1	1	1
0.001				0.80989	0.86493	0.88954
0.002				0.63043	0.7337	0.78118
0.003	0.012521		0.0126	0.47049	0.60983	0.67692
0.004	0.010841	0.012293	0.01196	0.33592	0.49624	0.57851
0.005	0.009857	0.011922	0.01164	0.22905	0.39504	0.4874
0.006	0.009172	0.010481	0.0117	0.14891	0.30743	0.40466
0.007	0.007733	0.009791	0.01037	0.09219	0.23376	0.33094
0.008	0.006674	0.008799	0.00992	0.05429	0.17357	0.26652
0.01	0.004758	0.007599	0.00873	0.01614	0.08894	0.16487
0.012	0.003274	0.006171	0.00759	0.00389	0.04123	0.09558
0.014	0.002265	0.004916	0.00669	0.00076	0.01724	0.05184
0.016	0.001433	0.003901	0.00553	0.00012	0.0065	0.02627
0.018	0.000877	0.003056	0.00464	1.5E-05	0.0022	0.01242
0.02	0.000482	0.002287	0.0038	1.5E-06	0.00067	0.00547
0.022	0.000257	0.001689	0.00308	1.2E-07	0.00018	0.00225
0.024	0.000131	0.001227	0.00247	7.8E-09	4.5E-05	0.00086
0.026	0.000064	0.000854	0.00195	4E-10	9.7E-06	0.0003
0.028	0.000024	0.000622	0.00153	1.6E-11	1.9E-06	0.0001
0.03		0.000409	0.00117	5.3E-13	3.3E-07	3.1E-05
0.032		0.000263	0.0009	1.4E-14	5.2E-08	8.8E-06
0.034		0.000154	0.0007	2.9E-16	7.3E-09	2.3E-06
0.036		0.000117	0.00049	4.7E-18	9.1E-10	5.7E-07
0.038			0.00039	6.2E-20	1E-10	1.3E-07
0.04			0.00031	6.4E-22	1E-11	2.8E-08
0.042				5.3E-24	9E-13	5.4E-09
0.043				4.4E-25	2.6E-13	2.3E-09
0.044				3.5E-26	7.2E-14	9.9E-10
0.045				2.6E-27	1.9E-14	4.1E-10
0.046				1.8E-28	5.1E-15	1.7E-10
0.047				1.2E-29	1.3E-15	6.7E-11
0.048				7.6E-31	3.2E-16	2.6E-11
0.049				4.5E-32	7.7E-17	1E-11
0.05				2.5E-33	1.8E-17	3.8E-12

t [s]	86400		172800		259200	average	stand. dev.
c_s [g/dm^3]	1	c_s [g/dm^3]	1	c_s [g/dm^3]	1	c_s [g/dm^3] 1.0000	0.0000
D [m^2/s]	1.000	D [m^2/s]	1.000	D [m^2/s]	1.000	D [m^2/s] 1.000	0.000
$\sum(\Delta c_1)^2$	0.393	$\sum(\Delta c_1)^2$	0.5545	$\sum(\Delta c_2)^2$	1.3464		
total difference	=K6+M6+O6						

- use the Solver tool to minimize the total difference by iterative variation of parameters c_s, D_a

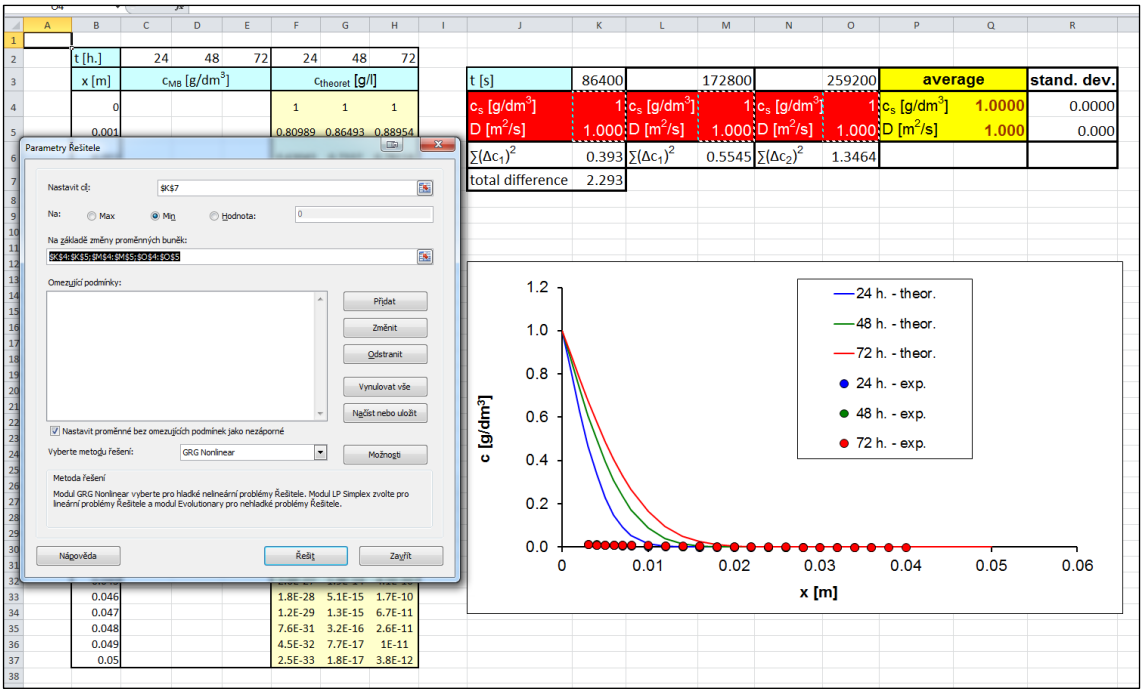

t [h.]	24	48	72	24	48	72
x [m]	c_{MB} [g/dm^3]			$c_{theoret}$ [g/l]		
0				1	1	1
0.001				0.80989	0.86493	0.88954
0.046				1.8E-28	5.1E-15	1.7E-10
0.047				1.2E-29	1.3E-15	6.7E-11
0.048				7.6E-31	3.2E-16	2.6E-11
0.049				4.5E-32	7.7E-17	1E-11
0.05				2.5E-33	1.8E-17	3.8E-12

t [s]	86400		172800		259200	average	stand. dev.
c_s [g/dm^3]	1	c_s [g/dm^3]	1	c_s [g/dm^3]	1	c_s [g/dm^3] 1.0000	0.0000
D [m^2/s]	1.000	D [m^2/s]	1.000	D [m^2/s]	1.000	D [m^2/s] 1.000	0.000
$\sum(\Delta c_1)^2$	0.393	$\sum(\Delta c_1)^2$	0.5545	$\sum(\Delta c_2)^2$	1.3464		
total difference	2.293						

- calculate the average value and standard deviations of the transient diffusion parameters

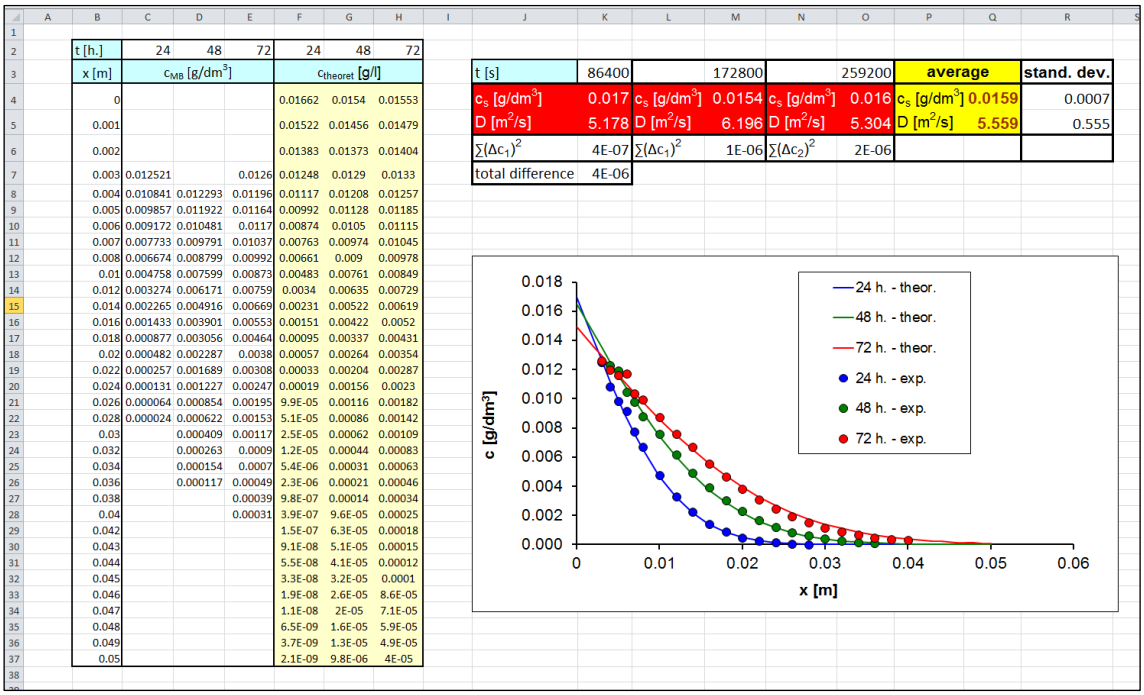

t [h.]	24	48	72	24	48	72
x [m]	c_{MB} [g/dm^3]			$c_{theoret}$ [g/l]		
0				0.01662	0.0154	0.01553
0.001				0.01522	0.01456	0.01479
0.002				0.01383	0.01373	0.01404
0.003	0.012521		0.0126	0.01248	0.0129	0.0133
0.004	0.010841	0.012293	0.01196	0.01117	0.01208	0.01257
0.005	0.009857	0.011922	0.01164	0.00992	0.01128	0.01185
0.006	0.009172	0.010481	0.0117	0.00874	0.0105	0.01115
0.007	0.007733	0.009791	0.01037	0.00763	0.00974	0.01045
0.008	0.006674	0.008799	0.00992	0.00661	0.009	0.00978
0.01	0.004758	0.007599	0.00873	0.00483	0.00761	0.00849
0.012	0.003274	0.006171	0.00759	0.0034	0.00635	0.00729
0.014	0.002265	0.004916	0.00669	0.00231	0.00522	0.00619
0.016	0.001433	0.003901	0.00553	0.00151	0.00422	0.0052
0.018	0.000877	0.003056	0.00464	0.00095	0.00337	0.00431
0.02	0.000482	0.002287	0.0038	0.00057	0.00264	0.00354
0.022	0.000257	0.001689	0.00308	0.00033	0.00204	0.00287
0.024	0.000131	0.001227	0.00247	0.00019	0.00156	0.0023
0.026	0.000064	0.000854	0.00195	9.9E-05	0.00116	0.00182
0.028	0.000024	0.000622	0.00153	5.1E-05	0.00086	0.00142
0.03		0.000409	0.00117	2.5E-05	0.00062	0.00109
0.032		0.000263	0.0009	1.2E-05	0.00044	0.00083
0.034		0.000154	0.0007	5.4E-06	0.00031	0.00063
0.036		0.000117	0.00049	2.3E-06	0.00021	0.00046
0.038			0.00039	9.8E-07	0.00014	0.00034
0.04			0.00031	3.9E-07	9.6E-05	0.00025
0.042				1.5E-07	6.3E-05	0.00018
0.043				9.1E-08	5.1E-05	0.00015
0.044				5.5E-08	4.1E-05	0.00012
0.045				3.3E-08	3.2E-05	0.0001
0.046				1.9E-08	2.6E-05	8.6E-05
0.047				1.1E-08	2E-05	7.1E-05
0.048				6.5E-09	1.6E-05	5.9E-05
0.049				3.7E-09	1.3E-05	4.9E-05
0.05				2.1E-09	9.8E-06	4E-05

t [s]	86400		172800		259200	average		stand. dev.
c_s [g/dm^3]	0.017	c_s [g/dm^3]	0.0154	c_s [g/dm^3]	0.016	c_s [g/dm^3]	0.0159	0.0007
D [m^2/s]	5.178	D [m^2/s]	6.196	D [m^2/s]	5.304	D [m^2/s]	5.559	0.555
$\sum(\Delta c_1)^2$	4E-07	$\sum(\Delta c_1)^2$	1E-06	$\sum(\Delta c_2)^2$	2E-06			
total difference	4E-06							

1. Transient diffusion of methylene blue in in 1 wt.% agarose hydrogel with the addition of 0.01 wt.% polyelectrolyte

Use the same data processing method as described above for transient diffusion of methylene blue in in 1 wt.% agarose hydrogel (for calculation of MB concentration in the gel, use the corresponding value of $\mu_{\text{AG/PE gel,665 nm}}$)

STUDENT SURVEY QUESTIONNAIRE

1. Do you consider the tested methods (through-diffusion experiments in the diffusion cells and non-stationary diffusion in cuvettes) useful in the advanced study of interactions between a polyelectrolyte and low-molecular solutes?

2. Have the tested methods extended your knowledge in the field of diffusion and transport processes in general?

3. Was the theoretical background of the tested methods explained clearly enough?

4. Were the experimental procedures explained clearly enough?

5. What do you consider the main pros and cons of the tested diffusion methods?

6. What do you suggest to improve in the workload of the tested laboratory experiments?
